Water stress detection using radar

van Emmerik, Tim

DOI
10.4233/uuid:46f0b6e6-5592-4b05-983b-a04c8f0f88a8

Publication date
2017

Document Version
Final published version

Citation (APA)
van Emmerik, T. (2017). *Water stress detection using radar*. [Dissertation (TU Delft), Delft University of Technology]. https://doi.org/10.4233/uuid:46f0b6e6-5592-4b05-983b-a04c8f0f88a8

Important note
To cite this publication, please use the final published version (if applicable).
Please check the document version above.

WATER STRESS DETECTION USING RADAR

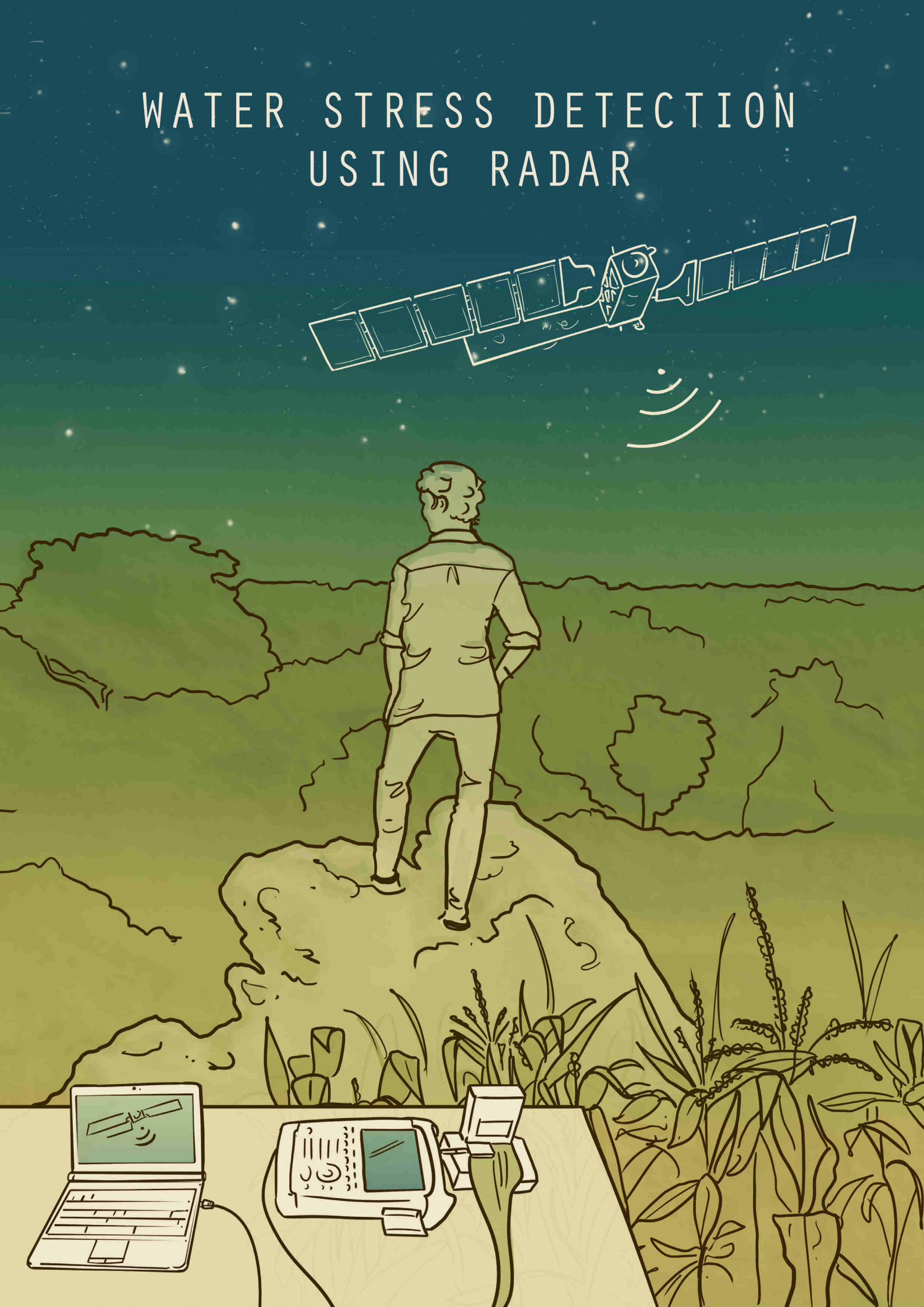

WATER STRESS DETECTION USING RADAR

WATER STRESS DETECTION USING RADAR

Proefschrift

ter verkrijging van de graad van doctor
aan de Technische Universiteit Delft,
op gezag van de Rector Magnificus prof. ir. K.C.A.M. Luyben,
voorzitter van het College voor Promoties,
in het openbaar te verdedigen op
vrijdag 1 december 2017 om 12:30 uur

door

Tim Hans Martin VAN EMMERIK

civiel ingenieur,
Technische Universiteit Delft,
geboren te Delft, Nederland.

Dit proefschrift is goedgekeurd door de

promotor: Prof. dr. ir. N. C. van de Giesen
copromotor: Dr. ir. S. C. Steele-Dunne

Samenstelling promotiecommissie:

Rector Magnificus	voorzitter
Prof. dr. ir. N. C. van de Giesen	Technische Universiteit Delft
Dr. ir. S. C. Steele-Dunne	Technische Universiteit Delft
Onafhankelijke leden:	
Prof. ir. P. Hoogeboom	Technische Universiteit Delft
Prof. dr. ir. R. Uijlenhoet	Wageningen University & Research
Prof. dr. Z. Su	Universiteit Twente
Jun.-Prof. dr. A. Hildebrandt	Friedrich-Schiller-Universität Jena, Duitsland
Prof. dr. ir. H.H.G. Savenije	Technische Universiteit Delft

Keywords: Radar, drought, water stress, hydrology, remote sensing, Amazon, rainforest, corn, tomato, vegetation

Printed by: Druk. Tan Heck

Front & Back: Sylvia Machgeels

ISBN 978-90-6824-060-3

An electronic version of this dissertation is available at
http://repository.tudelft.nl/.

Everything that sounds like wisdom could have been said by Mark Twain

Mark Twain

PREFACE

Nothing changes as much as the weather, according to my fellow Dutch speakers. I have a slightly different view, after having worked four years on this thesis. For some people, a Ph.D. is a continuous stream of pleasure and joy. Enjoying the academic freedom, exploring and challenging your mind, traveling around the world for fieldwork and conferences. For others, a Ph.D. is experienced as a never ending source of misery, insecurity, arguments, depression, and failure. Now, reality is not as binary, and there is quite a large range spanning these extremes. Or, and that is my case, a Ph.D. is a constant alternation of those two extremes. Living on a cloud when a paper gets accepted, followed by two months of distress when the next one is publicly destroyed. My professional and personal lives have been a complete roller coaster during the last four years. In some ways self-induced, and in some ways imposed on me by life. Therefore, I would like to argue that my relation with this very thesis has changed at least as much as the weather. It has been an incredible journey, and I am happy that the destination is reached. However, I also very much hope that it is just the beginning, and look forward to seeing where the (unlaid) tracks will bring me next.

Tim Hans Martin VAN EMMERIK
Delft, May 2017

SUMMARY IN ENGLISH

Vegetation is a crucial part of the water and carbon cycle. Through photosynthesis carbon is assimilated for biomass production, and oxygen is released into the atmosphere. During this process, water is transpired through the stomata, and is redistributed in the plant. Transpired water is refilled by uptake of water from the root zone in the subsurface. Transpiration by vegetation accounts for most of the total evaporation from land on a global scale. In some ecosystems, such as tropical rainforests, transpiration even makes up more than 70% of total evaporation.

Periods of low water availability, water stress, leads to irreversible damage to plants, and can eventually lead to plant death. To prevent this, various mechanisms are activated by the vegetation to survive. Transpiration is reduced as a result of vegetation water stress, which can affect the water and carbon cycle on local, regional, and even global scales. Additionally, water stress in crops is one of the major reasons for harvest losses, threatening food security. However, many effects of vegetation water stress on crops and tropical forests remains poorly understood.

New satellite observations provide opportunities for better detection and understanding of vegetation water stress. Recent research suggests that radar remote sensing might yield valuable insights into vegetation water content. Radar backscatter is sensitive to vegetation because of direct backscatter from the canopy, and through two-way attenuation of the signal as it travels through the vegetation layer. The degree of interaction of radar waves with the vegetation is mainly a function of the vegetation dielectric constant, which is in turn primarily influenced by vegetation water content.

Over the last years, various studies have reported links between anomalies in radar backscatter and vegetation water stress. This has led to the hypothesis that radar backscatter is sensitive to vegetation water stress. Additional field measurements of vegetation water content and dielectric constant, in combination with radar backscatter are necessary to test this hypothesis. This is what inspired this thesis. Based on a combination of field measurements using new sensors, models, and radar backscatter, this thesis focuses on understanding the effects of water stress on plant dynamics, identifying early signatures of vegetation water stress, and exploring the opportunities of early water stress detection using radar remote sensing.

This thesis studies the effects of vegetation water stress across scales, from individual leaves to rainforests. A new method is presented that allows measurements of leaf dielectric properties on living plants. First, the method is tested on tomato plants in a controlled environment. By measuring tomato plants with and without water stress, it is demonstrated that there is a significant difference in the leaf dielectric properties of stressed and unstressed tomato plants. Second, this same method is used under field conditions. Using data sets of corn plants with and without water stress, it is demonstrated that water stress changes plant water content, resulting in significant changes of leaf dielectric properties. Using the field data from the stressed corn field, a modeling

study was done to investigate the sensitivity of radar backscatter to water stress. Here, it is shown that total and leaf water content can change considerably during the day, leading to observable differences in radar backscatter.

To study the effects of water stress in tropical rainforests, accelerometers were placed on trees in the Brazilian Amazon to measure tree sway. Tree sway depends on various tree properties, and this thesis demonstrates that the measured tree acceleration is sensitive to tree mass, intercepted rainfall, and tree-atmosphere interactions. Using five months of acceleration data from 19 trees, an effect of the transition from the wet to the dry season was found. This thesis hypothesizes that this was caused by water related changes in tree mass, or leaf fall in response to increased tree water deficit.

Finally, coinciding field data on tree water content and tree water deficit, and radar backscatter, were used to demonstrate the sensitivity of radar backscatter to increased water stress. During the transition from wet to dry season, a strong drop was found in radar backscatter, which is explained by a rapid increase in measured tree water deficit.

For years, the hypothesis that radar backscatter is sensitive to vegetation water stress has been discussed. Yet, a lack of observations withheld this hypothesis to be tested. This thesis uses field data of crops, and trees in tropical forests, and modeling approaches to finally demonstrate that vegetation water stress results in significant changes in plant water status, which lead to observable variations in radar backscatter.

SAMENVATTING IN HET NEDERLANDS

Vegetatie is een cruciaal onderdeel van de water- en koolstofcyclus. Door middel van photosynthese wordt koolstof opgenomen voor biomassaproductie, waarbij zuurstof vrijkomt in de atmosfeer. Tijdens dit proces wordt water getranspireerd via de huidmondjes, en geredistribueerd in de plant. Het getranspireerde water wordt aangevuld via de wortels, die water opnemen uit de wortelzone in de bodem. Op een globale schaal heeft transpiratie door vegetatie het grootste aandeel in de totale verdamping vanaf het aardoppervlak. In sommige ecosystemen, zoals tropische regenwouden, maakt transpiratie zelfs meer dan 70 % uit van de totale verdamping.

Periodes met lage waterbeschikbaarheid, waterstress, kan bij planten leiden tot onomkeerbare schade en uiteindelijk zelfs tot sterfte. Om dit te voorkomen activeren planten mechanismen om te overleven. Tranpiratie wordt beperkt in reactie op waterstress, wat een significante invloed heeft op de locale, regionale, en globale water- en koolstofcyclus. Daarnaast is waterstress in gewassen een van de belangrijkste oorzaken van oogstverliezen, wat voedselzekerheid ernstig bedreigd. Helaas is de kennis over de effecten van waterstress in gewassen en tropische regenwouden nog beperkt.

Nieuwe satellietobservaties bieden mogelijkheden voor het beter detecteren en bestuderen van waterstress in planten. Recentelijk onderzoek suggereert dat remote- sensingtechnieken zoals radar waardevolle informatie kunnen leveren over het watergehalte van vegetatie. Radarweerkaatsing is gevoelig voor vegetatie wegens directe weerkaatsing van radargolven, alsmede de uitdoving van de golven wanneer het door de vegetatielaag reist. De mate van interactie van radargolven met vegetatie is voornamelijk een functie van de diëlektrische eigenschappen van de vegetatie. Diëlektrische eigenschappen zijn op hun beurt weer vooral afhankelijk van het watergehalte van de vegetatie.

In de laatste jaren hebben verschillende studies afwijkingen in radarweerkaatsing in verband gebracht met waterstress in vegetatie. Dit heeft geleid tot de hypothese dat radarweerkaatsing gevoelig is voor waterstress in vegetatie. Aanvullende veldmetingen van het watergehalte en diëlektrische eigenschappen van vegetatie, in combinatie met radarobservaties zijn noodzakelijk om deze hypothese te testen. Dit is wat als inspiratie heeft gediend van dit proefschrift. Gebruikmakende van een combinatie van innovatieve veldmetingen, modellen en radarobservaties, focust dit proefschift zich op (1) het beter begrijpen van de effecten van water stress op plantfysiologische processen, (2) het identificeren van vroege tekenen van water stress en (3) het verkennen van de mogelijkheden om radar te gebruiken voor waterstressdetectie in vegetatie.

Dit proefschift bestudeert de effecten van waterstress op verschillende scalen, van individuele bladeren tot tropische regenwouden. Een nieuwe methode gepresenteerd om diëlektrische eigenschappen van bladeren van levende planten te meten. Deze me-

thode is eerst getest op tomatenplanten in een gecontroleerde omgeving. Door het meten van bladeren van tomatenplanten met en zonder waterstress, wordt laten zien dat er een statistisch significant verschil is tussen de diëlektrische eigenschappen van bladeren van planten met en zonder waterstress. Vervolgens wordt dezelfde methode toegepast onder veldcondities. Met datasets van maisplanten met en zonder waterstress wordt laten zien dat waterstress een effect heeft op het watergehalte van planten, wat leidt tot significante verschillen in diëlektrische eigenschappen van de bladeren. De data van het veldwerk op het gestresste maisveld worden vervolgens gebruikt voor een modelstudie om de gevoeligheid van radarweerkaatsing voor waterstress te onderzoeken. Hier wordt laten zien dat het watergehalte van de hele plant, en vooral het watergehalte in de bladeren, drastisch kan veranderen gedurende de dag, wat leidt tot waarneembare verschillen in radarweerkaatsing.

Om het effect van waterstress in tropische regenwouden te onderzoeken zijn er accelerometers geïnstalleerd op bomen in de Braziliaanse Amazone om hun beweging te meten. De manier waarop bomen bewegen hangt af van verschillende eigenschappen. Dit proefschrift laat zien dat de beweging gevoelig is voor boommassa, de hoeveelheid water dat op het bladerdek blijft liggen (interceptie), en de mate van interactie tussen de boom en de atmosfeer. Vijf maanden accelerometerdata worden gebruikt van 19 bomen om te laten zien dat er ook een duidelijk verschil te zien is tussen het natte en het droge seizoen. De hypothese is dat deze verandering het resultaat is van veranderingen in boommassa, veroorzaakt door veranderingen in watergehalte, of het uitvallen van bladeren as reactie op toenemend watertekort.

Tot slot worden velddata van watertekorten in bomen in combinatie met radarobservaties gebruikt om te laten zien dat radarweerkaatsing zeer gevoelig is voor toenemende waterstress. Tijdens de overgang van het natte naar het droge seizoen is een duidelijke daling gevonden in radarweerkaatsing, wat verklaart kan worden door de snelle toename in gemeten watertekort in de bomen.

Al jaren wordt er gediscusseerd over de hypothese dat radarweerkaatsing gevoelig is voor waterstress in vegetatie. Helaas is er tot dusver altijd een tekort aan observaties geweest om deze hypothese te testen. Dit proefschrift gebruikt veldmetingen van watergehalte en diëlektrische eigenschappen van gewassen en bomen in tropische regenwouden, radarmodellen en radarobservaties om te laten zien dat watertekort in vegatie leidt in significante veranderingen in watergehalte en diëlektrische eigenschappen van planten, wat leidt tot waarneembare verschillen in radarweerkaatsing.

POETIC SUMMARY

Lonely Satellites

I'll tell you how my research went,
What we know from biology,
The functioning of ev'ry tree,
Depends on its water content

So what if there's a little less
Of this epic liquid of life
Will plants just stop to thrive
Or will we end up in a mess

Plant death is a catastrophe
For that we need to explore new ways
To ensure food security

Simply said, to save the human race
We need more lonely satellites
For drought detection from out'r space

NOMENCLATURE

List of abbreviations

ABA	Abscisic acid
ASCAT	Advanced scatterometer
DOY	Day of year
CCI	ESA Climate Change Initiative
ERS-1/2	European Remote-Sensing Satellite 1 and 2
ESA	European Space Agency
FAO	Food and Agriculture Organization of the United Nations
FAWN	Florida Automated Weather Network
FFT	Fast Fourier transform
ISS	International Space Station
LAI	Leaf area index
MIMICS	Michigan microwave canopy scattering model
MicroWEX-11	Eleventh Microwave Water and Energy Balance Experiment
MODIS	Moderate-resolution imaging spectroradiometer
NASA	National Aeronautics and Space Administration
RapidScat	ISS-RapidScat
QuickSCAT	NASA Quick Scatterometer
TRMM	Tropical Rainfall Measurement Mission
VPD	Vapor pressure deficit

List of symbols

Latin

a	Acceleration [m s^{-2}]
A	Water-cloud model parameter [-]
A_0	Amplitude [-]
A_{leaf}	Water-cloud leaf model parameter [-]
A_{st}	Water-cloud stalk model parameter [-]
A_t	Tree catch area [m^2]
B	Water-cloud model parameter [-]

B_{leaf}	Water-cloud leaf model parameter [-]
C	Wind energy spectrum constant [-]
c	Damping coeffcient [-]
C_d	Drag coefficient [-]
D_{BH}	Tree diameter at breast height [m]
$D_{b,act}$	Bark thickness [mm]
$D_{b,pot}$	Tree growth line [mm]
E	Water-cloud model parameter [-]
E_{def}	Evaporation deficit [mm d^{-1}]
E_{ref}	Penman-Monteith reference evaporation [mm d^{-1}]
E_{pot}	Potential evaporation [mm d^{-1}]
F	External force [N]
f	Frequency [Hz]
f_r	Microstrip line resonator resonant frequency [Hz]
f_0	Natural frequency [Hz]
H	Tree motion frequency spectrum [dB]
h	Plant height [m]
H_a	Aerodynamic transfer function [-]
H_m	Mechanical transfer function [-]
h_s	Surface roughness [m]
h_1	Height of leaf layer [m]
h_2	Height of stalk layer [m]
I	Applied irrigation [mm d^{-1}]
k	Wave number [-]
K_c	FAO crop factor [-]
k_s	Spring constant [N m^{-1}]
M	Tree mass [kg]
m	Mass [kg]
M_d	Dry weight [g]
$M_{d,l}$	Dry weight leaf [g]
$M_{d,s}$	Dry weight stem [g]
M_g	Gravimetric moisture content [-]
M_w	Fresh weight [g]
$M_{w,l}$	Fresh weight leaf [g]

$M_{w,s}$ Fresh weight stem [g]

P Precipitation [mm d^{-1}]

p Power spectrum of tree response [-]

P_u Power spectrum of the wind [dB]

P_y Power spectrum of tree response [dB]

p_0 Reference value [-]

s_a Tree acceleration frequency spectrum slope [dB/Hz]

s_w Wind frequency spectrum slope [dB/Hz]

t Time [s]

$\bar{u}$ Mean wind speed [m s^{-1}]

V Tree volume [m^3]

V_1 Water-cloud vegetation model parameter [-]

V_2 Water-cloud vegetation model parameter [-]

VWC Vegetation water content [kg/m^2]

x Horizontal displacement [m]

Greek

α Drag coefficient factor [-]

β Damping parameter [-]

γ Attenuation factor for vegetation layer [-]

γ_{leaf} Attenuation factor for leaf layer [-]

γ_{leaf} Attenuation factor for stalk layer [-]

Δf_r Difference in resonant frequency between leaf and reference [Hz]

$\frac{\Delta S}{\Delta t}$ Soil moisture change [mm d^{-1}]

ΔW Total tree water deficit [mm]

ϵ Dielectric constant of soil [-]

ϵ_d Dissipation rate [-]

κ Wind energy spectrum constant [-]

λ Wavelength [mm]

ρ Number of plants per m^2

ρ_a Air density [kg m^{-3}]

ρ_w Tree density [10^3kg m^{-3}]

σ^0_{hh} Horizontally polarized radar backscatter [dB]

σ^0_{leaf} Total backscatter [dB]

σ^0_{soil} Soil contribution to backscatter [dB]

σ^0_{stalk}	Total backscatter [dB]
σ^0_{tot}	Total backscatter [dB]
σ^0_{veg}	Vegetation contribution to backscatter [dB]
σ^0_{vv}	Vertically polarized radar backscatter [dB]
θ	Radar incidence angle [rad]
ϕ	Phase shift [rad]
ω_0	Natural frequency [rad/s]

CONTENTS

1

Introduction

Das Leben ist nicht immer nur Pommes und Disco,
Das sage ich Dir,
Manchmal ist das Leben einfach nur,
Eine Flasche Bier

Christian Steiffen

1

1.1 BACKGROUND

Radar remote sensing is used for many vegetation and soil moisture monitoring applications because of its sensitivity to the water content in the land surface layer. The key advantage of radar remote sensing is that radar waves penetrate clouds and do not require visible light, allowing measurements at any given moment in time (Brakke et al. (1981); Prevot et al. (1993)).

Current applications of radar include crop classification (Ulaby et al., 1982b; Hoogeboom, 1983; Foody et al., 1989; McNairn et al., 2009), biomass monitoring (Ferrazzoli et al., 1997; Paloscia et al., 1999; Chambers et al., 2007), fuel load estimation (Saatchi et al., 2007), and soil moisture estimation (Wagner et al., 1999; Bindlish and Barros, 2001; Joseph et al., 2008; Kim and van Zyl, 2009; Entekhabi et al., 2010; Brocca et al., 2017). Although vegetation water content (VWC) varies diurnally and seasonally (McNairn and Brisco, 2004), VWC is generally considered constant or to change only on a seasonal timescale (Wagner et al., 1999; Bindlish et al., 2009; Panciera et al., 2014; Kim et al., 2010; Steele-Dunne et al., 2017). Depending on the timescale of interest, diurnal variations in VWC can have a significant impact on backscatter.

Vegetation water stress affects diurnal variations in VWC significantly (Slayter et al., 1967; Hsiao, 1973), and recent work has hypothesized the sensitivity of radar backscatter to vegetation water stress (Friesen, 2008; Steele-Dunne et al., 2012). Due to a lack of ground data this hypothesis has not been tested thoroughly yet. Therefore it remains uncertain if, and in which order of magnitude, water stress affects backscatter. Understanding this relation is crucial for improving current applications such as soil moisture estimation, fuel load estimation, biomass estimation, and opens the door to potential new applications such as water stress detection and monitoring, and drought extend mapping.

1.2 RADAR RESPONSE TO VEGETATION

Radar backscatter over a canopy σ^0_{canopy} is the sum of the backscatter directly from the vegetation $\sigma^0_{vegetation}$ and the backscatter from the soil below the vegetation σ^0_{soil}, which is decreased in two ways by the vegetation attenuation γ (Attema and Ulaby, 1978; Champion et al., 2000; Dabrowska-Zielinska et al., 2007) while traveling through the vegetation layer.

$$\sigma^0_{canopy} = \sigma^0_{vegetation} + \sigma^0_{soil} \cdot \gamma^2 \tag{1.1}$$

The first systematic studies of vegetation effects on radar response were done by Ulaby et al. in the 1970s. Field experiments using truck mounted radar installations were used to investigate the influences of radar parameters and terrain parameters on radar backscatter (Ulaby, 1974, 1975). Backscatter over vegetation is governed by the following radar and surface parameters (Ulaby, 1974, 1975; Bindlish and Barros, 2001):

- **Frequency**: The penetration depth depends on the frequency of the used radar signal. For lower frequencies (longer wavelengths) the sensitivity to soil moisture is higher. For higher frequencies the attenuation by the vegetation layer is higher. Above certain frequencies, radar will be mainly sensitive to the vegetation surface

(see Fig. 1.1). For a wheat canopy, X-band backscatter was found to be mainly sensitive to vegetation water content, and did not depend on soil moisture (Taconet et al., 1994). At high frequencies (C-band and up) backscatter is dominated by the crown layer. At lower frequencies (P and L-band), backscatter is dominated by woody biomass (trunks and branches), and soil moisture (Bindlish and Barros, 2001).

- **Incidence angle**: The angle under which radar is sent strongly influences the attenuation by the vegetation. For lower incidence angles, the traveled distance through the vegetation layer increases and the attenuation will be stronger (see Fig. 1.1).

- **Polarization**: Different polarizations (geometric orientation of the waves) are sensitive to different parts of the vegetation (leaves, branches, fruits, stalks, trunk). Depending on the vegetation type, the response changes for different polarizations (see Fig. 1.1).

- **Geometry and roughness of the target**: Geometry includes the shape of the vegetation, and the amount and distribution of the vegetation parts. This affects the penetration depth into the vegetation (see Fig. 1.1). Surface roughness affects the spreading of the scattering. Roughness surfaces will lead to more diffuse backscatter, whereas smooth surfaces will have more specular reflection.

- **Complex dielectric properties of the target**: The dielectric constant is the main property that determines the interaction between electromagnetic waves and the material, and determines both the magnitude and phase of the backscatter. For vegetation and soil, the dielectric constant is a function of its water content. Vegetation with higher water content will have an increased dielectric constant associated with higher direct backscatter and higher two-way attenuation (see Fig. 1.1). Similarly, surfaces with high soil moisture will have an increased contribution of the soil to total backscatter.

The surface parameters (roughness, geometry, and dielectric constant) that determine the radar response over a given area can change over time, which results in temporal variation of radar backscatter. Over vegetation areas, both the soil and vegetation dynamics impact radar backscatter. Separating the influence of soil and vegetation remains challenging. Temporal changes in plant morphology have a significant effect on radar response to vegetation, because they change water content, geometry and roughness (Ulaby et al., 1975). These variations occur on diurnal and seasonal time-scales, and can change in response to water stress.

An important factor that determines the change in parameters of a vegetated surface is the phenology. For crops, temporal variations in backscatter have been observed, which were linked to the growing stage of the plants. Ulaby et al. (1981) found clear seasonal cycles in radar backscatter over various crops. Paris (1986) showed that the temporal variation in backscatter (17 GHz, vertically polarized) displayed the onset of the reproductive stage in corn plants. Prevot et al. (1993) found that backscatter of wheat is a function of the Leaf Area Index (LAI) over a growing season. Strong temporal variations

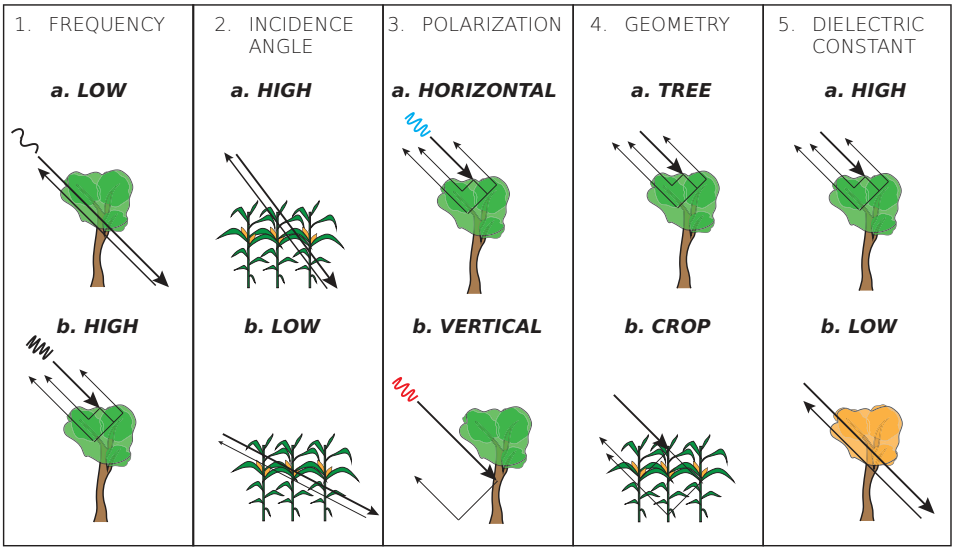

Figure 1.1: Examples of how 1. frequency, 2. incidence angle, 3. polarization, 4. geometry of the vegetation, and 5. vegetation dielectric constant influence radar backscatter. Note that the differences between the upper and lower figures are illustrative, and that the exact backscatter mechanisms are a combination of all factors. Arrows indicate the radar waves. Line width represent higher or lower radar backscatter.

of backscatter were also found over rice fields, which were related to the growing stages of the vegetation (Kurosu et al., 1995; Kim et al., 2000).

Various studies have found that backscatter increases with biomass (Ferrazzoli et al., 1992; Dobson et al., 1992; Le Toan et al., 1992). This sensitivity can saturate (backscatter does not change with changing vegetation biomass), which depends strongly on the used radar frequency (Dobson et al., 1992). Recently, ERS (European Remote-Sensing Satellite 1 and 2) backscatter, and ASCAT (Advanced Scatterometer) derived Vegetation Optical Depth (VOD) were linked to seasonal vegetation dynamics (Vreugdenhil et al., 2016a,b).

So far, we can conclude that vegetation dynamics have a significant impact on radar backscatter. However, this connection is mainly based on the vegetation growing cycle or phenology. The influence of shorter term (diurnal) variations in vegetation water status on backscatter remains largely unknown.

1.3 RELATION BETWEEN PLANT DYNAMICS AND DIELECTRIC PROPERTIES

The dielectric constant is a property describing the interaction of a material with the electromagnetic field (McDonald et al., 2002). In the microwave range, dielectric constant of water is an order of magnitude larger than dry soil or dry vegetation, and therefore the dielectric constant of vegetation material is strongly influenced by the dielectric constant of its water component (Brakke et al., 1981; Ulaby and Jedlicka, 1984). Water in

vegetation material occurs in 'free' and 'bound' form. Bound water is tightly held to organic material in the vegetation, and free water is water that can move freely within the material (El-Rayes and Ulaby, 1987; Ulaby and El-Rayes, 1987). When water content of vegetation changes, it mainly affects the amount of free water. Only after severe drying the bound water content decreases. Dielectric properties of plant materials are governed by water content, temperature, and salinity. Measurements of dielectric properties of leaves, branches and trunks have shown that dielectric constant is most dependent on water content.

The experimental data from Ulaby and Jedlicka (1984) and El-Rayes and Ulaby (1987) showed that within the 0.2 - 20 GHz range, leaves and stalks of corn and wheat plants show a similar, significant dependence on moisture content. Considerable additional work was done in the 1990s, when it was hypothesized that vegetation dielectric properties are likely to be related to the vegetation water status. McDonald et al. (1992) suggested that strong correlations may exist between dielectric constant of trees and xylem water potential, as evaporation of water occurs through the leaves. Measurements under controlled conditions showed that the xylem dielectric constant responds directly to changes in xylem water potential. After application of water to the trees, both water potential and dielectric constant in the xylem increased. Burke et al. (2005) used lab measurements of leaf dielectric constants to show the relation between relative water content and the dielectric constant. Dobson et al. (1991) found that dielectric constant of loblolly pine trunks were partially correlated to canopy layer physiological observations, such as transpiration, stomatal conductance and xylem water potential.

Also differences in temporal variation in xylem dielectric constant were observed. Although higher water content results in higher dielectric constant, the lag effects between changing water potential and dielectric constant are different (Salas et al., 1991). Zimmermann et al. (1994) measured coniferous and deciduous trees and found that although all trees showed seasonal variation, not all showed diurnal variation. Also differences were found in the lag between xylem dielectric constant and xylem sap flow. Relations between water status and dielectric properties vary between species.

Observations of vegetation dielectric properties suggest a strong relation between vegetation water status and dielectric properties. In some cases changes in water status resulted in variations in dielectric constant that are suggested to be detectable by radar.

1.4 EFFECT OF WATER STRESS ON PLANT DYNAMICS

Plants use photosynthesis to convert carbon dioxide and water into oxygen and sugar (biomass), fueled by light energy. For terrestrial plants, radiation is the main source of energy for evaporation (Steduto and Hsiao, 1998a,b). Pores on the leaf surface (stomata) allow CO_2 intake and O_2 exhaust. When stomata are opened for CO_2 intake, water transpires through stomatal aperture. Stomata play a dominant role in regulating the amount of water transpired by vegetation (Jarvis, 1976). Transpiration depends on stomatal conductance, net radiation, vapor pressure deficit (VPD), temperature and wind speed (Morison and Gifford, 1983; Jones and Tardieu, 1998). Transport of water from the soil to the atmosphere depends on the water potential gradient from atmosphere to soil, through the leaf, xylem and roots. The water potential gradients caused by transpiration induce xylem water flow, propagating from leaves to stem to roots to soil. Photosynthe-

sis is governed by leaf water status and depends on the difference between transpiration rate and water supply from soil and through the xylem (Manzoni et al., 2014). To prevent excessive water loss, plants regulate transpiration by adjusting the stomatal aperture, leading to a change in stomatal conductance (Olioso et al., 1996). Stomatal conductance varies with the balance between loss of water through transpiration and supply of water to leaf from soil (Tuzet et al., 2003). Diurnal variations in solar radiation, meteorological and environmental variations lead to diurnal patterns of leaf stomatal conductance (Ding et al., 2014).

Water stress is one of the most important environmental factors that influence plant water status, limits plant growth and production (Jiang and Zhang, 2002), and it can cause early plant death (Jones and Tardieu, 1998). In response to water deficit, transpiration is reduced with increasing water stress (Jarvis, 1976; Carlson et al., 1991). Control of transpiration is determined by stomatal aperture (Jarvis, 1976; Jones and Sutherland, 1991; Yu et al., 1998) to prevent dehydration and physiological damage (Oren et al., 1999). This enhances survival, but reduces photosynthesis and productivity. During periods of low water availability, stomatal regulation is always a trade-off between optimization of survival and production. Plants can respond to water stress through defense mechanisms (Bohnert and Jensen, 1996), which can be divided into two categories: (1) passive hydraulic and (2) active chemical mechanisms.

The hydraulic root-to-leaf system provides a passive mechanism for water stress signaling through a plant (McAdam and Brodribb, 2014). For photosynthesis, transpiration from leaves is supplied from soil through the soil-to-leaf hydraulic system. Water transport from soil to the leaves is driven by the difference in water potential between the atmosphere and leaves, approximated by VPD. If VPD becomes higher than a certain threshold value, partial cavitation of the xylem and leaf tissue occurs (Manzoni et al., 2013; Huber et al., 2014). This is either caused by an increased atmospheric water demand or an increased soil water deficit. This leads to lower turgor pressure in the leaves resulting in decreasing the pressure in the guard cells surrounding the stomata. The stomatal aperture and conductance are decreased, resulting in lower water losses.

The production and release of Abscisic acid (ABA) is an active mechanism to regulate stomatal aperture (McAdam and Brodribb, 2014). ABA is a stress hormone that is produced in the plant roots. Stomatal conductance can be controlled by soil water status via root chemical messaging of ABA, independently of leaf water potential (Davies and Zhang, 1991; Shinozaki and Yamaguchi-Shinozaki, 1997). When water stress increases, build up of ABA in roots follows, which is transported through xylem flow and regulates stomatal conductance through regulation when ABA arrives at guard cells (Davies and Meinzer, 1990; Zhang and Davies, 1990; Davies and Zhang, 1991; Tardieu et al., 1992b). Roots sense drying soil early in the drying cycle, before water deficit develops. Mild dehydration already causes ABA release by the roots into the transpiration stream, increasing xylem ABA. The concentration of xylem ABA affects stomatal aperture (Tardieu et al., 1992a; Correia and Pereira, 1995; Tardieu et al., 1996). Increased ABA therefore results in closuring of the stomata, decreasing water losses through the leaves.

How plants cope with water stress depends on whether a plant species is isohydric or anisohydric. Isohydric plants (e.g., maize, soybean) maintain daytime leaf water status through active stomatal control, regardless of soil water status (Jones and Tardieu, 1998;

Tuzet et al., 2003; Martínez-Vilalta et al., 2014). Plant water status does not depend on soil water until extreme water stress conditions (Egea et al., 2011). When leaves experience low critical water potential, partial closure of stomata prevents water potential from dropping further by reducing transpiration. Leaf water potential and content are regulated and kept higher than or equal to a certain threshold value which is higher than the permanent wilting point (i.e. when damage occurs) (Buckley, 2005; Huber et al., 2014).

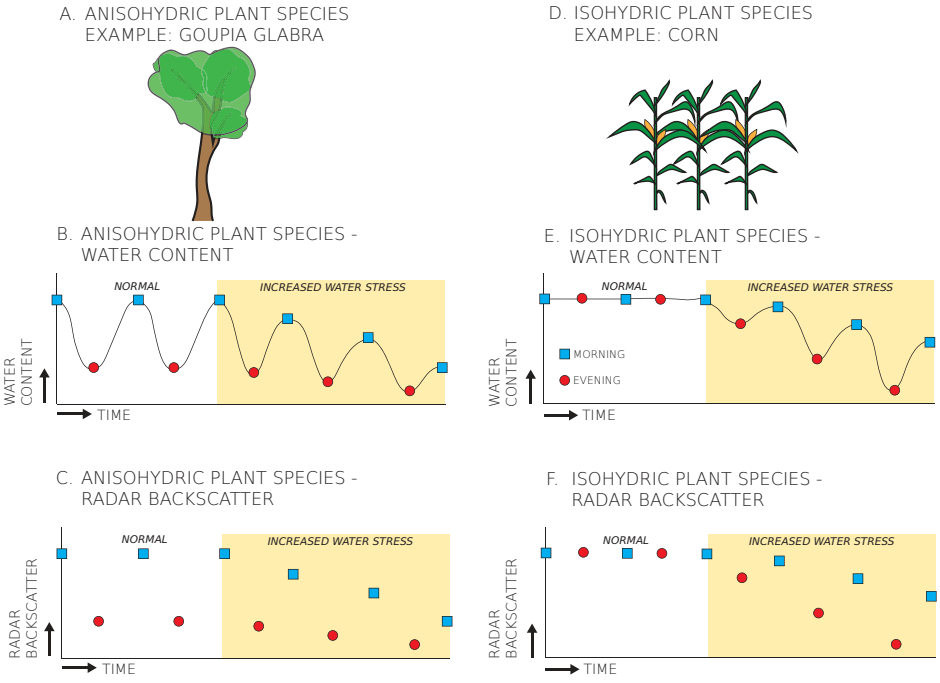

Figure 1.2: A. Example of anisohydric plant species, *Goupia glaba* tree, and illustration of B. plant water content and C. expected change in radar backscatter from the transition from normal conditions to increased water stress, and D. example of isohydric plant species, corn, and illustration of E. plant water content and F. expected change in radar backscatter from the transition from normal conditions to increased water stress.

Stomata of anisohydric plant species (e.g., sunflower, sorghum) are insensitive to changes in leaf water potential and stomata remain fully open during soil drying and higher evaporative demand (Martínez-Vilalta et al., 2014). Leaf water potential shows strong fluctuations with changes in soil water availability and transpiration rates (Buckley, 2005; Huber et al., 2014), leading to large diurnal variations in leaf water potential and leaf water content (Egea et al., 2011). In contrast to isohydric species, leaf water potential of anisohydric species tend to correlate closely with stomatal conductance (Tardieu et al., 1996; Tuzet et al., 2003). An illustration of the effect of water stress on anisohydric and isohydric plant species is presented in Fig. 1.2.

For both isohydric and anisohydric plant species, there is a direct effect of water stress on the diurnal variations in plant water status. For isohydric species, diurnal variations in water content increase with water stress. For anisohydric species, decreasing

diurnal variations are a sign of water stress. In both cases the onset of water stress can be detected from day-to-day observations of the diurnal variation in water content.

1.5 CURRENT STATE OF KNOWLEDGE

Radar backscatter over vegetated areas through direct backscatter and two-way attenuation of signal as it travels through the vegetation layer. Depending on the used radar frequency, polarization, and incidence angle, backscatter is affected by different parts of the vegetation. The backscatter and attenuation by the vegetation is primarily driven by the vegetation dielectric properties, which are in turn a function of water content. The vegetation dielectric properties are closely related to the vegetation water status. Small changes in plant moisture content can cause a significant change in dielectric properties and thus backscatter (Brakke et al., 1981). Changing diurnal variation in plant water content is a sign of water stress (Slayter et al., 1967; Hsiao, 1973). Depending on the degree of isohydricity of the plant, they either increase or decrease after the onset of water stress (Tardieu and Simonneau, 1998). Such variations have been measured in plant dynamics, as well as in trunk and xylem dielectric properties. It has been suggested that these changes are detectable by radar. If this is the case, radar might also be used for water stress detection and monitoring over vegetation surfaces.

1.6 ARE DIURNAL DIFFERENCES A SIGN OF WATER STRESS?

1.6.1 DIURNAL VARIATIONS IN DIELECTRIC PROPERTIES

Measurements have shown that the dielectric constant of xylem can change diurnally. The lowest dielectric constants were found during the highest atmospheric evaporative demand, when depletion of water in the xylem was the highest (McDonald et al., 2002). Zimmermann et al. (1995) found diurnal changes in xylem dielectric constant and water status. The lowest dielectric constant was measured in the afternoon. Salas et al. (1994) found hysteresis between diurnal variations in branch water potential and trunk sapwood dielectric constant. The dielectric properties were positively correlated with tree moisture content. These measurements suggested that diurnal variations in tree dielectric properties are related to diurnal fluctuations in tree water status. Weber and Ustin (1991) measured diurnal variation in trunk dielectric constant, which corresponded well to leaf water potential, especially in the morning. The measured lag in dielectric constant was hypothesized to be the result of gradual refilling of xylem tissue with water.

1.6.2 DIURNAL VARIATIONS IN BACKSCATTER

The earliest observations of diurnal variation in radar backscatter were reported by Ulaby et al. Ulaby and Batlivala (1976). Differences up to 2-5 dB for L- and C-band were found between morning and evening backscatter, and it was suggested that this was caused by changes in orientation of the leaves, or plant moisture content. Later observations by Brisco et al. (1990) and McDonald et al. (1990) found diurnal patterns in L-, C-, and Ku-band. McDonald et al. (1990) observed and modeled diurnal variation in backscatter. At the same time, diurnal variation in canopy dielectric properties were measured, which have a direct effect on backscatter. Brisco et al. (1990) found that the diurnal variation was evident for all used frequencies, although the effect of L- and C-band was different.

This was attributed to the increased geometric effect of the vegetation canopy at higher frequencies.

Birrer et al. (1982) were the first to report diurnal variations in space-born radar backscatter. Radar response over the Amazon rainforest was studied to determine the suitability as a standard calibration target for scatterometers, and a large homogeneous region would be an ideal solution. However, it was found for the SeaSat scatterometer that morning measurements were 0.5 - 1 dB higher than measurements at any other time of the day.

Satake and Hanado (2004) found diurnal variation in TRMM backscatter of 0.5 dB, with the highest daily value around 6 A.M. They suggested three explanations for the observed diurnal variations: (1) changes of water vapor in the air, (2) changes of dew on the leaves, and (3) changes of vegetation water status. Changes in water vapor were estimated to attenuate the backscatter by 0.1 dB at most. A crude model was used to test whether dew could explain the diurnal cycle. By assuming only small variations in vegetation water status, it was suggested that dew caused the observed diurnal variations in backscatter. However, no field data on vegetation water status, or dielectric properties were available.

Frolking et al. (2006) studied the sensitivity of K_u backscatter to vegetation dynamics by comparing QuikScat backscatter to MODIS derived LAI. Using data for non-frozen periods from 2000 to 2002, they demonstrated that the backscatter response to growing season canopy dynamics. A later study by Frolking et al. (2011) compared 10 years of QuikScat backscatter to an expression of water deficit anomalies using TRMM precipitation estimates. Strong negative anomalies were found in morning overpass backscatter and water deficit anomalies during the dry season. It was hypothesized that the dry season reduction in backscatter was due to changes in water status of the canopy. Dew was not considered as a plausible explanation, as the anomalies in morning backscatter and water deficit anomalies also corresponded to a reported increase in tree mortality during this period. Yet, no field data of tree water status was available to confirm the sensitivity of backscatter to canopy water content.

More recently, Jaruwatanadilok and Stiles (2014) analyzed 10 years of QuikScat backscatter to investigate trends in backscatter at potential calibration targets. It was found that backscatter over tropical forests such as the Amazon are very stable and homogeneous on longer time scales. However, backscatter was also found to consistently show diurnal variations, which corresponds to the expectations that morning backscatter is higher due to increased vegetation moisture content.

Crucial work that led to the hypothesis that radar backscatter is sensitive to vegetation water stress was done by Friesen (2008) and Friesen et al. (2007, 2012). Friesen et al. (2007) observed diurnal differences in ERS 1/2 C-band backscatter up to 1 dB over West Africa. It was found that the patterns shift temporally in accordance with the transition from wet to dry seasons. Because of the absence of any additional data, five possible explanations were given for the diurnal differences: (1) diurnal variation in vegetation water content, (2) diurnal variation in water stored on the leaves and topsoil due to diurnal rainfall patterns, (3) diurnal variation in soil moisture, (4) azimuthal anisotropy and (5) diurnal differences in Bragg scatter from open water.

Not all explanations were considered as likely to explain the observed diurnal varia-

tions in backscatter. Diurnal variation in rainfall or dew would only explain diurnal differences in the wet/rainy season, and not the observed diurnal differences in backscatter in other times of the year. Although soil moisture varies over the day, the regional patterns in soil moisture did not correspond to the observed patterns in backscatter. On the other side, Bragg scatter by wind might be relevant as the diurnal variation of wind speed is significant in West Africa. Azimuthal anisotropy due to changes in structural features of the surface can have an effect of 1-5 dB. Finally, it was found that the region with the largest diurnal variation backscatter had trees that are subject to limiting soil moisture, influencing vegetation water content significantly.

Using regional vegetation modeling, Friesen (2008) investigated the diurnal plant water fluxes, which showed that diurnal variations in tree water status can be the main cause of the observed diurnal variation in backscatter. The diurnal variation in backscatter coincided with the onset of water stress over West Africa. The largest diurnal differences were found during the dry season, which ruled out interception, dew, or topsoil as drivers over diurnal variation in backscatter. It was also found that the greatest differences were found in areas with the presence of vegetation, shortly after the rainy season (Friesen et al., 2012), at the onset of the dry season.

To test diurnal variation vegetation water status as explanation of the observed diurnal differences in radar backscatter, Steele-Dunne et al. (2012) modeled the sensitivity of L- and C-band backscatter to changing vegetation water content. Using the Michigan Microwave Canopy Scattering Model (MIMICS, (Ulaby et al., 1990)), it was demonstrated that during periods of low soil moisture availability, radar backscatter is sensitive to changes in vegetation water content. Results for L- and C-band suggest that observed diurnal variation in backscatter can be caused by diurnal variation in vegetation dielectric properties.

Recently, the non-sun-synchronous RapidScat mission was used to identify diurnal changes in backscatter globally (Paget et al., 2016; Madsen and Long, 2016). Over some areas, such as the Amazon and the Congo, the changes in backscatter can be correlated with vegetation. This supports the theory of the sensitivity of backscatter to changing vegetation moisture content in e.g. the Amazon and Congo regions (Paget et al., 2016). Diurnal variations in RapidScat backscatter over Central African forests also demonstrate seasonal variation, that are consistent with patterns in stomatal closure in this region (Konings et al., 2017). However, only in situ observations of moisture content, dielectric properties and backscatter can determine whether diurnal variation in backscatter is affected by vegetation water stress.

1.7 THIS THESIS: TESTING THE HYPOTHESIS

From previous work it is clear that vegetation water status and dielectric properties are affected by water stress. At the same time, significant changes in diurnal variations of radar backscatter have been found. All fingers point in the direction of vegetation as the explanation for these observations. This thesis therefore aims to test the hypothesis that:

- Vegetation water stress has an observable effect on radar backscatter

This thesis studies the missing link between vegetation water content, dielectric properties and radar backscatter, in response to water stress. To test the hypothesis that radar backscatter is sensitive to vegetation water stress, ground measurements of vegetation water status, and dielectric properties, in combination with backscatter are required. First, this thesis focuses on measuring the vegetation response to water stress at the field scale by developing and employing sensors to measure dielectric properties, and mass variations of vegetation in vivo. Second, ground measurements of the vegetation response to water stress are linked to radar response on field and forest scale.

The hypothesis that water stress affects radar backscatter is tested in two different ecosystems. The first half of this thesis focuses on agricultural canopies. Water stress in crops leads to decreased biomass production and plant death. Early detection of water stress might therefore be useful to optimize irrigation strategies, and increase food security. The second half focuses on tropical forests in the Brazilian Amazon. The Amazon rainforest has a significant influence in the global water and carbon cycle. Yet, the effects of water stress are poorly understood. Water stress detection and monitoring will therefore give new insights in the dynamics and extent of drought in the Amazon, and its broader impact on the water and carbon cycle.

1.8 HOW TO READ THIS THESIS

Chapters 2 to 4 focus on agricultural canopies. Chapter 2 presents a controlled experiment on a greenhouse grown tomato canopy. This experiment was used to test and demonstrate a novel sensor that allows in vivo measurements of leaf dielectric properties. Measurements were done on plants with and without water stress, to allow demonstrating differences in leaf dielectric properties.

Chapter 3 discusses dielectric properties measurements under field conditions. In this chapter, results from two measurements campaigns on corn canopies are presented. One campaign was done on a corn canopy with water stress, and one campaign on a corn canopy without water stress. This chapter shows the effect of water stress on variations in dielectric properties at individual corn leaves.

Chapter 4 links the measured changes in vegetation water content of a corn canopy in response to water stress to modeled radar backscatter. A sensitivity study was performed to demonstrate the response of radar backscatter to changes in VWC during a period of low soil moisture availability. Radar backscatter time series were modeled to show the change in diurnal variation in backscatter in response to vegetation water stress.

Chapters 5 to 7 focus on tropical forests. Chapter 5 demonstrates a new concept of using accelerometers to measure tree properties and responses. Accelerometers measure tree sway, which is sensitive to mechanical tree properties. Using five months of tree acceleration data, collected on 19 trees, it is shown that tree acceleration is sensitive to tree mass, precipitation intercepted by the canopy, and canopy-atmosphere turbulent exchange.

Chapter 6 uses tree accelerometer data to study the spatiotemporal variation in tree-atmosphere interaction across Amazon trees. A time series of tree-atmosphere interaction during the transition from the wet to the dry season is presented, showing the response to increased tree water deficit.

Chapter 7 links simultaneous ground measurements of tree water status to RapidScat radar backscatter over the Amazon rainforests. Data of a nine-month period is used to demonstrate the effect of changing tree water status on the diurnal variation in backscatter. An additional analysis is presented that demonstrates the effect of increased tree water deficit on morning radar backscatter.

Finally, Chapter 8 presents the conclusions of this thesis, and provides an outlook to future research directions.

2

A Comparison Between Leaf Dielectric Properties of Stressed and Unstressed Tomato Plants

Knowledge is knowing that a tomato is a fruit.
Wisdom is not putting it in a fruit salad

Miles Kington

Leaf dielectric properties influence microwave scattering from a vegetation canopy. The dielectric properties of leaves are primarily a function of leaf water content. Understanding the effect of water stress on leaf dielectric properties will give insight in how plant dynamics change as a result of water stress, and how radar can be used for early water stress detection over agricultural canopies.

This chapter presents in-vivo *measurements of leaf dielectric properties. Different relationships between leaf water content and leaf dielectric properties were found for tomato leaves at various heights. The dielectric properties of live stressed and unstressed tomato plants were measured during a controlled, two-week experiment. A clear difference was found between the leaf dielectric properties of stressed and unstressed leaves, which can be attributed to increase in water stress.*

The results show changes in plant dynamics due to water stress lead to a difference in leaf dielectric properties between stressed and unstressed plants.

Parts of this chapter have been published in the Proceedings of the Geoscience and Remote Sensing Symposium (IGARSS), 2015 IEEE International, (van Emmerik et al., 2015a)

2.1 INTRODUCTION

This chapter presents observations of leaf dielectric properties of stressed and unstressed tomato plants in the field. The vegetation dielectric properties are a crucial factor that determines the interaction of a canopy with electromagnetic waves. Dielectric properties of individual vegetation components (e.g., leaves, branches, stems, fruit) are therefore an important driver of the impact of vegetation on microwave emission and scattering.

Vegetation dielectric properties depend on e.g., salinity and temperature (Nelson, 1991; Ulaby and Jedlicka, 1984), but are primarily a function of water content (Nelson, 1991). Recent studies have shown that microwave scattering at various frequencies, polarizations and incidence angles, radar backscatter from forest (Steele-Dunne et al., 2012) canopies is mainly sensitive to leaf water content, especially during times of water stress. However, behavior of leaf dielectric properties in response to changes in leaf water content and water stress is still poorly understood. This is mainly caused by the lack of *in-vivo* measurements of the dielectric properties (El-Rayes and Ulaby, 1987; Steele-Dunne et al., 2012).

Previous studies have investigated the dielectric properties of vegetation, see for example Nelson (1991); Ulaby and Jedlicka (1984); El-Rayes and Ulaby (1987). However, this has mainly been done using destructive sampling or *in-vivo* on tree trunks (McDonald et al., 1999, 2002), but not on leaves. *In-vivo* measurements of leaf dielectric properties should give insight in the effect of changing leaf water content and water stress on leaf dielectric properties. Leaf water content is related to the amount of water present in the soil. However, this relation can be different for various types of crops (Tardieu and Simonneau, 1998; Sade et al., 2012).

Detailed *in-vivo* measurements of the leaf dielectric properties will give insight in response of dynamics of different plant species to water stress, allowing further study of how water stress affects radar backscatter. During a two-week experiment, leaves of both a stressed and unstressed tomato plant were measured throughout per day. Water stress was induced by switching off water supply for one row of tomato plants, while irrigation continued for the other. The goals of this chapter are to (1) determine the relationship between the sensor response and leaf moisture content, and (2) identify the effects of water stress on leaf dielectric properties of tomato plants.

2.2 METHODS

2.2.1 STUDY SITE AND PLANT MATERIAL

The experiment for this chapter was conducted in the greenhouses at the Wageningen University and Research Center Glastuinbouw, located in Bleiswijk, Zuid-Holland, The Netherlands. Measurements were conducted from November 10 to 22, 2014. All measurements were done on tomato plants (*Solanum lycopersicum*, Tomimaru Muchoo), sown on May 1, 2014 and planted on June 20, 2014 in rock wool After the emergence of the 8th cluster of fruit, the head of the plant was cut to prevent further growth. Measurements were done in the mature stage of the plant, when all fruits were fully developed. Temperature, relative humidity, CO_2 concentration, and irrigation was all regulated throughout the cultivation of the plants. Each tomato plant had an individual drip

irrigation nozzle.

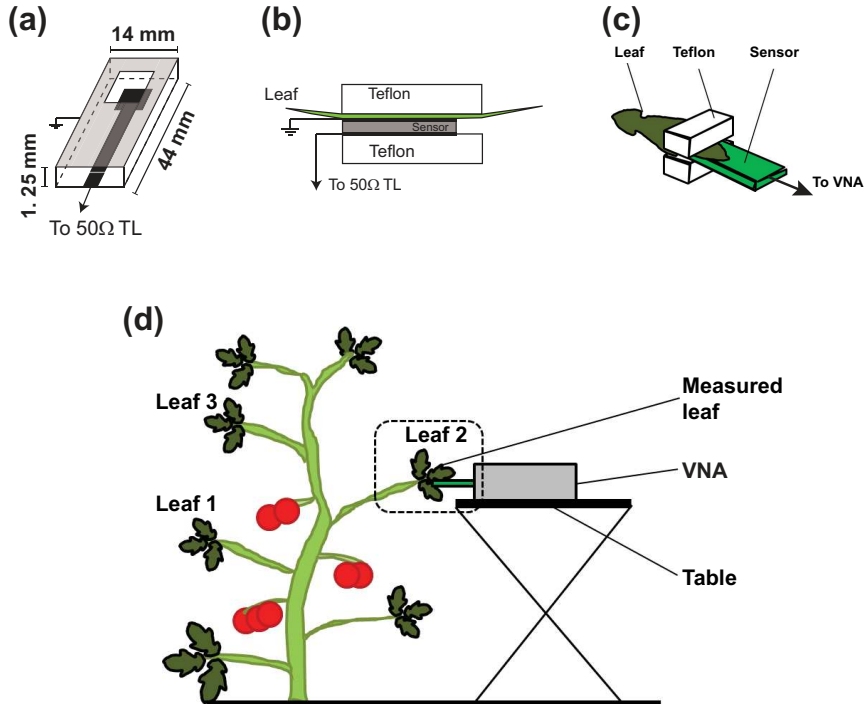

Figure 2.1: (a) Microstrip line resonator used for Δf_r measurements, (b) illustration of leaf sample placement, (c) 3D schematic of the sensor setup for a measurement, and (d) measurement set-up. Note that the leaves are numbered from the bottom upwards.

2.2.2 DIELECTRIC PROPERTIES MEASUREMENTS

Fig. 2.1(a) shows the sensor, a microstrip line resonator (44mm x 14mm x 1.25mm) which senses the leaf through a "sampling window" (9mm x 9mm), cut in the ground plane. Teflon blocks (1cm x 4cm x 3cm) are placed under the sensor and on top of the leaf (Fig. 2.1(b)) to ensure that environmental effects are limited to those of a known dielectric constant, and that the leaf is held in place against the sensor with a constant pressure. The sensor was directly attached to Port 1 of a ZVH8 Cable and Antenna Analyzer (ZVH8, 100kHz to 8GHz, Rohde & Schwarz, München, Germany) with the K42 Vector Network Analysis and K40 Remote Control options. For each measurement, the magnitude (dB) of the reflection coefficient S_{11}, which depends on the dielectric constant of the sample, was measured at 1201 frequencies over a predefined range. The resonant frequency f_r is the frequency at which the magnitude of $S11$ is at a minimum. An increase in the real part of the dielectric constant of the sample leads to a decrease in the resonant frequency, f_r.

For wet leaves the dielectric constant is high (El-Rayes and Ulaby, 1987), f_r is lower, and the dip in the signal is sharper. For drier leaves the dielectric constant is lower, lead-

ing to a higher f_r and a shallower dip in the signal. As the leaf dries out, the difference in f_r between the leaf and the Teflon block decreases, due to a decreasing dielectric constant of the leaf. In the subsequent figures and analysis, this difference in f_r will be referred to as Δf_r [GHz]. A high value of Δf_r corresponds to a high value of the dielectric constant of the leaf, and a low Δf_r corresponds to a low dielectric constant. The moisture content of single scatterers (leaves) is expressed here in terms of gravimetric moisture because it is used in the dual-dispersion model (Ulaby and El-Rayes, 1987), as well as models in which dielectric properties of individual scatterers are required (e.g. MIMICS (Ulaby et al., 1990)).

2.2.3 CALIBRATION EXPERIMENT

The relationship between Δf_r and leaf gravimetric moisture content M_g depends strongly on the species. A calibration experiment was performed to establish the relationship between the M_g and Δf_r for the measured tomato plants. This was done by taking dielectric measurements of a drying leaf. First one measurement was done when the tomato leaf was attached to the plant. Then, the leaf was cut, measured, weighed, air-dried and measured again. This was repeated for 12 values of M_g. After a dielectric measurement, the leaf was weighed to determine the fresh mass. Finally, the leaf was dried in an oven at 70 °C for 24 hours and weighed again to determine the dry mass. The gravimetric moisture content was calculated using Ulaby and Jedlicka (1984):

$$M_g = \frac{M_w - M_d}{M_w} \tag{2.1}$$

where M_w and M_d are the fresh and dried leaf weights.

2.2.4 DIELECTRIC PROPERTIES TIME SERIES

For one row of plants, all irrigation nozzles were removed on November 10, 2014 at 9 A.M. For the other row, irrigation continued throughout the experiment. *In-vivo* measurements were taken five times per day (7 A.M., 9 A.M., 11 A.M., 1 P.M., 3 P.M.). At the same time, volumetric moisture content was determined by taking the mean value of 3 measurements along the row. From 10 to 15 November the dielectric properties of an individual irrigated and non-irrigated plant were measured. From 17 to 22 November, another individual irrigated and non-irrigated plant were measured. For every plant, three leaves at different heights were measured, see Fig. 2.1d. The time series were tested on the presence or absence of trends by calculating Spearman's correlation coefficient Gauthier (2001). For the two separate weeks, the correlation coefficient was determined of both the stressed and unstressed time series. A trend was considered present if the confidence level was higher than 80%.

2.3 RESULTS AND DISCUSSION

2.3.1 CALIBRATION EXPERIMENT

Fig. 2.2 presents the results of the calibration experiment for leaf 1, 2 and 3. For every leaf, a different relationship was found between leaf moisture content M_g and Δf_r. Leaf 1 and 2 have a similar relationship, but leaf 3 shows that Δf_r is generally lower. Δf_r

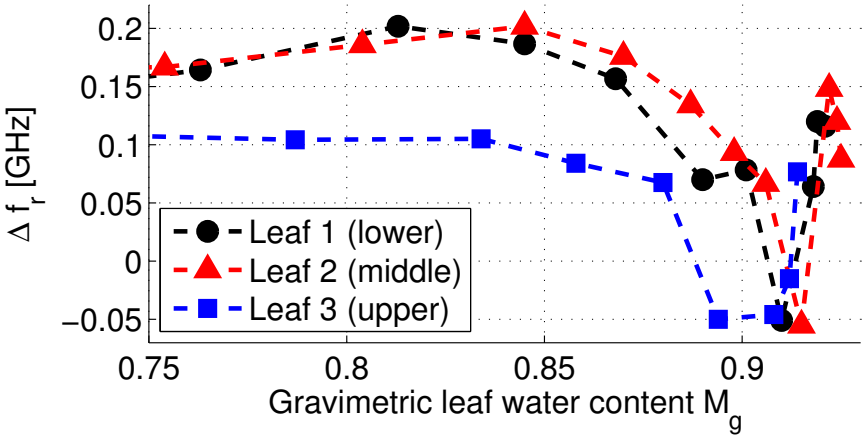

Figure 2.2: Relationship between M_g and Δf_r for three leaves: the lower leaf 1 (black circles), the middle leaf 2 (red triangles) and the upper leaf 3 (blue squares).

first decreases with decreasing water content. If the leaf water content drops below 0.92, the resonant frequency increases steeply. For leaf water content below 0.75, Δf_r is insensitive to changes in M_g. It can be seen that for tomato leaves, the relation between M_g and Δf_r is non-monotonic, since the same Δf_r values were measured for M_g values between 0.86 and 1. This is related to the drying mechanism of the leaves. If leaves dry out without further changes to the structure or salinity, one can expect a monotonic relation between M_g and Δf_r. The non-monotonic relation for tomato leaves might indicate that when leaves dry out, the structure or salinity is also changed, in addition to the water content.

2.3.2 SOIL MOISTURE

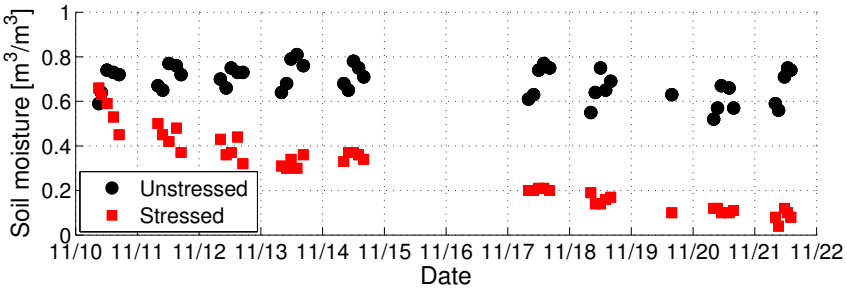

Figure 2.3: Volumetric soil moisture measured at the irrigated (black squares) and non-irrigated (red dots) tomato plants.

Fig. 2.3 presents the soil moisture measured at the irrigated and non-irrigated tomato plants. The soil moisture measurements showed a clear difference between the irrigated

and non-irrigated plants. On average, the soil moisture was 0.75 for the irrigated row. Soil moisture at the non-irrigated row dropped directly after irrigated was withheld. After two weeks, soil moisture was lower than 0.1.

2.3.3 LEAF DIELECTRIC PROPERTIES TIME SERIES

Table 2.1: Confidence boundaries for the presence or absence of trends in resonant frequency difference between leaf and Teflon Δf_r and leaf gravimetric moisture content M_g for the stressed and unstressed tomato plants, calculated using Spearman's Rank Coefficient. Positive and negative signs indicate an increasing or decreasing trend, respectively. A (-) indicates no trend was observed. Confidence boundaries were tested for the complete period (November 10 - 21), and for the first (November 10 - 15) and second week (November 16 - 21) separately

Leaf No.	Stressed		Unstressed	
	Δf_r	M_g	Δf_r	M_g
	November 10 - 21 (complete period)			
1	0.99	-0.99	0.86	-0.82
2	0.83	-0.97	-	-0.87
3	0.98	-0.98	-	-
	November 10 - 15 (1st week)			
1	-	-	-	-
2	0.84	-	-	-0.84
3	-	-	-	-
	November 16 - 21 (2nd week)			
1	-	-	-0.84	-
2	0.98	-	-	-
3	0.99	-	-0.98	-

Fig. 2.4 (a)-(c) show the leaf water content M_g for leaves 1 to 3. For both the stressed and unstressed plants, M_g appears stable over time. In the second week M_g of the stressed plant is visibly lower than for the unstressed plant. In Table 1 it can be seen that for the stressed plants, all leaves showed a strong decreasing trend. The unstressed plant showed a weak decreasing trend in leaves 1 and 2.

Fig. 2.4 (d)-(f) shows the difference in resonant frequency between leaf and Teflon Δf_r for leaves 1 to 3. All stressed leaves show an increasing trend in Δf_r. For the unstressed plant, only the first leaf shows a weak increasing trend (Table 1). In the first week the values of the stressed and unstressed plant are similar and no trend was observed in both the irrigated and non-irrigated plant. The rock wool contained sufficient water for root water uptake by the non-irrigated plant.

In the second week Δf_r of the stressed and unstressed leaves diverge. Δf_r of stressed leaves is higher than the unstressed leaves, and also strong increasing trends were observed in leaves 2 and 3, while for the unstressed plants only decreasing trends were found for leaves 1 and 3. The calibration (Fig. 2.2) showed that for Δf_r below 0.85, an increasing Δf_r corresponds to a drier leaf. From November 11 to 22, Δf_r is higher for the stressed leaves than for the unstressed, indicating a lower leaf water content. This is consistent with the lower measured M_g for stressed leaves. From the measurements it is

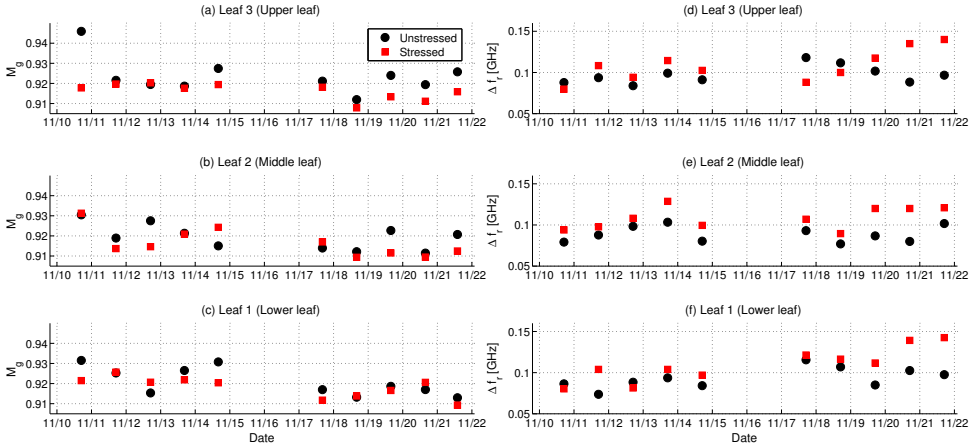

Figure 2.4: Gravimetric leaf moisture content M_g of (a) leaf 3 (upper leaf), (b) leaf 2 (middle leaf) and (c) leaf 1 (lower leaf), and the difference in resonant frequency between leaf and Teflon Δf_r of (d) leaf 3 (upper leaf), (e) leaf 2 (middle leaf) and (f) leaf 1 (lower leaf). M_g and Δf_r of the unstressed plants are shown as black dots, the stressed plants as red squares.

clear that water stress leads to different dynamics in the leaves. Both M_g and Δf_r in the stressed leaves show different trends than the unstressed plants.

Note that the measurements took place in mid-November, during days on which the incoming radiation was around 10 % of typical summer values. Also, the plants were restrained from growing further and all fruits were developed. The photosynthetic activity was therefore most likely very low, leading to low transpiration, and hence water loss rates. Even during these times of low plant activity a difference in Δf_r was found. In case a similar experiment would be done in the vegetative or early reproductive stage (fruits are developing), the effects of water stress would probably be noticeable not only earlier, but also to a greater extent.

2.4 CONCLUSIONS

Measurements using a microstrip line resonator were used to show that the dielectric properties of tomato leaves are affected by (mild) water stress.

Considerably different trends in leaf water content M_g and Δf_r were observed for stressed and unstressed tomato plants, suggesting a similar difference in leaf dielectric constant. This shows that the impact of water stress on plant dynamics results in dynamics in leaf dielectric properties.

In this chapter, we show the difference in dielectric properties between irrigated and non-irrigated tomato plants as a result of water stress. This is a first step in the development of a better understanding of the relation between water stress, leaf water content, and leaf dielectric properties. In the next chapter, the presented method for measuring leaf dielectric properties *in-vivo* is used under field conditions on a corn canopy to study the effect of vegetation water stress.

3

Dielectric Response of Corn Leaves to Water Stress

Rain makes corn,
Corn makes whisky,
Whisky makes my baby,
Feel a little frisky

Luke Bryan

Radar backscatter from vegetated surface is sensitive to direct backscatter from the canopy, and two-way attenuation of the signal as it travels through the canopy. Both mechanisms are affected by the dielectric properties of the individual elements of the canopy, which are primarily a function of water content. Leaf water content of corn can change considerably during the day and in response to water stress, and model simulations suggested that this significantly affects radar backscatter. Understanding the influence of water stress on leaf dielectric properties will give insight into how the plant water status changes in response to water stress, and how radar can be used to detect vegetation water stress. We used a microstrip line resonator to monitor the changes in its resonant frequency at corn leaves, due to variations in dielectric properties. This study presents in vivo resonant frequency measurements during field experiments with and without water stress, to understand the dielectric response due to stress. The resonant frequency of the leaf around the main leaf of the stressed plant showed increasing diurnal differences. The dielectric response of the unstressed plant remained stable. This study shows the clear statistically significant effect of water stress on variations in resonant frequency at individual leaves.

Parts of this chapter have been published in IEEE Geoscience and Remote Sensing Letters, 14 (1), 8–12 (van Emmerik et al., 2017c).

3.1 INTRODUCTION

This study is motivated by the potential use of radar for early water stress detection in agricultural canopies. Radar backscatter is sensitive to vegetation because of the direct backscatter from the canopy itself, and two-way attenuation of the signal as it travels through the canopy. Both mechanisms are affected by the dielectric constant, architecture, shape and orientation of all individual scattering elements (leaves, branches, stem, fruits) within the canopy. In turn, the dielectric properties of these individual scatterers are primarily a function of water content, but also depend on salinity (Nelson, 1991) and temperature (Ulaby and Jedlicka, 1984). Whether radar backscatter is sensitive to changes in the dielectric properties of certain individual elements depends on the radar frequency, polarization and incidence angle.

Water content in vegetation changes on a diurnal and seasonal scale. Several studies have reported diurnal differences in radar backscatter due to water stress (Frolking et al., 2011; Friesen et al., 2007; Friesen, 2008; Friesen et al., 2012). Recent studies on tree and corn canopies have demonstrated that during periods of low soil moisture availability, total radar backscatter is mainly sensitive to changes in leaf water content. A modeling study using the Michigan Microwave Canopy Scattering Model (MIMICS, (Ulaby et al., 1990)) showed that total C-band backscatter from a forest canopy is sensitive to the water content of leaves and trunks, especially when at the onset of water stress (Steele-Dunne et al., 2012). This study highlighted the significant influence of leaf water content on radar backscatter during water stress.

Water stress influences plant water dynamics, and might cause early plant death (Jones and Tardieu, 1998). To prevent excessive water loss and physiological damage, plants regulate transpiration by adjusting the stomatal aperture (Jarvis, 1976). Stomatal closure is the result of hydraulic signalling from the roots to the leaves, and an increase of the stress hormone Abscisic acid (ABA) (McAdam and Brodribb, 2014), which is transported through xylem flow and regulates stomatal conductance (Tardieu et al., 1992b).

It remains unclear how hydrological and plant physiological signatures of water stress affect radar backscatter. A better understanding of how dielectric properties of individual scattering elements, individual leaves in particular, change in response to water stress gives more insight in how radar can be used for water stress detection. Unfortunately, few datasets on *in vivo* leaf dielectric properties are available (Steele-Dunne et al., 2012). Previous studies have investigated the dielectric properties of vegetation, but most studies focused on tree trunks McDonald et al. (2002), or used *in vivo* methods that were not suited for leaves (Way et al., 1991). However, measurements presented in Chapter 2 showed a significant dielectric response of tomato leaves to water stress in a greenhouse. In current radar backscatter models and soil moisture algorithms vegetation is often modeled as a homogeneous layer (Attema and Ulaby, 1978) or as a combination of individual scattering elements (Ulaby et al., 1990) with equal moisture content.

This study uses *in vivo* measurements made during two field experiments with a microstrip line resonator, the resonant frequency of which depends on the dielectric constant of the sampled leaf. The first experiment was done on a corn canopy without plant water stress. During the second experiment, water stress was induced by withholding irrigation. The objective of this study is to understand the dynamics of resonant frequency variation in response to changing dielectric constant of individual leaves, induced by

water stress and plant development.

3.2 METHODS

3.2.1 DIELECTRIC RESPONSE MEASUREMENTS

All measurements were done using the microstrip line resonator measurement setup as presented in Chapter 2. Fig. 3.1 shows the leaf numbering used for the corn leaf measurements. Note that leafs are numbered starting at the lowest leaf. Fig. 3.2 shows the reflection coefficient S_{11} between 3.3 and 3.8 GHz for a typical background measurement of the Teflon blocks, and two measurements of single corn leaves with high and low gravimetric water content (Ulaby and Jedlicka, 1984), defined as:

$$M_g = \frac{M_w - M_d}{M_w} \tag{3.1}$$

where M_w and M_d are the fresh and dried leaf weights. Fig. 3.2b shows the relationship between Δf_r and M_g for individual leaves from a corn canopy. When leaves are measured as the plant dries down, the decrease in M_g clearly results in a decrease in Δf_r. During both field experiments, the resonant frequency was measured at both sides of the middle of the leaf.

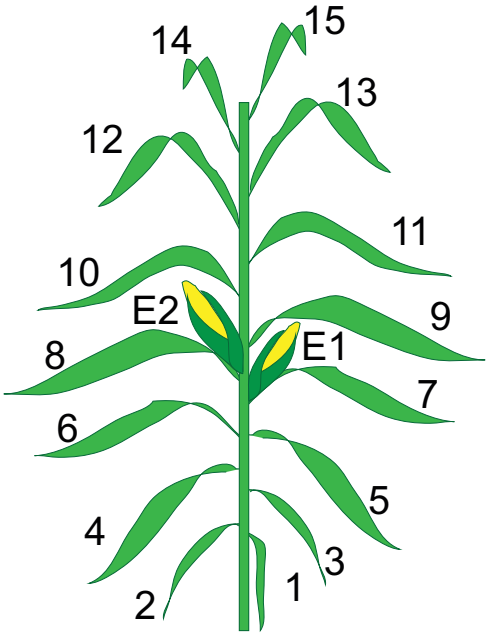

Figure 3.1: Schematic figure of a corn plant including leaf and ear numbering.

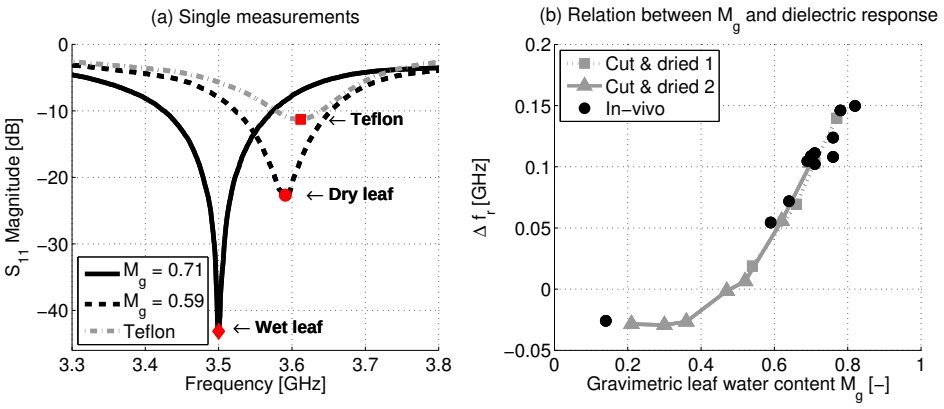

Figure 3.2: (a) Measurements of a Teflon block, a wet leaf, and a dry leaf, showing the shift in resonant frequency f_r associated with the change in the real part of the dielectric constant of the leaf, and (b) a relation between Δf_r and M_g, obtained by measuring a leaf before cutting (*in vivo*), and after (Cut & dried) cutting.

3.2.2 UNSTRESSED FIELD MEASUREMENTS

Unstressed field measurements were done on a rain fed corn field from July 8 to September 6, 2013 (DOY 189 to 249) near Zeewolde, The Netherlands (52.36°N, 5.54°E). Field corn (100-day growing period) was planted on a site of 100 m x 100 m, with a row spacing of 0.7 m, a plant density of 6.6 plants per meter and a clay soil. This study uses observations of the late vegetative, reproductive and mature stages of corn (DOY 211 to 220). The plants had a mature average height of 2.20 m, fifteen leaves and two ears, located at leaves 7 and 9. No irrigation was applied during the experiment. Precipitation was measured using a HOBO weather station (Onset Computer Co., Bourne, MA, USA). Soil moisture profiles were measured at 0.1, 0.2, 0.4 and 0.8 m, using EC-5 soil moisture sensors (Decagon Devices, Inc., Pullman, WA, USA) with a measurement interval of 15 min.

The influence of water stress on bulk vegetation water content was determined using destructive vegetation samples every morning and evening. VWC is used here because it is used to describe the moisture content of the canopy in the water-cloud model (Attema and Ulaby, 1978). To determine total, leaf, and stem VWC, one corn plant was cut, weighed with leaves, stems, and ear separated, dried in a 70°C oven for 48 (leaves) or 120 hours (stems and ears), and weighed again. VWC values of leaves and stems were determined from the fresh and dry masses (M_w and M_d), using:

$$VWC = \eta[(M_{w,l} - M_{d,l}) + (M_{w,s} - M_{d,s})] \tag{3.2}$$

where η is the number of plants/m^2, and the superscripts l and s indicate leaves and stems. Resonant frequency measurements were made between 3.1 and 4.1 GHz at 6 A.M. and 6 P.M., immediately preceding the destructive vegetation sampling. Between DOY 211 and 220, leaves 1 to 12 were measured, and measurements were taken every day. Trends were calculated for the total data series, A.M. measurement, P.M. measurements, and the diurnal difference (P.M. - A.M.), using Spearman's correlation coefficient,

expressed as confidence boundaries. Only values higher than 0.9 were considered statistically significant trends.

Note, from Fig. 3.2a, that Δf_r is related to the gravimetric moisture content of an individual leaf, and not to the bulk moisture content of the canopy. Unfortunately, M_g data is not available for the field trial described here.

3.2.3 STRESSED FIELD MEASUREMENTS

Fieldwork during a period of increased vegetation water stress was conducted near Citra, FL (29.41°N, 82.18°W), as part of the MicroWEX-11 experiment (Bongiovanni et al., 2015) from April 25 to December 9, 2012 (DOY 115 to 343). Sweet corn (78-day growing period) was planted on a site with a sandy soil of 183 m x 183 m, 1 m row spacing and plant density of five plants per meter. This study used observations during the late vegetative and reproductive periods (DOY 281 to 292). Water stress was induced by withholding irrigation at the vegetation sampling location. The corn plants had an average mature height of 1.8m, twelve leaves and one ear, located at leaf 8. Precipitation data was obtained from the Florida Automated Weather Network (FAWN). The soil moisture profile was measured at six depths of 0.02m, 0.04m, 0.16m, 0.32m, 0.64m and 1.2m at the site using Campbell Scientific CS616 time-domain water content reflectometers (Campbell Scientific, Inc., Logan, UT, USA). From DOY 281 to 292, daily destructive samples were taken at 6 A.M. and 6 P.M.. To determine total leaf and stem water content, two corn plants were cut, weighed with leaves and stems separated, dried in a 70°C oven for 48 and 120 hours, respectively, and weighed again. Resonant frequency measurements were made between 2.1 and 4.1 GHz from DOY 281 to 292, at 6 A.M. and 6 P.M., immediately preceding the destructive vegetation sampling. All measurements were performed on the same corn plant throughout the experiment.

3.3 RESULTS

3.3.1 UNSTRESSED FIELD MEASUREMENTS

Fig. 3.3(a) shows the precipitation and root zone soil moisture in the unstressed canopy. Although only few rainfall events occurred during the measured period, the root zone soil moisture remained high (0.4 - 0.45 m^3/m^{-3}). Fig. 3.3(b) and (c) present the total stem and leaf water content. Stem water content decreased gradually during the reproductive phase. Leaf water content is constant after DOY 211. Fig. 3.4 (a)-(c) present the differences in resonant frequency (Δf_r) of leaves 7, 9 and 11. Δf_r is stable for all three leaves, and only for leaf 7 diurnal variations were observed. From DOY 211 to 214, the 6 A.M. values were higher than the 6 P.M. values. Table 1 presents the trends in Δf_r. Leaf 7 shows an increasing trend in the P.M. values, and leaf 9 shows positive trends in the total, and in the A.M. data. During measurement period, the plant was still in the vegetative stages, which led to an increased leaf water content (and hence dielectric constant) in the leaves around the ears (leaf 7 and 9). Lab measurements found the instrument error to be 0.001 GHz, and the reproducibility error, defined as the error when moving and reapplying the sensor to be 0.009 GHz. Both errors were significantly smaller than the observed diurnal differences of Δf_r at leaf 7 (0.04 GHz) and the total change of Δf_r at leaf 7 and 9 (0.05 GHz).

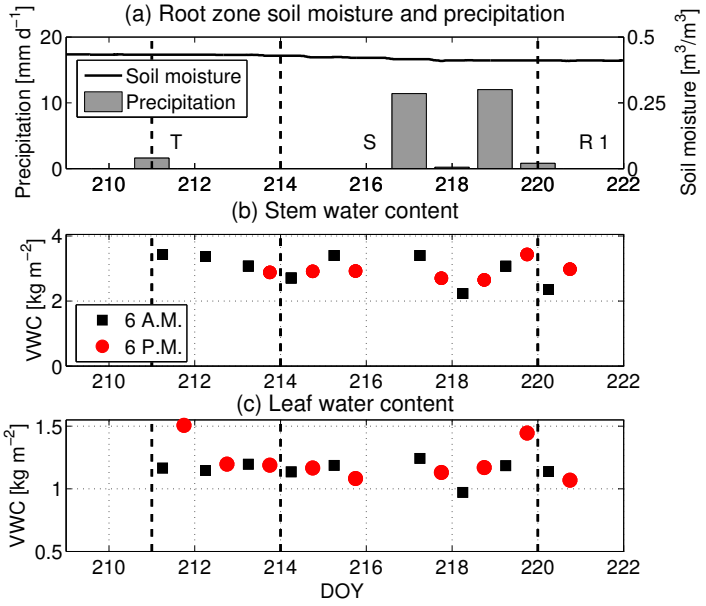

Figure 3.3: Unstressed canopy: (a) Precipitation and root zone soil moisture, (b) stem water content and (c) leaf water content. The stages are included in (a), T=Tasseling, S= Silking, R1=Reproductive stage).

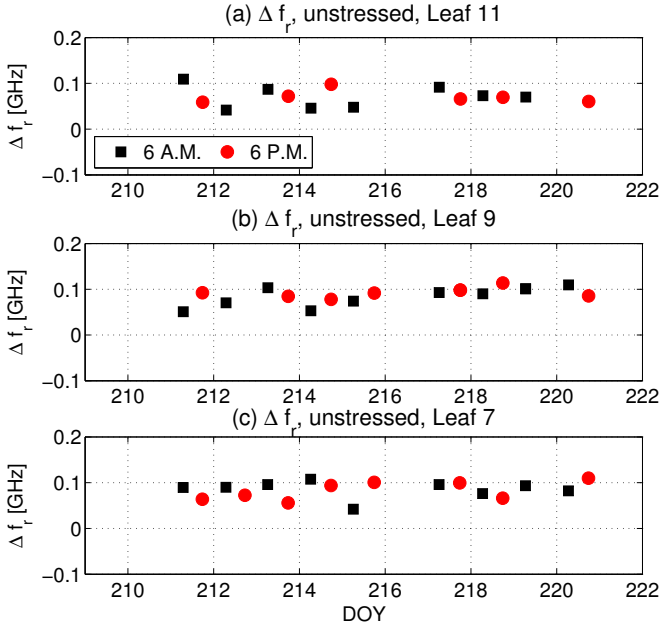

Figure 3.4: Unstressed canopy: Dielectric response Δf_r on (a) leaf 11, (b) leaf 9 and (c) leaf 7.

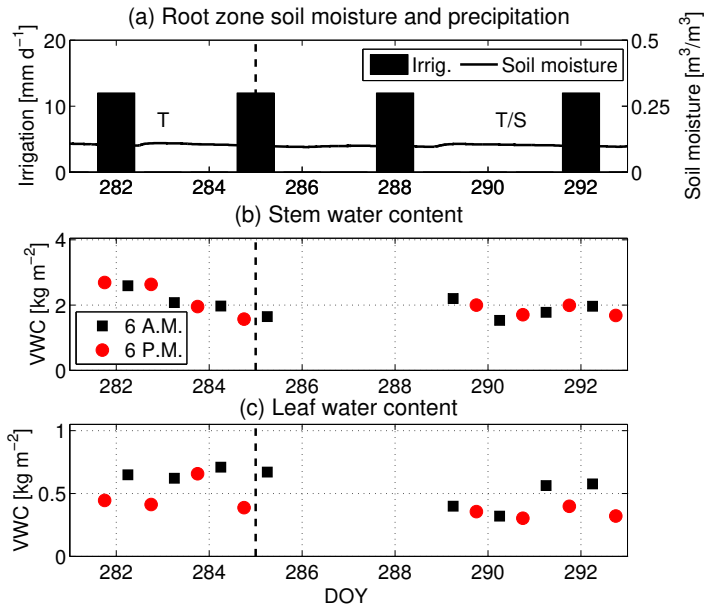

Figure 3.5: Stressed canopy: (a) Precipitation (not between DOY 281 and 293), irrigation at the soil moisture measurement site only, and root zone soil moisture, (b) stem water content and (c) leaf water content. The stages are included in (a), T=tasseling, T/S= start silking.

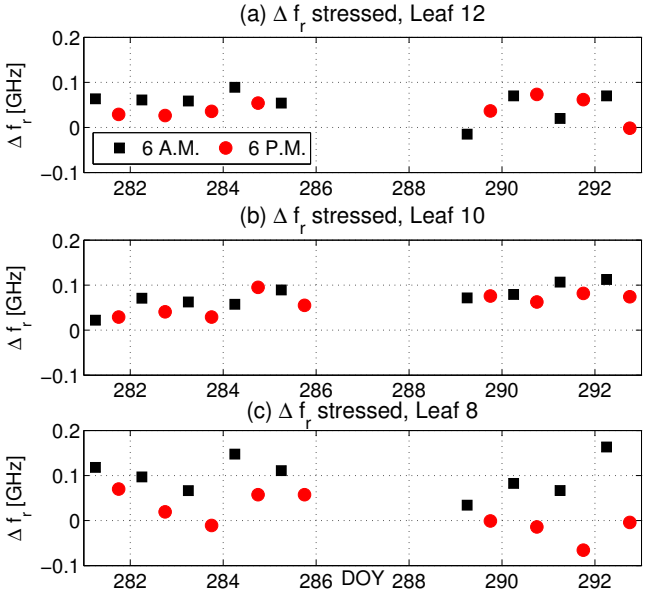

Figure 3.6: Stressed canopy: Dielectric response Δf_r on (a) leaf 12, (b) leaf 10 and (c) leaf 8.

Table 3.1: Trends in Δf_r for the stressed and unstressed canopies, calculated using Spearman's rank coefficient. Positive trends are indicated with (+), negative trends with (-), and no significant trends with (n.t.). Total means all data points of the time series, A.M. and P.M. are the morning and evening values only. Diurnal difference refers to differences between A.M. and P.M.

Leaf No.	Total	A.M.	P.M.	Diurnal difference
Flevoland (unstressed)				
11	n.t.	n.t.	n.t.	n.t.
9	+ 0.99	+ 0.99	n.t.	n.t.
7	n.t.	n.t.	+ 0.92	n.t.
Florida (stressed)				
12	n.t.	n.t.	n.t.	n.t.
10	+ 0.99	+ 0.99	+ 0.95	n.t.
8	n.t.	n.t.	- 0.96	+ 0.94

3.3.2 STRESSED FIELD MEASUREMENTS

During the measurement period in the stressed canopy, no precipitation events occurred (Fig. 3.5(a)). Root zone soil moisture remained low during this period (0.1 m^3/m^{-3}). Note that, although irrigation was switched off at the vegetation sampling location, it continued at the soil moisture probes. These events are indicated as I_x, meaning that soil moisture at the vegetation sampling site is overestimated. Fig. 3.5 shows total stem (b) and leaf water content (c). After the onset of water stress on DOY 280, stem water content, and 6 A.M. and 6 P.M. leaf water content decreased. The diurnal differences in leaf water content are the highest between DOY 281 and 284, just after the onset of water stress. Fig. 3.6 (a)-(c) show the difference in resonant frequency Δf_r time series at leaves 8, 10 and 12. Leaf 10 and 12 show a very stable signal from DOY 281 to 292. There are small diurnal differences in Δf_r, similar in magnitude to the measurements in the unstressed canopy. A positive trend was observed in the A.M. and P.M. values of leaf 10 (Table 1). Leaf 8 shows a clear decreasing trend in the 6 P.M. values, and an increasing trend in the diurnal variation. The diurnal variation of leaf 8 (increasing from 0.048 GHz to 1.675 GHz) is considerably higher than in other leaves (about 0.030 GHz).

3.4 DISCUSSION

Leaf water content of the stressed corn canopy decreased significantly, in contrast to the unstressed canopy, where leaf water content remained stable during the measurement period. Water stress also had an effect on the diurnal differences in leaf water content, which increased just after the onset of water stress. The resonant frequency measurements revealed a dynamic vertical profile of the dielectric response in both the unstressed and the stressed canopy. During normal conditions, the slowly increasing resonant frequency at leaves 7 and 9 are a sign of the growing canopy, suggesting increasing leaf water content and dielectric constant of these leaves. The leaves of the stressed canopy also demonstrated dynamic behavior, depending on the height of the leaf. The contrasting trends of the resonant frequencies at leaves 8 and 10 suggest a change in the vertical water distribution between leaves. However, the effect of water stress was mostly visible through the increasing diurnal variation in resonant frequency of leaf 8. Such di-

urnal variations only occur during times of severe water stress, as isohydric species are unable to prevent water loss for all leaves. Individual leaves respond differently to an increase in stress hormone ABA, which is not reflected in the bulk leaf water content. The older, lower leaves are less responsive to ABA (Zhang and Davies, 1990) and are therefore likely to have caused the large diurnal differences in total leaf water content. Also, the highest photosynthetic rates occur at the leaf close to the main ear, and stomatal control at this leaf is limited to maximize CO_2 uptake. The leaf at the ear (leaf 8) provides carbon for the development of the ear. If the stomata would close too soon, carbon assimilation will decrease and the development of the ear would be jeopardized (Dwyer and Stewart, 1986). Therefore it is important for corn to keep the leaf at the ear transpiring water, even when this leads to higher water losses in the leaf. The upper leaves, smaller and less important for survival, showed no trend in diurnal variation. Therefore, results suggest that the decline in total leaf water content is primarily due to changes in the larger leaves close to the ear (e.g., leaf 8). Our observations are consistent with previously observed response of corn to water stress, which have shown a vertical profile in plant physiological variables, such as photosynthetic rate, transpiration rate and stomatal conductance (Dwyer and Stewart, 1986; Turner, 1974; Acevedo et al., 1979; Rochette et al., 1991). The coupling between plant physiological effects of water stress and the dielectric properties of individual leaves is important to assess the potential of water stress detection using radar. Water stress does not cause a homogeneous reaction of the canopy as a whole. In radar backscatter models or soil moisture retrieval algorithms, vegetation is often modeled as a single layer (water-cloud), or as a layer of individual scatterers. In both cases, the vertical profile of leaf water content, and thus leaf dielectric constant, is not taken into account. We show that when a change in total vegetation was observed, leaves do not necessarily react similarly. Whether radar backscatter is sensitive to a changing vertical profile of leaf dielectric properties depends on the used radar frequency, polarization and incidence angle.

3.5 CONCLUSIONS

This chapter shows that after the onset of water stress, the dielectric response of the leaves around the ear are mainly affected. The results of this first field application are promising, as these results demonstrate the dynamic behavior of leaf dielectric constant. Leaf dielectric properties change with time, and its response to plant growth and water stress depends on the height and age of the leaf.

The *in vivo* resonant frequency measurements suggest that leaf dielectric properties are dynamic in time and space. The variation in leaf dielectric properties, in response to plant growth or water stress, depends on the height of the leaf. Resonant frequency measurements on the stressed canopy clearly showed an effect of water stress on the leaf dielectric response. The leaf at the ear showed an increase in diurnal differences in Δf_r, as well as a negative trend in 6 P.M. values. This highlights the importance of understanding the effect of water stress on the dielectric properties of individual elements within the canopy.

In the next chapter, a radar backscatter sensitivity study is presented to investigate the impact of vegetation water stress on radar backscatter for different frequencies, polarizations, and incidence angles. Field data from this study is used for a modeling study

to (1) look at the sensitivity of radar backscatter to vegetation water content and soil moisture during periods of increased water stress, and (2) look at the influence of vegetation water stress on radar backscatter time series.

4

Impact of Diurnal Variation in Vegetation Water Content on Radar Backscatter From Corn During Water Stress

Traveling through hyperspace ain't like dusting crops, farm boy

Han Solo - A New Hope

Microwave backscatter from vegetated surfaces is influenced by vegetation structure and vegetation water content (VWC) which varies with meteorological conditions and moisture in the root zone. Radar backscatter observations are used for many vegetation and soil moisture monitoring applications under the assumption that VWC is constant on short timescales. This research aims to understand how backscatter over agricultural canopies changes in response to diurnal differences in VWC due to water stress. A standard water-cloud and a two-layer water-cloud model for corn were used to simulate the influence of the observed variations in bulk/leaf/stalk VWC and soil moisture on the various contributions to total backscatter at a range of frequencies, polarizations and incidence angles. The bulk VWC was found to change up to 30 % and leaf VWC up to 40% on a diurnal basis during water stress and may have a significant effect on radar backscatter. Total backscatter time series are presented to illustrate the simulated diurnal difference in backscatter for different radar frequencies, polarizations and incidence angles. Results show that backscatter is very sensitive to variations in VWC during water stress, particularly at large incidence angles and higher frequencies. The diurnal variation in total backscatter was dominated by variations in leaf water content, with simulated diurnal differences of up

Parts of this chapter have been published in IEEE Transactions on Geoscience and Remote Sensing 53 (7) (van Emmerik et al., 2015b).

to 4 dB in X- through K_u-bands (8.6 - 35 GHz). This chapter highlights a potential source of error in current vegetation and soil monitoring applications and provides insights into the potential use for radar to detect variations in VWC due to water stress.

4.1 Introduction

The influence of vegetation on radar backscatter is significant in many applications, including soil moisture retrieval, (Entekhabi et al., 2010; Dubois et al., 1995; Kim and van Zyl, 2009; Joseph et al., 2008, 2010; Bindlish and Barros, 2001), crop classification (Foody et al., 1989; McNairn et al., 2009; Ulaby et al., 1982b; Hoogeboom, 1983), biomass Paloscia et al. (1999), Ferrazzoli et al. (1997) and forest monitoring (Chambers et al., 2007; Saatchi et al., 2007). Radar observations of the land surface are sensitive to vegetation because its presence results in two-way attenuation of the reflection signal from the soil surface, and the vegetation contributes to total backscatter by surface and volume scattering from the canopy itself (Bindlish and Barros, 2001; Paloscia et al., 1999), (Ferrazzoli et al., 1997). Understanding the influence of diurnal vegetation water content (VWC) dynamics in response to water stress on radar backscatter could improve soil moisture retrievals using microwave remote sensing, and provide insights into the potential use for radar to directly monitor vegetation water status.

Radar is used for many vegetation and soil moisture monitoring applications. In algorithms for crop classification (Foody et al., 1989; McNairn et al., 2009; Ulaby et al., 1982b; Hoogeboom, 1983) and biomass monitoring for carbon studies (Chambers et al., 2007), (Saatchi et al., 2007), only a few radar images are used over time. Based on the assumption that VWC mainly changes on a seasonal scale O'Neill et al. (2011), diurnal variations in VWC are often neglected. The water content of soil and vegetation varies diurnally and seasonally (McNairn and Brisco, 2004). Depending on the timescale of interest, these variations could have a significant impact on radar backscatter. In cases where one is interested in seasonal changes in VWC, diurnal differences might be less important. However, Chambers et al. (2007) stated that current hypertemporal remote sensing observations already changed our understanding of canopy VWC and phenology in tropical forests, suggesting that also for applications based on radar with longer revisit times a better understanding of diurnal differences in VWC may improve current retrieval algorithms. When studying soil and vegetation water status dynamics on a daily timescale, diurnal variations might be significant. Soil moisture retrieval algorithms for radar missions require an estimate of VWC, which is generally considered constant or to change only on a seasonal time scale (Wagner et al., 1999; Naeimi et al., 2009; Bindlish et al., 2009; Kim et al., 2010; Panciera et al., 2014). In the latter case, seasonal variation is assumed to be due to canopy growth rather than diurnal moisture dynamics. Diurnal differences in VWC can thus introduce an error in soil moisture retrieval algorithms. For applications like estimating the fuel load of vegetation (Saatchi et al., 2007), where foliage water content is significant (Chambers et al., 2007), accounting for diurnal variation in VWC might improve vegetation fire threat monitoring. It is important to understand under what conditions diurnal variations can be observed in VWC, to quantify their effect on microwave backscatter and the errors introduced in different applications if they are unaccounted for. Finally, observable diurnal differences in microwave backscatter due to variation in VWC could be an interesting new source of information for hydrological,

agricultural and terrestrial ecosystem monitoring applications. Specifically early detection of variation in VWC associated with the onset of water stress in agricultural crops could be useful for crop and water management and food security applications.

Several studies have found diurnal variation in backscatter due to VWC. Differences have been observed between morning and evening overpasses of backscatter observations from satellites (Birrer et al., 1982; Satake and Hanado, 2004), aircraft and ground-based platforms (Ulaby and Batlivala, 1976; Brisco et al., 1990; McDonald et al., 1990). Frolking et al. (2011) showed that the morning overpass of the SeaWinds scatterometer (13.4 GHz) on QuikSCAT was 0.5 - 1.0 dB higher than the evening overpass over the Amazon and used the diurnal differences as an indicator of water stress to study the 2005 drought in this region. Jaruwatanadilok and Stiles (2014) found similar diurnal differences in SeaWinds data over other rain forests (Amazon, Congo, Indonesia). Friesen (2008) and Friesen et al. (2007, 2012) identified a statistically significant diurnal difference between the morning and evening passes of the ERS-1/2 wind scatterometer in vegetated areas. Friesen (2008) used hydrological modeling to demonstrate that the timing and location of the largest difference between morning and evening measurements in West Africa coincided with the onset of water stress. Steele-Dunne et al. (2012) performed a synthetic sensitivity study on a forest canopy using the Michigan Microwave Canopy Scattering (MIMICS) model (Ulaby et al., 1990) to investigate whether variations in leaf water content and hence dielectric properties, could explain these differences in backscatter. Steele-Dunne et al. (2012) confirmed that total backscatter from a forest canopy was sensitive to water content in both leaf and trunk, particularly around the onset of water stress when the soil is dry. This study also highlighted the lack of *in-situ* data on diurnal variations in leaf water content for rigorous analyses.

In Chapter 2 and 3 it was shown that leaf dielectric properties are significantly affected by vegetation water stress. It is hypothesized that this can result in observable differences in radar backscatter. In this chapter, we characterize the diurnal variations in VWC of an agricultural canopy, how these vary in response to water stress and quantify their impact on modeled backscatter for different frequencies, polarizations and angles of incidence. Water stress was induced on a corn canopy in North Central Florida, between September 1 and October 20, 2012. A water cloud model (Attema and Ulaby, 1978) was used with parameter sets obtained from three published experiments to investigate the influence of VWC variations on modeled backscatter for ranges of measured soil moisture and VWC, frequencies, polarizations and incidence angles. Using measured diurnal VWC and soil moisture data, radar backscatter time series were simulated to investigate the effect of water stress and highlight the possible diurnal variation in backscatter due to changes in VWC.

4.2 METHODS AND MATERIALS

4.2.1 STUDY AREA

The fieldwork of this study was conducted at the University of Florida Plant Science Research and Education Unit, located in North Central Florida near Citra, FL (29.41°N, 82.18°W). Measurements were made as part of the Eleventh Microwave Water and Energy Balance Experiment (MicroWEX-11, (Bongiovanni et al., 2015)) from April 25 to

December 9, 2012. For this research sweet corn (*Zea mays L.*, 78-day growing period) was planted on a site of 183 m x 183 m with 89% by volume fine sand, 1 m row spacing and plant density of 5 plants/m. This study used observations during the late vegetative (corn is growing and developing, (Abendroth et al., 2011)) and reproductive (corn is fully grown) periods, from September 1 through October 20, 2012. Typically the crop is heavily irrigated due to sandy soils however, there was no irrigation at the vegetation sampling location from September 29 to October 20, 2012. The growth of plants was restricted only by competition among plants.

4.2.2 WATER STRESS

WATER BALANCE

Meteorological data such as precipitation, soil and air temperature, relative humidity, wind speed and solar radiation at the field site were obtained from the Florida Automated Weather Network (FAWN), managed and maintained by the University of Florida (FAWN website: http://fawn.ifas.ufl.edu). All data were obtained from September 1 to October 20, 2012 with 15 minutes intervals.

To quantify water stress, a water balance was estimated using the following equations:

$$E_{def} = E_{pot} - (P + I) - \frac{\Delta S}{\Delta t} \tag{4.1}$$

where the evaporation deficit E_{def} [mm d^{-1}] is determined as the difference between maximum potential evaporation E_{pot} [mm d^{-1}] and the water available for evaporation, i.e. precipitation P [mm d^{-1}], applied irrigation I [mm d^{-1}] and soil moisture change $\frac{\Delta S}{\Delta t}$ [mm d^{-1}].

The maximum potential evaporation was calculated using

$$E_{pot} = E_{ref} \cdot K_c \tag{4.2}$$

where E_{ref} [mm d^{-1}] is the Penman-Monteith reference evaporation, and K_c [-] is the FAO crop factor for corn which takes the growth stage into account (Allen et al., 1998). From September 1 to 10 K_c was 0.3. Between September 10 and October 1 K_c increased linearly from 0.3 to 1.2 and between October 1 and 20 K_c was 1.2. Daily E_{ref} is provided by FAWN. The soil moisture profile was measured every 15 minutes at six depths of 0.02m, 0.04m, 0.16m, 0.32m, 0.64m and 1.2m at the site using Campbell Scientific CS616 time-domain water content reflectometers (Campbell Scientific, Inc., Logan, UT, USA). Soil moisture was measured several meters away from the vegetation sampling area. At the location of the soil moisture probes, irrigation continued until October 20, 2012. At the vegetation sampling location, the last irrigation event was on September 29, 2012. Therefore, the evaporation deficit calculated using the soil moisture measurements underestimates the evaporation deficit at the vegetation sampling location, providing a conservative estimate of the degree of water stress.

SOIL WATER TENSION

Soil water tension was measured at the vegetation sampling location from September 11 to October 19, 2012 using two UMS T4/e Pressure Transducer Tensiometers (UMS

GmbH, Munich, Germany). One was installed at 50 cm with an angle of 35° with respect to the vertical and one was installed at 30 cm depths with an angle of 40°.

4.2.3 VEGETATION WATER CONTENT

Vegetation water content (VWC) was measured at 6AM and 6PM on 19 days from September 24 to October 19, 2012. Concurrently, two corn plants were cut, weighed with leaves and stalks separated, dried in a 70°C oven for 48 and 120 hours, respectively, and weighed again. VWC values were determined from the fresh and dry masses (m_f and m_d), using the following equation:

$$VWC = \eta[(m_{f,l} - m_{d,l}) + (m_{f,s} - m_{d,s})] \tag{4.3}$$

where η is the number of plants per square meter, and the superscripts l and s indicate leaves and stalks.

4.2.4 WATER-CLOUD MODEL

Radar is influenced by vegetation by three main mechanisms (Ulaby and Jedlicka, 1984): direct backscatter from plants, two-way attenuation of soil backscatter and the multiple scattering between soil and vegetation. For this study, the water-cloud model (Attema and Ulaby, 1978) was used to estimate radar backscatter, which assumes that a canopy can be represented by a cloud of randomly distributed water droplets, based on the assumption that the vegetation dielectric constant is dominated by the dielectric constant of water.

Here, we use three published datasets (Joseph et al., 2010), (Ulaby and Jedlicka, 1984), (Dabrowska-Zielinska et al., 2007), each of which requires a slightly different form of the original water-cloud model of Attema and Ulaby (Attema and Ulaby, 1978). To allow a comparison between model output of all different radar frequencies, incidence angles and polarizations, vegetation and soil backscatter were calculated separately. Vegetation backscatter was determined based on the equations provided by the individual models. For soil backscatter contribution, the bare soil scattering model of (Dubois et al., 1995) was used.

All modeled backscatter will be presented in decibels [dB]. The water-cloud parameters used in the three modeling approaches can be found in Table 1. To evaluate the diurnal differences in modeled radar backscatter for different frequencies, polarizations and incidence angles, a T-test was performed to determine the statistical significance. This was also done for the morning and evening values for VWC and soil moisture.

L-BAND (HH, 35°) AND C-BAND (VV, 23°)

Dabrowska-Zielinska et al. (2007) used a simplified water-cloud model, based on Prevot et al. (1993) and Champion et al. (2000), to simulate C-band (VV, 23°) and L-band (HH, 35°) radar backscatter. Total backscatter σ^0_{tot} is described as:

$$\sigma^0_{tot} = \sigma^0_{veg} + \gamma^2 \sigma^0_{soil} \tag{4.4}$$

with vegetation contribution σ^0_{veg}, soil contribution σ^0_{soil} and two-way attenuation γ^2. σ^0_{veg} and γ^2 are formulated as:

Table 4.1: Used parameters for water-cloud models.

Model	Radar parameters				Vegetation parameters					
	Band	Freq. [GHz]	Angle [°]	Pol.	A	B	α	E	A_{st}	α_{st}
Ulaby *et al.* (1984)	X	8.6	50	VV	0.22	2.6	0,411		0.025	0
	K_u	17	50	VV	0.30	2.7	0,418		0.022	0
	K_a	35	50	VV	0.36	2.0	0,360		0.034	0
Dabrowska-Zielinska *et al.* (2007)	L	1.275	35	HH	0.01	0.04		0.0		
	C	5.3	23	VV	0.08	0.15		2.9		
Joseph *et al.* (2010)	C	4.8	15	HH	0.03	0.09				
	C	4.8	15	VV	0.01	0.13				
	C	4.8	35	HH	15.96	$1.18 \cdot 10^{-4}$				
	C	4.8	35	VV	3.05	$1.38 \cdot 10^{-4}$				
	C	4.8	55	HH	5.57	$4.16 \cdot 10^{-4}$				
	C	4.8	55	VV	2.96	$1.96 \cdot 10^{-4}$				

$$\sigma^0_{veg} = AV_1^E cos\theta(1-\gamma^2) \tag{4.5}$$

$$\gamma^2 = exp(\frac{-2BV_2}{cos\theta}) \tag{4.6}$$

with model parameters A, B and E, incidence angle θ, and vegetation parameters V_1 and V_2. Model parameters A, B and E are parameters depending on the used radar frequency, incidence angle, polarization and crop. For V_1 and V_2, VWC is used (Joseph et al., 2008; Bindlish and Barros, 2001; Prevot et al., 1993).

C-BAND (HH AND VV, 15°, 35° AND 55°)

The water-cloud model of Joseph et al. (2010) is similar to those of Bindlish and Barros (2001) and Ulaby and Jedlicka (1984). Joseph et al. (2010) calibrated their model for C-band backscatter with HH and VV polarization and three incidence angles, i.e. 15°, 35° and 55°. σ^0_{tot} is given by equation (4.4). The vegetation term is formulated as:

$$\sigma^0_{veg} = (1-\gamma^2)AV_1 cos\theta \tag{4.7}$$

with VWC V_1, model parameters A and E and incidence angle θ. The two-way attenuation is determined using equation 4.6.

X, K_u AND K_a-BAND (VV, 50°)

Ulaby and Jedlicka (1984) account for the leaves and stalks separately such that total backscatter σ^0_{tot} is given by:

$$\sigma^0_{tot} = \sigma^0_{leaf} + \sigma^0_{stalk} + \sigma^0_{soil} \tag{4.8}$$

leaf and stalk backscatter σ^0_{leaf} and σ^0_{stalk}, respectively, and soil contribution σ^0_{soil}. σ^0_{leaf} and σ^0_{stalk} are given by:

$$\sigma^0_{leaf} = A_{leaf}[1-exp(\frac{-B_{leaf}V_1}{h_1})][1-\gamma^2_{leaf}]cos\theta \tag{4.9}$$

$$\sigma^0_{stalk} = A_{stalk} \cdot V_2 \cdot \frac{h_2}{h} \cdot \gamma^2_{leaf} \tag{4.10}$$

with leaf vegetation parameters A_{leaf} and B_{leaf}, leaf VWC V_1, height of the leaf layer h_1 (see Fig. 4.1), leaf attenuation factor γ^2_{leaf}, angle of incidence θ, stalk vegetation parameters A_{st}, stalk VWC V_2, height of the stalk layer h_2 and total plant height h (see Fig. 4.1). The leaf and stalk attenuation factors γ^2_{leaf} and γ^2_{stalk} determine how much of the original signal makes is attenuated by the leaf and stalk layer and are given by:

$$\gamma^2_{leaf} = exp(-2 \cdot \alpha_{leaf} \cdot V_1 \cdot h_1 \cdot sec\theta) \tag{4.11}$$

$$\gamma^2_{stalk} = exp(-2 \cdot \alpha_{stalk} \cdot V_2 \cdot h_2 \cdot sec\theta) \tag{4.12}$$

with model parameters α_{leaf} and α_{stalk}.

From October 7 to 21, the ratio of leaf water content over bulk water content was 0.20, with a standard deviation of 0.05. For the sensitivity study, this value is used to separate bulk vegetation water content into leaf and stalk water content.

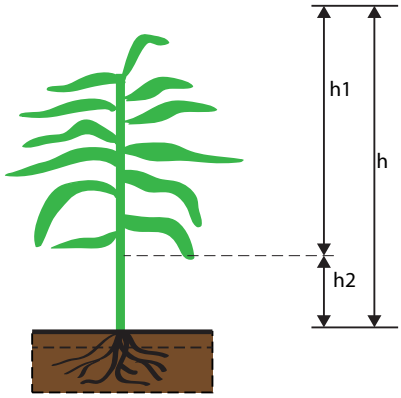

Figure 4.1: Vegetation heights h, h_1 and h_2 as used in the water-cloud model

SOIL BACKSCATTER

This empirical backscattering approach is based on field data sets, and describes HH or VV polarized radar backscatter as a function of the angle of incidence θ, frequency f, surface roughness h_s, wave number k, the dielectric constant of soil ϵ and wavelength λ, using the following equations:

$$\sigma^0_{hh} = 10^{-2.75} \cdot \frac{cos^{1.5}\theta}{sin^5\theta} \cdot 10^{0.028\epsilon \cdot tan\theta} (kh_s sin\theta)^{1.4} \cdot \lambda^{0.7} \tag{4.13}$$

$$\sigma^0_{vv} = 10^{-2.35} \cdot \frac{cos^3\theta}{sin^3\theta} \cdot 10^{0.046\epsilon \cdot tan\theta} (kh_s sin\theta)^{1.1} \cdot \lambda^{0.7} \tag{4.14}$$

A value for RMS height (h_s = 1 cm) was assumed for the entire period. This value is based on reported values in the literature for similar conditions

4.3 Results

4.3.1 Water stress

Fig. 4.2 (a) shows rainfall and irrigation. In the last week of September, irrigation was necessary to ensure the corn had enough moisture during the end of the growing phase. After October 7, irrigation was withheld at the vegetation sampling area to induce water stress. Fig. 4.2 (b) shows the volumetric soil moisture profile in the soil over time. It is clear that this sandy soil remained very dry for the duration of the experiment. After September 30, near surface soil moisture varies between 0.04 and 0.15 m^3m^{-3} at the near-surface (0.02 m depth) and between 0.08 and 0.09 m^3m^{-3} at 1.2 m. Increases in near-surface soil moisture were observed on October 9, 12, 15 and 19. Because the soil moisture sensors were placed outside the vegetation sampling area, the available soil moisture is overestimated. Fig. 4.2 (c) shows the surface soil moisture values at 6AM and 6PM. Peaks are observed after rainfall or irrigation events. Fig. 4.2 (d) shows the calculated daily evaporation decreasing with time. The evaporation deficit, an indicator of water stress in this study, is shown in Fig. 4.2 (e). The deficit increases gradually until October 7 because irrigation is provided to supplement the precipitation. After October 7, the cumulative evaporation deficit increases rapidly in the absence of irrigation. For comparison, Fig. 4.2 (e) shows the soil water tension measured at 30 cm and 50 cm. The values measured are consistent with the published values for dry sandy soils (van Genuchten and Nielsen, 1985; Simunek and van Genuchten, 1995). The dynamics of soil water tension reflect those of the moisture in Fig. 4.2 (b), with drier soil and higher soil water tension closer to the surface. The soil water tension at depth exhibits a slower, damped response to the absence of precipitation or irrigation. After October 7, soil tension at 30 cm and 50 cm increase in agreement with the rising cumulative evaporation deficit. The rapid increase in cumulative evaporation deficit is particularly apparent in the soil water tension at 30 cm.

Table 2 shows the statistical significance of diurnal variation in VWC and soil moisture. Low values (< 0.9) mean an absence of statistically significant diurnal variation. No statistically significant diurnal difference in soil moisture was observed. Because soil moisture was measured in the irrigated field, diurnal differences might have occurred at the vegetation sampling size. However, since irrigation was absent, it is assumed that if present, these variations are very low. Observed diurnal differences in VWC were clearly significant.

4.3.2 Vegetation Water Content

The vegetation water content is shown in Fig. 4.3. Fig. 4.3 (a) shows the bulk VWC and Fig. 4.3 (b) shows the VWC for stalks and leaves separately. As the corn reaches the final vegetative stages (V10 and V11), most of the water in the plant is stored in the stalks. Consequently, the temporal variations in bulk and stalk VWC are very similar. Up to October 7, the corn is still developing and growing, and therefore the stalk and bulk VWC increase. After the corn is fully developed, the increasing water stress causes a decrease in stalk and bulk VWC. The leaf VWC is quite stable until September 30, but then shows a decreasing trend from the onset of water stress onwards.

On 13 days leaf and stalk VWC was measured at both 6AM and 6PM. VWC of leaves

Table 4.2: T-test results to determine statistical significance of diurnal differences, (-) means a decrease between 6AM and 6PM, (+) means an increase between 6AM and 6PM. Diurnal differences are statistically significant for 1 - $P \geq 0.9$

Model	Radar parameters				T-test	
	Band	Freq. [GHz]	Angle [°]	Pol.	1 - P	+/-
Ulaby *et al.* (1984)	X	8.6	50	VV	1.00	-
	K_u	17	50	VV	1.00	-
	K_a	35	50	VV	1.00	-
Dabrowska-Zielinska *et al.* (2007)	L	1.275	35	HH	0.98	-
	C	5.3	23	VV	0.92	+
Joseph *et al.* (2010)	C	4.8	15	HH	0.97	+
	C	4.8	15	VV	0.96	+
	C	4.8	35	HH	0.99	-
	C	4.8	35	VV	0.83	-
	C	4.8	55	HH	0.98	-
	C	4.8	55	VV	0.87	-
Surface soil moisture					0.06	-
Total soil moisture					0.08	+
Bulk VWC					0.98	-
Leaf VWC					1.00	-
Stalk VWC					0.89	-

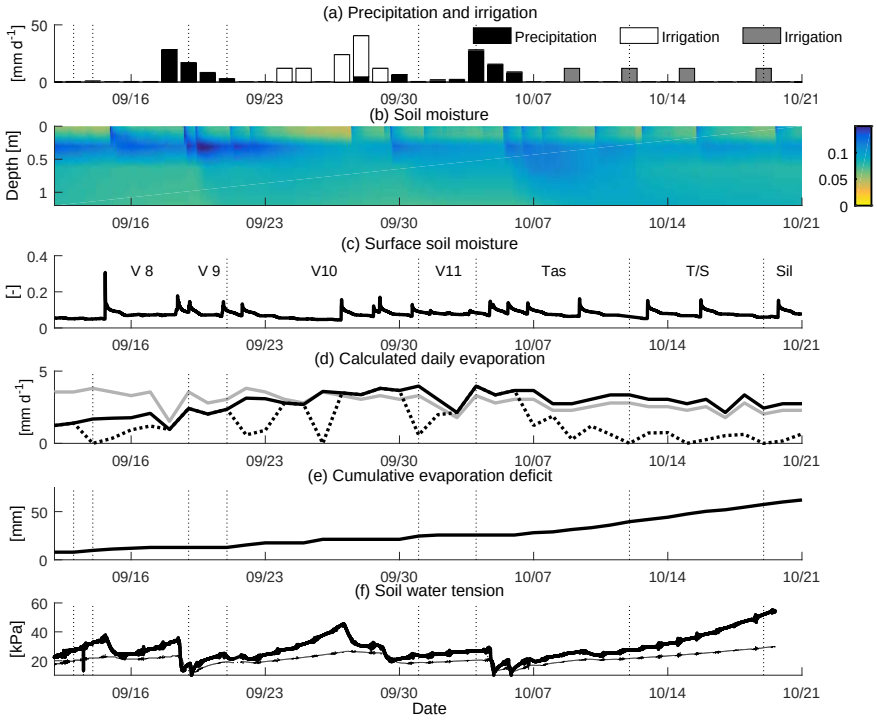

Figure 4.2: (a) Precipitation and irrigation at the measurement site, (b) soil moisture profile over time, (c) calculated daily evaporation at the measurement site, (d) water stress quantified by cumulative evaporation deficit, (e) water stress quantified by soil water tension at 30cm and 50cm depth.

and stalks was higher at 6AM than at 6PM on 11 and 9 days, respectively. On 17 and 18 October the evening bulk VWC was higher than the morning VWC. This is unexpected, since on most days VWC decreased during 6AM and 6PM. It is likely that the observed increase is due to spatial variation. Especially on 17 October, a relatively low VWC was observed in the morning.

Diurnal difference in total VWC were statistically significant (Table 2). This was expected since transpiration of corn occurs mainly during the day, with the peak transpiration rate around noon, causing the VWC of corn to decrease between morning and evening. The morning leaf measurements decrease as stress continues, suggesting that the plant cannot replenish all water lost during the day. The trend is less significant in the evening leaf measurements.

4.3.3 BACKSCATTER SENSITIVITY STUDY

L- AND C-BAND

Fig. 4.4 shows the horizontally co-polarized backscatter at 1.275 GHz and an incidence angle of 35°, simulated using equations 4.4 to 4.6 and the parameters from the water cloud model of Dabrowska-Zielinska *et al.* (Table 1). During the observation period,

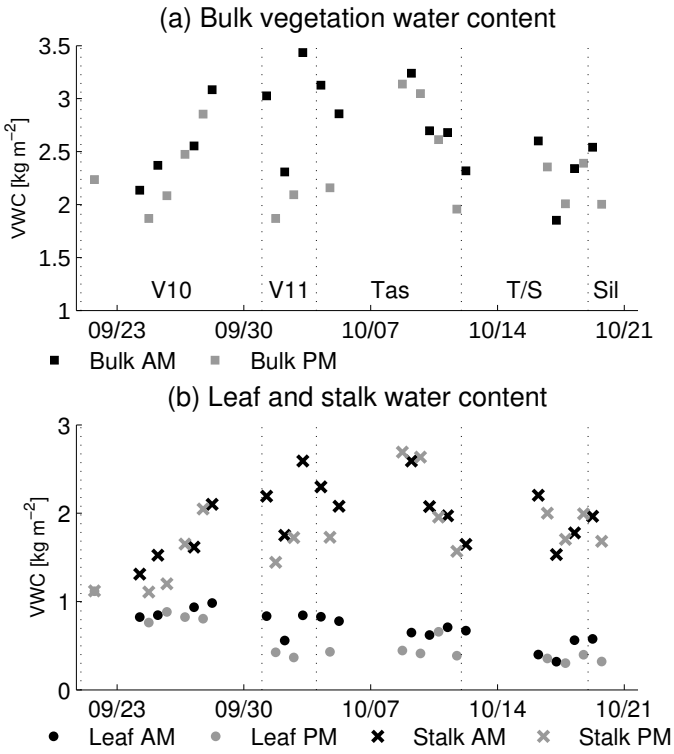

Figure 4.3: Results of vegetation sampling, (a) bulk vegetation water content at 6AM and 6PM, (b) leaf and stalk vegetation water content at 6AM and 6PM.

surface soil moisture was low (between 0.04 and 0.15 $m^3\ m^{-3}$) so the range of backscatter from bare soil is about 1.5 dB (Fig. 4.4 (a)). VWC varies between 1.7 and 3.5 $kg\ m^{-2}$, which leads to a range of around 2 dB in attenuated soil backscatter (Fig. 4.4 (b)). Fig. 4.4 (c) illustrates that backscatter from the vegetation itself varies between -24 dB and -10 dB, which is considerably larger than the range of values simulated for the attenuated soil backscatter. Furthermore, at VWC values greater than 2.3 $kg\ m^{-2}$, σ°_{veg} is greater than $\gamma^2\sigma^\circ_{soil}$. Consequently, total backscatter dynamics are primarily a function of VWC, as shown in Fig. 4.4 (d).

VWC affects the transparency of the canopy layer. At an incidence angle of 35°, changes in soil moisture have a small effect on total backscatter because the path through the canopy layer is large (Ulaby et al., 1982c) (Section 11-5). Increasing VWC will decrease the penetration capacity. At L-band, low VWC makes vegetation transparent and the soil moisture signal governs total backscatter. However, the effect of changes in soil moisture on backscatter are limited. High VWC results in a low penetration capacity, so the backscatter signal mainly consists of vegetation contribution. In case soil moisture variation is low, backscatter mainly reflects the dynamics in VWC. Dabrowska-Zielinska

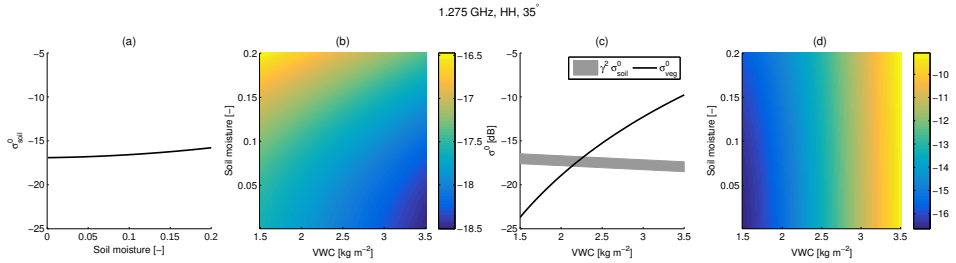

Figure 4.4: Sensitivity of L-band (1.2GHz, HH, 35°) radar backscatter modeled using Dabrowska-Zielinska et al. (2007) to soil moisture and vegetation water content, (a) soil backscatter as function of soil moisture, (b) attenuated soil backscatter as function of VWC and soil moisture, (c) vegetation backscatter as function of VWC, including minimum and maximum contribution of attenuated soil backscatter, (d) total backscatter as function of VWC and soil moisture.

et al. (2007) investigated the effect of plant and soil variables on L-band radar. It was found that for L-band (35°) the dominant signal to total backscatter comes from vegetation in case of VWC greater than 3 kg m^{-2} and soil moisture varying between 0 and 0.6. We measured surface soil moisture between 0.04 and 0.15 and VWC between 1.7 and 3.5 kg m^{-2}. Compared to Dabrowska-Zielinska et al. (2007), we show that in case of low soil moisture variability, total backscatter is also mainly sensitive to variations in VWC within this lower range. This is interesting because this means that the effect of VWC on L-band radar backscatter might be larger than previously found. We show that especially at times of low soil moisture variability, total backscatter is mainly influenced by dynamics in VWC.

Fig. 4.5 shows the vertically co-polarized backscatter at 5.3 GHz and an incidence angle of 23° for the same model and appropriate parameters from Table 1. In this case, the range of attenuated soil backscatter for a given value of VWC is 3.5 dB, which is larger than the range of simulated σ°_{veg} values (2.5 dB variation). The magnitudes of the two backscatter terms are comparable, with the vegetation term dominating when VWC exceeds 3.0 kg m^{-2}. As a result, total backscatter is sensitive to both VWC and soil moisture (Fig. 4.5 (d)). Because the incidence angle is relatively low, the path through the vegetation is short. Closer to nadir, agricultural canopies are more transparent and microwaves can more easily penetrate through the vegetation layer. Therefore, backscatter is relatively sensitive to changes in soil moisture. However, higher VWC leads to a lower penetration capacity and the contribution from vegetation is larger than the soil contribution. Dabrowska-Zielinska et al. (2007) found that for VWC equal to 5 kg m^{-2} soil contributes 50% to total backscatter, mainly due to larger soil moisture variations (0-0.6). We show that this is also the case for lower values of VWC. Between 2.5 and 3.0 kg m^{-2}, soil contributes 50% to total backscatter. For VWC higher than 3.0 kg m^{-2}, the vegetation is the main contributor to total backscatter. In the range of VWC and soil moisture observed, Fig. 4.5 shows that C-band (VV, 23°) total backscatter is sensitive to both VWC and soil moisture.

The modeled sensitivity of backscatter to diurnal variation in VWC was done for agricultural canopies. Interestingly, for various vegetation types a strong sensitivity of backscatter to diurnal dynamics in VWC has been found in case of low soil moisture

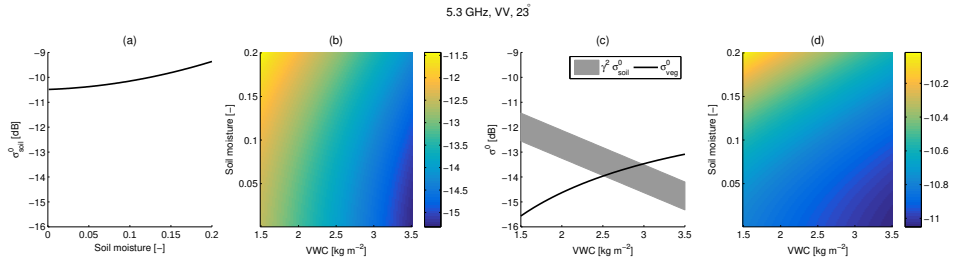

Figure 4.5: Sensitivity of C-band (5.3 GHz, VV, 23°) radar backscatter using Dabrowska-Zielinska et al. (2007) to soil moisture and vegetation water content, (a) soil backscatter as function of soil moisture, (b) attenuated soil backscatter as function of VWC and soil moisture, (c) vegetation backscatter as function of VWC, including minimum and maximum contribution of attenuated soil backscatter, (d) total backscatter as function of VWC and soil moisture.

4

variation. Over savannas in West Africa,Friesen et al. (2012) *et al.* found a statistically significant diurnal difference in ERS backscatter and hypothesized that this was caused by diurnal variation in VWC. For tree forests, Steele-Dunne et al. (2012) showed that at L- and C-band changes in leaf moisture lead to a significant change in total backscatter over a forest canopy. Although agricultural canopies are less densely vegetated than forests, the results in this chapter show that total backscatter at L- and C-band is sensitive to both VWC and soil moisture. During periods of water stress, soil moisture is likely to be low and change little during the day, hence total backscatter will be mainly influenced by VWC dynamics of savannas, forests and agricultural canopies.

INFLUENCE OF INCIDENCE ANGLE AT C-BAND

In this section, results are presented for C-band (4.8GHz) vertically and horizontally co-polarized backscatter for three different incidence angles, simulated using equations 4.4-4.7 and the parameters from Joseph et al. (2010) provided in Table 1.

Fig. 4.6 shows the simulated horizontally co-polarized backscatter at 15°, 35° and 55° for the observed range of surface soil moisture and VWC. From Fig. 4.6 (a)-(c), the direct vegetation contribution is similar (-15 to -22 dB) for all three incidence angles. The magnitude of the attenuated soil backscatter decreases from -6.5 dB at 15° to -21.5 dB at 55°. As shown in Fig. 4.6 (d)-(f), the influence of VWC on the attenuated soil backscatter is different at low and high incidence angles. At 15° (Fig. 4.6 (d)), the attenuated soil backscatter decreases considerably with increasing VWC. At 35° and 55° the path through the vegetation is longer, and the water-cloud model vegetation parameter B (representing the extinction coefficient for a canopy (Ulaby et al., 1982c) (Section 11-5)) is very small (Table 1) so γ^2 is close to unity and independent of VWC.

It was expected that attenuation γ^2 would have been higher for increasing incidence angles, leading to more attenuation of σ^0_{soil}. The reason for low γ^2 can be found in the calibration of the water-cloud model, where parameter A was significantly higher at 35° and 55°, leading to higher σ^0_{veg} and lower γ^2. When one looks at the total backscatter modeled by Joseph et al. (2010), the complete effect of vegetation is captured (direct backscatter and attenuation). However, these parameter sets do not capture the dynamics of the individual contributions from soil and vegetation. At 15°, total backscatter is

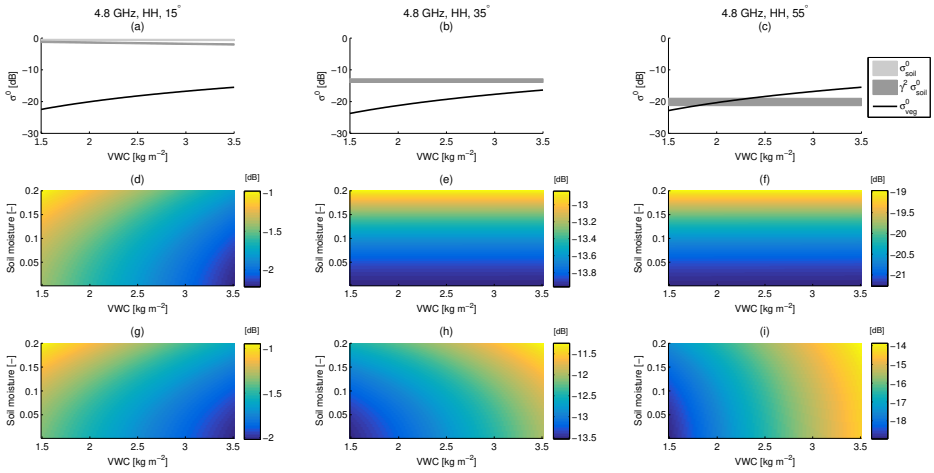

Figure 4.6: Sensitivity of C-band (4.8 GHz) HH radar backscatter at difference incidence angles using Joseph et al. (2008), (a)-(c) vegetation and attenuated soil contributions as a function of VWC for 15°, 35° and 55° respectively, (d)-(e) attenuated soil backscatter as a function of VWC and soil moisture for 15°, 35° and 55° respectively, (f)-(i) total backscatter as a function of VWC and soil moisture for 15°, 35° and 55°, respectively.

dominated by the attenuated soil backscatter (Fig. 4.6 (a)), so total backscatter (Fig. 4.6 (g)) depends on both soil moisture and VWC. At this incidence angle, a decrease in VWC would lead to an increase in backscatter. Interestingly, at 55° and HH polarization, the direct backscatter from the canopy (highly sensitive to VWC) is similar in magnitude to the attenuated soil backscatter (insensitive to VWC). As the incidence angle increases total backscatter becomes increasingly sensitive to VWC. At 35° and 55°, a decrease in VWC leads to a decrease in total backscatter.

Similar results were obtained for vertically co-polarized C-band backscatter (Fig. 4.7). In this case even at the larger incidence angles, the attenuated soil backscatter dominates, so the total backscatter at 35° and 55° is less sensitive to VWC than the horizontally co-polarized case.

Joseph et al. (2010) also found that for increasing incidence angles, changes in backscatter showed more resemblance to changes in VWC and less to variation in soil moisture. Horizontally co-polarized backscatter was more sensitive to changes in VWC at 35° and 55° than vertically co-polarized backscatter. Ulaby et al. (1982c) (Section 11-5) found that the sensitivity to soil moisture over an agricultural canopy decreases with an increasing incidence angle. Total backscatter also decreased with increasing incidence angles. Because at higher angles the path through vegetation increases and the penetration capacity decreases. A larger portion of the incoming microwaves will scatter and not make it to the soil.

Joseph et al. (2010) found that at 15° attenuated soil is the more dominant contributor to total backscatter and that at 35° and 55° scattering from vegetation becomes more dominant. It was mentioned that for VWC equal to 5.1 kg m^{-2} backscatter was sensitive for changes in soil moisture. Our results add that for 15° - 55° and low variation in soil moisture (0-0.2), changes in VWC (1.5-3.5 kg m^{-2}) can also affect total backscatter.

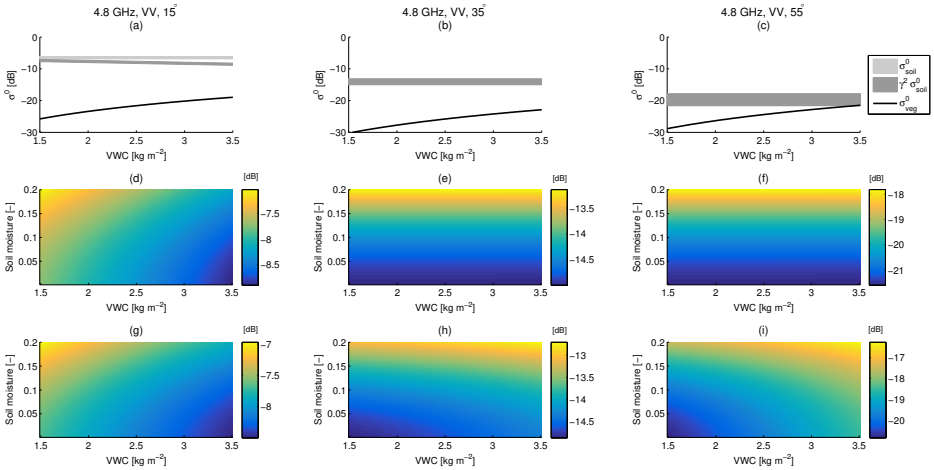

Figure 4.7: Sensitivity of C-band (4.8 GHz) VV radar backscatter at difference incidence angles using Joseph et al. (2008), (a)-(c) vegetation and attenuated soil contributions as a function of VWC for 15°, 35° and 55° respectively, (d)-(f) attenuated soil backscatter as a function of VWC and soil moisture for 15°, 35° and 55° respectively, (g)-(i) total backscatter as a function of VWC and soil moisture for 15°, 35° and 55° respectively.

This is particularly evident in C-band horizontally co-polarized backscatter (Fig. 4.6) and becomes more significant with increasing incidence angle. Rather than looking at vegetation as something to correct for in soil moisture retrieval algorithms, this suggests that the sensitivity of radar to changes in VWC might also be a new source of information.

HIGH FREQUENCIES

Fig. 4.8 shows the sensitivity of high frequency (8.6 GHz, 17 GHz and 35 GHz, VV-polarized, 50°) radar backscatter to soil moisture and VWC. Fig. 4.8 (a)-(c) show that the direct vegetation backscatter is equal to the backscatter from the leaves at all frequencies. For increasing frequencies, the magnitude of the vegetation contribution increases from -17 to -12 dB at 8.6 GHz to -16 to -10 dB at 35 GHz. This corresponds to the original results presented by Ulaby and Jedlicka (1984), where it was found that the variation in backscatter over a corn field is higher for increasing frequencies. The attenuated soil backscatter is smaller than the vegetation term (Fig. 4.8 (d)-(f)) for VWC below 1.5 kg m^{-2} at 8.6 and 17 GHz and 1.7 kg m^{-2} at 35 GHz. Consequently, the total backscatter is primarily sensitive to VWC, or more precisely to leaf VWC. At high frequencies, a larger fraction of the incoming microwaves will be scattered by the canopy surface. A lower amount of volume scattering thus means a lower sensitivity to total VWC, since from our results it can be seen that leaf VWC mainly determines the amount of surface scattering. This is particularly interesting because the results in Fig. 4.3 illustrate that the dynamics of leaf VWC are different from those of bulk VWC.

4.3.4 TIME SERIES OF MODELED RADAR BACKSCATTER

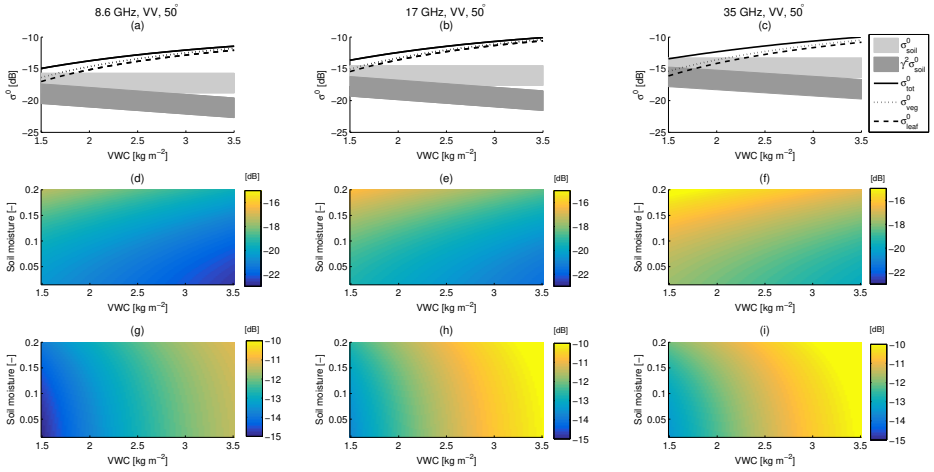

Figure 4.8: Sensitivity of radar backscatter at 8.6 GHz (a, d, g), 17 GHz (b, e, h) and 35 GHz (c, f, i) using Ulaby and Jedlicka (1984) to soil moisture and VWC, (a) - (c) leaf and total vegetation backscatter as function of VWC, (d)-(f) attenuated soil backscatter as funtion of soil mosture and VWC, (e)-(i) total backscatter as function of soil moisture and VWC.

L- AND C-BAND

Fig. 4.9 (a) shows the time series of L-band (35°, HH) total backscatter simulated using equations 4.4 to 4.6 and the parameters from Dabrowska-Zielinska et al. (2007). Fig. 4.9 (c), (e) and (g) show the contributions from vegetation, attenuated soil and soil backscatter, respectively.

Fig. 4.9(g) shows the variation in σ^0_{soil} due to the limited variations observed in surface soil moisture. Recall that soil moisture was measured in the irrigated field. While no diurnal differences were observed there (Table 2), they may have occurred at the vegetation sampling site. However, in the absence of irrigation, it is reasonable to assume that variability in surface soil moisture at the vegetated sampling site would be even less than that observed at the irrigated field. For the observed variation in soil moisture, the range of simulated backscatter from the soil is about 0.4dB. Fig. 4.9(e) shows the impact of the measured variations in VWC on the simulated attenuated soil backscatter. The difference in dynamics between Fig. 4.9(e) and 9(g) is due to the measured variations in VWC. On 9 days, $\gamma^2\sigma^0_{soil}$ was lower at 6AM than at 6PM due to diurnal variations in VWC, though the total range of values is less than 1dB. Recall from Fig. 4.4(c) that the range of simulated vegetation backscatter at L-band (35°, HH) is 13dB for the range of observed VWC, and that above VWC=2.3 kg m^{-2}, this term is the dominant contribution to total backscatter. Hence, the variations in σ^0_{veg} (Fig. 4.9(c)) are due to the observed changes in the bulk VWC. In late September, the VWC increases as the plants grow which results in an increase in σ^0_{veg}. The decline in VWC after October 7 results in a decrease in σ^0_{veg}. Vegetation backscatter is significantly higher in the morning than in the evening due to the diurnal difference in VWC (see Table 2), with differences of up to 7 dB between October 1 and 20, 2012. From Fig. 4.9(a) and (c), it is clear that diurnal variations observed in VWC dominate the simulated dynamics in total L-band (35°, HH) backscatter and ex-

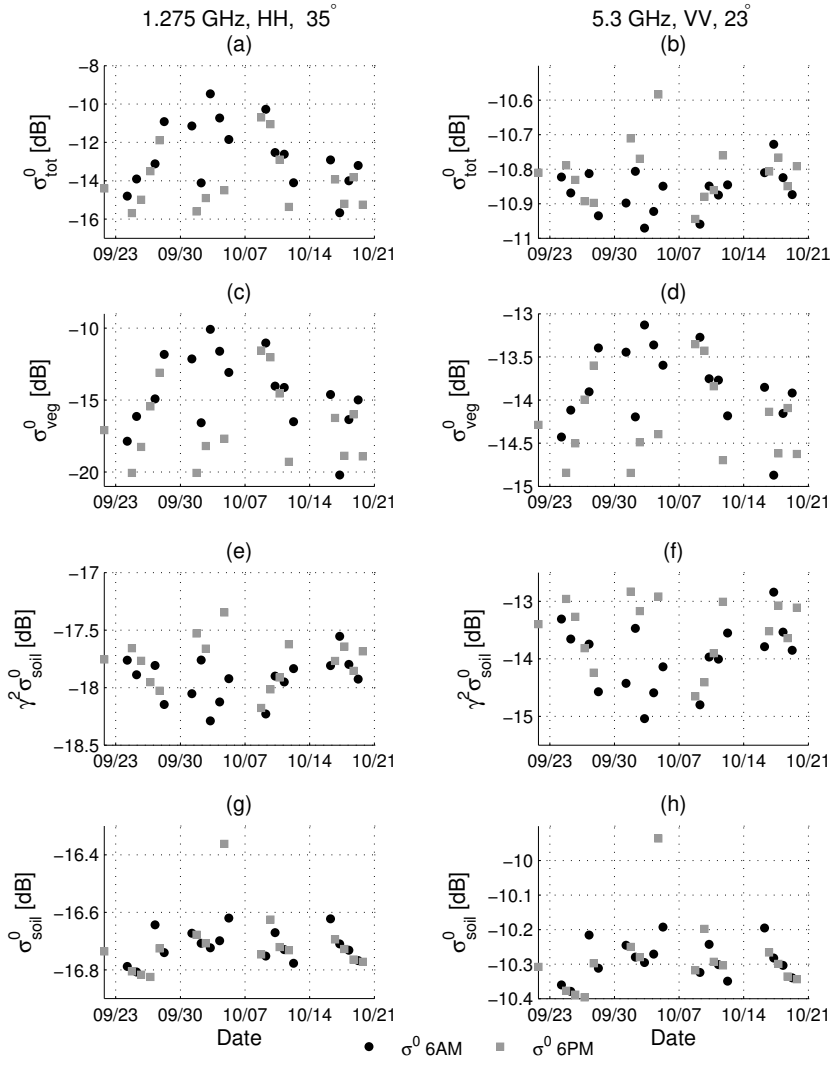

Figure 4.9: Modeled radar backscatter time series at L-band (1.275 GHz, HH, 35°) and C-band (5.3 GHz, VV, 23°) using Dabrowska-Zielinska et al. (2007), (a) - (b) total backscatter, (c) - (d) vegetation contribution, (e) - (f) attenuated soil backscatter and (g) - (h) soil contribution.

plain the statistically significant difference simulated between 6AM and 6PM values.

It is generally accepted that L-band penetrates further through canopies (e.g. (Jackson and Schmugge, 1991; Joseph et al., 2008)). Ulaby et al. (1982c) showed that at increasing incidence angles, the penetration through canopy decreases, resulting in a lower sensitivity to soil moisture. Fig. 4.9 shows that at a 35° incidence angle and HH co-polarization, the effect of vegetation and its diurnal dynamics cannot be neglected in

case of low soil moisture variability. Both attenuation and direct backscatter caused by diurnal variation in VWC can have a significant influence on total backscatter. From Table 2 it can be seen that diurnal differences in L-band backscatter are statistically significant. This is interesting for soil moisture and vegetation monitoring using L-band radar. Before, the main focus was on soil moisture, attributing variation in backscatter to changes in soil moisture. However, Fig. 4.9(a) shows that during times of low soil moisture availability, diurnal differences in L-band (35°, HH) backscatter can be attributed to changes in VWC. This does not only highlight potential errors in soil moisture retrieval algorithms, it also points out the potential of radar for vegetation and water stress monitoring.

At C-band (23°, VV) the range of total backscatter values over the whole time series, shown in Fig. 4.9 (b), is just 0.4 dB. Recall from Fig. 4.5 that the total backscatter in this configuration was dominated by the attenuated soil moisture signal up to a VWC of 3 kg m^{-2}. The limited variation in measured surface soil moisture results in a range in simulated σ^0_{soil} of less than 0.4dB (Fig. 4.9(h)). The impact of VWC in attenuating this soil signal is shown in Fig. 4.9(f). Simulated attenuated soil backscatter is up to 2dB lower in the morning due to the diurnal variations in measured VWC. The VWC has an opposite effect on σ^0_{veg}, with higher 6AM VWC values producing simulated σ^0_{veg} up to 1.5dB higher in the morning. Recall from Fig. 4.5(d) that these two effects are comparable in magnitude. Hence, there is limited variation in simulated total C-band (23°, VV) backscatter. Though Table 2 shows that there is a statistically significant difference between morning and evening values, it is clear from Fig. 4.9(b) that the magnitude of the difference is very small.

As mentioned in Section I, diurnal variations in ERS backscatter (also C-band, VV) were observed by Friesen et al. (2007). The largest differences coincided with the onset of water stress, when Friesen *et al.* argued that VWC still varies diurnally, but soil moisture is low and does not change significantly. Steele-Dunne et al. (2012) showed that the diurnal difference observed by Friesen et al. (2007) could be explained by variations in leaf moisture content. However, this was for a forest canopy where the VWC is much higher than that considered in Fig. 4.9.

INFLUENCE OF INCIDENCE ANGLES AT C-BAND

Fig. 4.10 and 4.11 show the time series of backscatter simulated using equation 4.4 to 4.8 for C-band at different incidence angles and horizontal and vertical polarization, respectively. For both HH and VV polarization, backscatter decreases with increasing incidence angles (-1.2 to -2 dB at 15°, -14 to -20 at 55°). As expected from the sensitivity study, the influence of VWC on backscatter at different incidence angles causes some interesting differences in the diurnal backscatter variations. For all horizontally polarized incidence angles and 15° vertically polarized, a statistically significant diurnal difference was found.

At 15° the maximum diurnal difference was only 0.4 dB, at 55° the maximum diurnal difference was 3.5 dB. More interestingly, at 15° total backscatter was dominated by the attenuated soil backscatter, so the drop in VWC during the day results in an increase in backscatter. At 55°, total backscatter is dominated by the direct vegetation contribution and relatively insensitive to soil moisture. In this case, the decrease in VWC during the day leads to a decrease in backscatter.

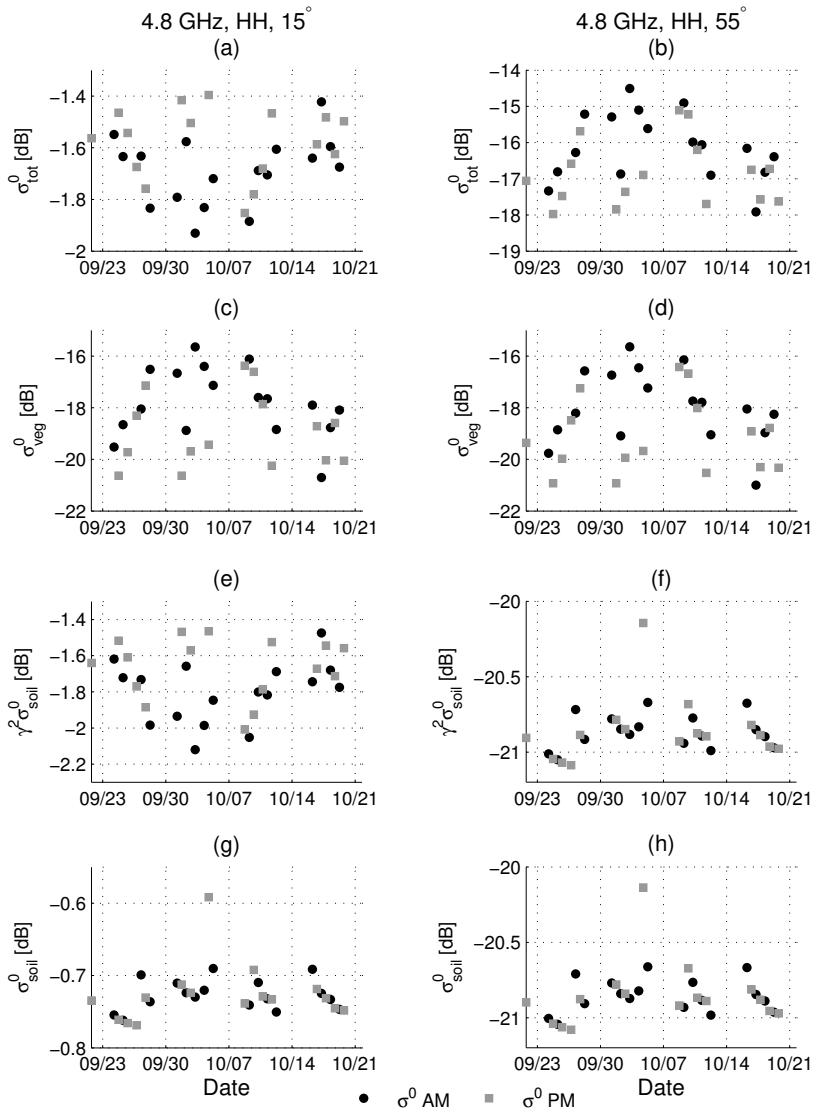

Figure 4.10: Modeled radar backscatter time series at horizontally polarized C-band (4.8 GHz) using Joseph et al. (2010), (a) - (b) total backscatter, (c) - (d) vegetation contribution, (e) - (f) attenuated soil backscatter and (g) - (h) soil contribution.

In general, vertically co-polarized backscatter is less than horizontally co-polarized backscatter due to the different impact of corn geometry on the two polarizations. Increasing incidence angles still result in a transition to vegetation dominated total backscatter, but the magnitude of backscatter values and the diurnal differences are smaller than the in horizontally co-polarized case. Diurnal differences for both 35° and 55° were not

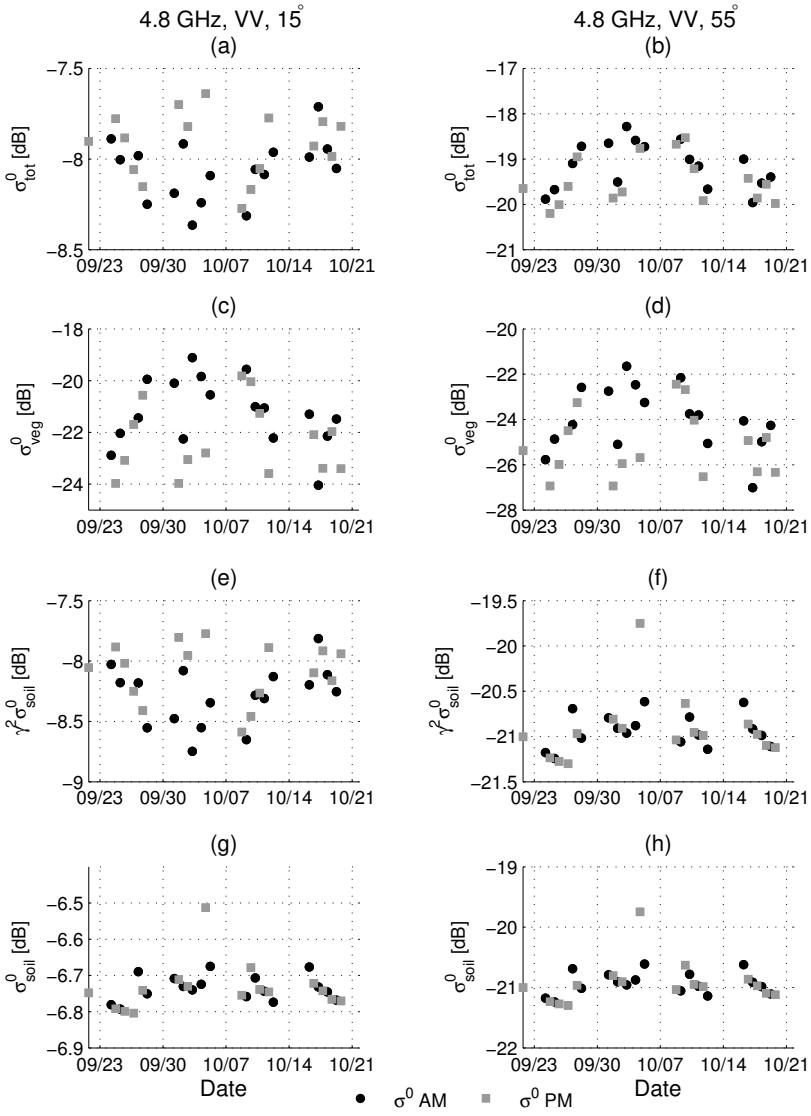

Figure 4.11: Modeled radar backscatter time series at vertically polarized C-band (4.8 GHz) using Joseph et al. (2010), (a) - (b) total backscatter, (c) - (d) vegetation contribution, (e) - (f) attenuated soil backscatter and (g) - (h) soil contribution.

statistically significant.

At C-band, diurnal differences can be attributed to changes in VWC. Close to nadir, it is mainly the attenuation that is affected. At higher angles VWC mainly influences the vegetation contribution to backscatter, which is the main contribution to total backscatter. These results have some interesting implications. First, this shows that one should be

aware of the incidence angle when measuring or combining backscatter data. At different angles, two different mechanisms are influencing backscatter (attenuation by vegetation vs. direct vegetation backscatter), which might lead to errors in soil moisture retrieval algorithms, if not taken into account properly. Second, results in Fig. 4.10 show that diurnal variations in C-band (HH) backscatter can be attributed to changes in VWC, which highlights the potential for vegetation and water stress monitoring using radar.

HIGH FREQUENCIES

Fig. 4.12 shows the modeled time series of vegetation and attenuated soil contributions to total backscatter time series for high frequencies (8.6 GHz, 17GHz and 35 GHz) using equations 4.8 to 4.14 and the parameters of Ulaby and Jedlicka (1984). For all frequencies, the direct vegetation contribution is higher than the attenuated soil contribution. As a result, the time series of total backscatter is almost identical to that of the direct vegetation contribution. The magnitude of these terms shifts slightly with increasing frequency. The vegetation contribution shifts from a -10 to -17 dB range at 8.6 GHz to a -8 to -15 dB range at 35 GHz. The attenuated soil contribution decreases from a -18 to -25 dB range at 8.6 GHz to a -20 to -27 dB range at 35 GHz. Note that the temporal change in backscatter differs significantly from that shown in Fig. 4.9 and 4.10.

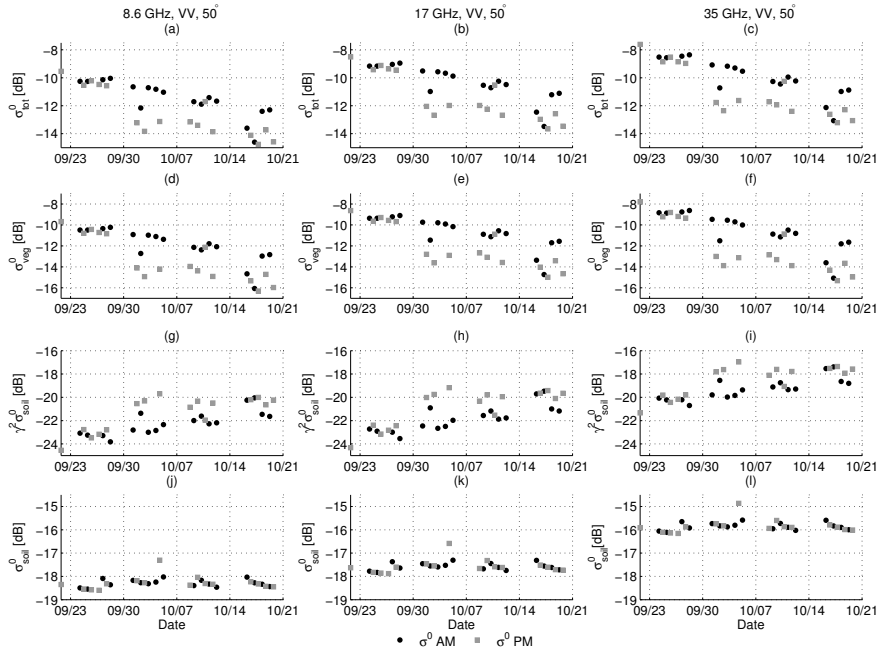

Figure 4.12: Modeled time series of vegetation and attenuated soil contributions to total radar backscatter at 8.6, 17 and 35 GHz (VV, 50°) using Ulaby and Jedlicka (1984), (a) - (c) total backscatter, (d) - (f) vegetation contribution, (g) - (i) attenuated soil backscatter and (j) - (l) soil contribution.

In Fig. 4.12, separate values for leaves and stalk water content were used with equations 4.8 to 4.12. The results in Fig. 4.11 illustrated that at high frequencies, total backscat-

ter is mainly influenced by leaf water content. Therefore, the modeled backscatter follows the change in leaf water content, rather than bulk vegetation water content. The decreasing trend in simulated backscatter is caused by the decrease observed in leaf water content. The clear distinction between morning and evening backscatter (up to 4dB at 35GHz) between September 30 and October 14, 2012 is due to the observed decrease in leaf VWC during this period. Note that this change in leaf water content is quite small relative to the bulk VWC.

A decrease in VWC can lead to either a decrease or increase in σ^0_{tot} depending on the governing contribution to σ^0_{tot}. At higher frequencies and incidence angles, where the dominant contribution is the signal from vegetation itself, a decrease in VWC during the day leads to a decrease in σ^0_{tot}. Where the attenuated σ^0_{soil} is the main contributor to σ^0_{tot}, a decrease in VWC leads to an increase of σ^0_{tot}.

This research shows that even using vertically co-polarized microwaves, the diurnal differences in backscatter can clearly be attributed to changes in VWC. It would be interesting to see how sensitive HH polarized high frequency microwaves are to changes in VWC. As shown in Fig. 4.11, HH polarized microwaves are more sensitive to changes in VWC. The close correlation between leaf VWC and backscatter highlights the potential of vegetation and water stress monitoring using high frequency radar.

4.4 DISCUSSION

Previous research investigated the influence of VWC on σ^0_{tot} from the perspective of soil moisture retrieval. Assuming that VWC changes only on a seasonal scale, vegetation is parameterized. However, given the sensitivity of radar to diurnal differences in VWC, information is lost during this process. This study shows that for different frequencies, polarizations and incidence angles, diurnal changes in VWC lead to observable variations in σ^0_{tot}. During periods of water stress, diurnal differences in radar backscatter can be attributed to vegetation, rather than changes in soil moisture. This sensitivity highlights use of VWC as a source of information for early water stress detecting in agricultural canopies and to improve vegetation and soil moisture monitoring applications using radar.

Results from this study show that for a corn canopy, diurnal variation in VWC can be the main influence on total backscatter during periods of low soil moisture variability. Data from this study suggest that VWC dynamics vary in response to water stress. During the day the amount of water stored in crops (leaves, stalks) decreases during the day by transpiration (Slayter et al., 1967; Larcher, 1995). As soil moisture decreases, more energy is required for root water uptake (Slayter et al., 1967). Plants take longer to refill, causing a change in the diurnal cycle of VWC. To fully understand the influence of canopy water dynamics on radar backscatter, more comprehensive experimental data are required.

The observed diurnal difference in VWC (30%-40%) is high and can be attributed to the structure of corn. For other crop types (e.g. alfalfa, beat, sorghum, soybean) a significant decrease in VWC results in an increase of crop transparency Consequently, the underlying soil becomes more visible and contributes more to total backscatter. Similar studies with other crops might shed light on the effect of diurnal variation in VWC of other crops on backscatter.

From Chapters 2 to 4 we see how VWC is connected to dielectric properties and radar backscatter. The significant changes in VWC affect the leaf dielectric properties (see Chapter 3). In this chapter, it is shown that this results in observable changes in radar backscatter.

4.5 CONCLUSIONS

In this chapter, we investigated the diurnal variations in vegetation water content of a corn canopy and their influence on radar backscatter. Leaf and stalk water content were determined using destructive sampling at 6AM and 6PM over a period of several weeks. A water-cloud model was used to investigate the influence that the observed differences in VWC would have on backscatter at a range of frequencies and angles.

Results from the destructive sampling showed that bulk VWC can vary considerably (up to 1 kg m^{-2}, 30%) between 6AM and 6PM, primarily due to changes in stalk VWC. Leaf VWC showed a diurnal difference up to 40 % between morning and evening. Furthermore, leaf VWC decreased with water stress. This was particularly noticeable in the early morning values.

The sensitivity study using a water-cloud model and bulk VWC demonstrated that at high frequencies and incidence angles, σ^0_{tot} is influenced by variation in both VWC and soil moisture. Fluctuations in VWC have a significant impact on σ^0_{tot}, especially when surface soil moisture is dry and fairly constant.

Using a two-layer water-cloud model at high frequencies, it was shown that the simulated difference in σ^0_{tot} could be explained by changes in leaf VWC rather than the bulk VWC. Although most of the bulk VWC is in the stalks, fluctuations in the leaf VWC can have a significant impact on radar backscatter.

Statistically significant diurnal differences in backscatter were found for 8.6, 17, 35 GHz (VV, 50°), 1.275 GHz (VV, 35°), 5.3 GHz (HH, 23°) and 4.8 GHz (HH, 15° - 35°; VV, 15°). Morning VWC was statistically significantly higher than evening VWC. When σ^0_{tot} is more sensitive to VWC, diurnal variation is caused by direct backscatter from canopy. When soil backscatter is the main contribution, changes in VWC affect the attenuation, leading to diurnal differences in σ^0_{tot}. During periods of water stress, soil moisture variation is limited and diurnal differences in σ^0_{tot} can be attributed to diurnal variation in VWC.

The results from this chapter highlight the importance of understanding the mechanisms that control vegetation and leaf water content. A more detailed understanding of leaf water content dynamics and their influence on backscatter may improve soil moisture, biomass and fuel load retrieval algorithms and shed additional light on how microwave remote sensing could be used to monitor water stress in agricultural canopies.

In chapters 2 to 4 it was demonstrated that water stress in agricultural canopies results in significant changes in leaf dielectric properties, leading to observable differences in diurnal variation in backscatter. In the following chapters we will focus on water stress in tropical forests, to investigate the impact of water stress on VWC and radar backscatter.

5

MEASURING TREE PROPERTIES AND RESPONSES USING LOW-COST ACCELEROMETERS

I'm completely lost

Bob - Lost in Translation

Trees play a crucial role in the water, carbon and nitrogen cycle on local, regional and global scales. Understanding the exchange of momentum, heat, water, and CO_2 between trees and the atmosphere is important to assess the impact of drought, deforestation and climate change. Unfortunately, ground measurements of tree properties such as mass and canopy interception of precipitation are often expensive, or difficult due to challenging environments. This chapter aims to demonstrate the concept of using robust and affordable accelerometers to measure tree properties and responses. Tree sway is dependent on mass, canopy structure, drag coefficient, and wind forcing. By measuring tree acceleration we can relate the tree motion to external forcing (e.g. wind, precipitation and related canopy interception) and tree physical properties (e.g. mass, elasticity). Using five months of acceleration data of 19 trees in the Brazilian Amazon, we show that the frequency spectrum of tree sway is related to mass, canopy interception of precipitation, and canopy-atmosphere turbulent exchange.

Parts of this chapter have been published in Sensors, 17 (5) (van Emmerik et al., 2017a).

5.1 INTRODUCTION

Trees are important contributors to the local, regional, and global water and carbon cycle (Reichstein et al., 2013; Schlesinger and Jasechko, 2014; Patton et al., 2016). Trees play a key role in the carbon cycle as they store carbon as a result of their primary production. Through photosynthesis carbon is assimilated for biomass production, and oxygen is released to the atmosphere. During this process, water is transpired through the stomata for cooling and is redistributed throughout the plant. Transpiration by trees accounts for most of the total evaporation from land on the global scale, making them a dominant contributor to the global water cycle (Jasechko et al., 2013; Schlesinger and Jasechko, 2014). The role of trees in the water cycle is even higher in tropical rainforests, where transpiration makes up to 70% of total evaporation (Schlesinger and Jasechko, 2014). Through transpiration, trees also have a large influence on soil moisture and groundwater, as their roots take up water to transport it to the stomata. Finally, canopy interception of precipitation makes up a significant part of the water cycle, as it can amount up to 15-50% of precipitation (Gerrits, 2010; Gerrits and Savenije, 2011).

The exchange of CO_2 and water are determined by the turbulent exchange between the canopy and the atmosphere (Baldocchi et al., 1991; Hollinger et al., 1994). Vegetation is a rough surface that interacts with the atmospheric boundary layer (Sellers et al., 1997). Higher turbulence results in higher rates of CO_2 and water exchange, through increased mixing (Baldocchi and Amthor, 2001). Studying the momentum transfer from wind to trees through tree sway might therefore yield information on turbulent regulation of tree photosynthesis and transpiration rates.

Measurements of tree properties such as mass, canopy interception, and tree- atmosphere interaction, offer additional insights in the role of trees in the water and carbon cycle, and how this might be affected by drought, climate change, and deforestation. Some changes in drought-induced tree mortality, and tree species distribution in response to climate change have been observed (Thuiller et al., 2011; Lindner et al., 2014). Also, it has been shown that tropical deforestation results in warmer, drier conditions at local scales (Lawrence and Vandecar, 2015). Yet, recent analyses are not conclusive, and various studies have highlighted the lack of broad empirical assessments (Stephenson et al., 2014).

Recent developments in remote sensing have allowed new analyses of the effects of droughts on vegetated areas. Friesen (2008) used radar backscatter and hydrological modeling to hypothesize that vegetation water stress affects diurnal variations in radar backscatter. This was extended by Steele-Dunne et al. (2012), where backscatter modeling was used to demonstrate the high sensitivity of backscatter to changes in vegetation water content during periods of low soil moisture availability. In this thesis (Chapter 2 to 4), actual field data was used to demonstrate that diurnal differences in vegetation water content can be associated with water stress, and have a significant effect on radar backscatter. Additional ground measurements are necessary to relate tree properties to space borne radar backscatter. Other work by Huete et al. (2006) found a green-up of the vegetation in the Amazon during severe droughts using MODIS spectral imagery, which led to a long discussion about the possible explanations for these observations. Morton et al. (2014) recently hypothesized that the original analyses were in fact based on an optical illusion, and that no actual green-up of the forest occurred. This exposed the critical

lack of ground-based observations of tree properties for calibration and validation of remote sensing data (Soudani and François, 2014). In this chapter, it is explored whether accelerometers can be used to measure relevant tree properties and responses for this purpose.

Unfortunately, key variables and fluxes such as transpiration, mass, interception capacity, canopy drag, and turbulent exchange are not easy to measure accurately. Conventional measurement equipment, such as sap flow sensors and dendrometers, use invasive techniques to measure tree water fluxes (Helfter et al., 2007), or are often expensive. Furthermore, these devices are not always robust enough to withstand the challenging field conditions in environments such as tropical forests. Using dendrometers that only measure stem diameter might also give inaccurate results, as it is required to know the relative contributions of the phloem and bark (Drew and Downes, 2009). Few methods exist to measure canopy interception and throughfall, and they often involve complicated and labor intensive techniques (Gerrits et al., 2007). Finally, many tree measurement techniques are only fit for indoor experiments (e.g., drag coefficient in tunnels (Mayhead, 1973)), or require a significant power supply (for e.g., drag coefficient (Koizumi et al., 2010) or sap flow (Burgess et al., 2001)), making them unsuitable for long term field campaigns, especially in challenging environments such as tropical forests. In this chapter we show that accelerometers are a cheap (+/-200 USD) and robust alternative for obtaining longterm data series of tree motion, which is used to infer tree properties and tree-related fluxes, such as mass, canopy precipitation interception, and turbulent exchange.

Accelerometers mounted on a tree trunk measure the sway movement of the tree. Tree sway is determined by tree properties such as mass, elasticity, wood density, and drag coefficient, and momentum in the atmosphere (Moore and Maguire, 2004). Tall, wide trees will respond differently to the same wind forcing as small, slim trees. Similarly, trees with different crown architecture (e.g., leaf size, distribution, orientation) will most likely respond differently to similar wind load. Several studies (Amtmann, 1985; Mayer, 1987; Gardiner, 1995; Peltola, 1996; Hassinen et al., 1998; Flesch and Wilson, 1999; Lohou et al., 2003; Sellier et al., 2008; Schindler et al., 2013) measured tree sway to determine the response to wind loads, mainly to study tree wind damage and tree failure mechanisms. Studying tree sway and bending in response to wind load is important for forestry, as storm damage to trees is a large source of economic loss (Mayer, 1987; Moore and Maguire, 2004). Mayer (1987) found that the primary sway of a tree (1st harmonic) is related to tree throw. Tree throw is one of the failure mechanisms which removes the whole tree, including roots, from the soil due to wind load. Mayer (1987) used accelerometers to identify the peak of the 1st harmonic in the frequency spectrum, and suggested that this can be changed to reduce the risk of storm damage, e.g., by cutting off tops, the crown, or chaining trees. To optimize wind shelter, and thereby reduce storm risk, Flesch and Wilson (1999) used tilt sensors (which measure tree inclination) to assess the influence of silvicultural management techniques on the reduction on wind throw. By comparing frequency spectra of trees for different cut-block dimensions (clear areas in forests), they provided suggestions for maximizing risk reduction. Further development of research tools to study the origin and modes of tree failures caused by wind was done by Sellier et al. (2008). They used tilt sensors to identify peaks in the frequency

spectrum of tree sway, and compared different trees to study the influence of crown architecture of trees on stability.

Earlier work by others mainly determined frequency spectra for a single moment in time using 30 minutes to 1 hour of data. Lohou et al. (2003) presented the evolution of the acceleration frequency spectrum during a day, to better understand canopy-atmosphere interactions. It was shown that tree sway primarily depends on available momentum in the wind. More recent work discussed the importance of taking temporal tree dynamics into account in analyzing tree sway. Schindler et al. (2013) deployed inclinometers on the trunk, and primary and secondary branches in broadleaved trees, and identified multiple vibration modes, which were linked to different parts of the tree. They discussed the importance of foliage phenology that might cause seasonal variation in the tree motion acceleration spectrum, as the tree properties determining the tree sway will change over time. Additional opportunities of using accelerometers to study temporal variations in tree sway has not been discussed until recently. Selker et al. (2011) suggested that changes in the frequency spectrum were related to mass variations, resulting from leaf loss or intercepted precipitation. This was based on Stewart et al. (2012), who used accelerometers for the design of hydrological measurement equipment. Stewart et al. (2012) developed a rain gauge that was able to detect changes in mass due to precipitation and evaporation. By estimating the peak frequency in the wind driven motion of a bucket on a stick, precipitation amounts were estimated with an accuracy up to 1 mm. Although trees do not exhibit similar simple behavior, the general idea that mass changes influence the frequency spectrum is still valid. Llamas et al. (2013) hypothesized that even diurnal variations in mass, e.g., as a result of changing in storage, might influence the frequency spectrum. Temporal dynamics in the frequency spectrum, and the analysis of other spectrum parameters in addition to the peak frequencies, are yet to be explored.

This study focuses on the analysis of tree sway time series collected for 19 trees in the Amazon rainforest over a five month period. The analysis aims to demonstrate the potential of using accelerometers to measure three crucial tree properties and responses: (1) mass variations, (2) interception of precipitation, and (3) tree-atmosphere turbulent interaction. Tree mass varies as a result of growth, leaf drop or development, and changes in water content. Tree mass changes diurnally, mainly due to variation in tree water content. During the day,, transpiration exceeds water uptake during the day, leading to a decrease in water content from sunrise to sunset. At night, water uptake exceeds transpiration, and water content increases again. During periods of water stress, the soil moisture availability might be insufficient for the required nocturnal refilling. In this case the diurnal variations in tree water content, and thus mass, change as a response to water stress (Slayter et al., 1967; Hsiao, 1973). Drought causes lower transpiration and carbon assimilation rates and can eventually lead to tree mortality. Therefore, field measurements of diurnal and day-to-day mass variations of trees will increase understanding of tree response to water stress. Measurements of longer-term mass changes gives insights in tree growth, and phenology. Interception of precipitation has a large impact on the hydrological cycle. Despite recent advances in simpler measurement methods (see e.g., (Friesen, 2008)), it remains difficult to quantify interception by individual trees. This is especially challenging in tropical forests, because of a substantial flow along the

trunk. Finally, tree-atmosphere interaction is the driving force that determines tree sway. The momentum transfer from the atmosphere to the canopy also regulates the exchange of heat, vapor and CO_2. Accelerometers have not explicitly been used to study temporal changes in tree-atmosphere interactions, as most measurements have been done in wind tunnels (Mayhead, 1973), or at instanteanous time (Koizumi et al., 2016).

In this chapter we discuss the concept of using accelerometers to study tree properties and responses. We give examples of several applications, which are based on measurements from a field study in the rainforest of the Brazilian Amazon. We show that measurements of tree sway can be related to tree mass variations, canopy interception of precipitation, and tree-atmosphere interaction. Finally, we provide an outlook on how accelerometers could be used in combination with auxiliary measurements to study additional tree properties and responses.

5.2 MATERIALS AND METHODS

5.2.1 THEORY

In previous work, it has been assumed that trees behave like damped harmonic oscillators (Gardiner, 1995; Peltola, 1996). To illustrate what information we can derive from tree sway measurements, we can simplify a tree as a damped mass-spring system, assuming small displacements. The displacement of such a system can be derived from Newton's second law:

$$F(t) = m\frac{d^2}{dt^2}x(t) - k_s x(t) - c\frac{d}{dt}x(t) \tag{5.1}$$

With external force $F(t)$, horizontal displacement $x(t)$, mass m, acceleration a, damping coefficient c, spring constant k_s and time t. For trees, k_s would be related to the elasticity, or wood density of the tree. Higher wood density would translate in less tree sway. In absence of external forcing F, the solution of a damped oscillator equation is:

$$x(t) = A_0 e^{-\zeta 2\pi f_0} \sin(\sqrt{1-\zeta^2}\omega_0 t + \phi) \tag{5.2}$$

With:

$$\zeta = \frac{c}{4\pi\sqrt{mk_s}} \tag{5.3}$$

$$\omega_0 = 2\pi f_0 = \sqrt{\frac{k_s}{m}} \tag{5.4}$$

With amplitude A_0, natural frequency ω_0 [rad/s] or f_0 [Hz], and phase shift ϕ. Taking the Fourier transform of equation 5.1, and multiplying with the the wind force yields (Stewart et al., 2012):

$$|H(\omega)| = \omega_\alpha \frac{1}{\sqrt{\omega_0^2 - 2\zeta^2 - \omega^2} + 4\zeta^2(\omega_0^2 - \zeta^2)} \tag{5.5}$$

where $H(\omega)$ is tree motion frequency spectrum as a function of forcing frequency, and ω_α is the amplitude of the driving wind force. It is clear from equation 5.5 that tree

motion, and its frequency spectrum is a function of mass, and the elasticity of the tree. Here, change in tree mass, elasticity, or a combination thereof should influence the amplitude spectrum, and the resonance frequency ω_0 in particular.

To approach a tree as a mass-spring system is an oversimplification. In reality, trees have a significantly more complex geometry, and therefore can be seen as a combination of multiple, possibly nonlinear, oscillators. From the momentum balance equation however, the spectrum of the tree response as function of frequency $P_y(f)$ can be estimated using (Mayer, 1987):

$$P_y(f) = |H_m(f)|^2 \rho_a^2 C_D^2 A_t^2 \bar{u}^2 H_a(f)^2 P_u(f) \tag{5.6}$$

with mechanical transfer function H_f, air density ρ_a, drag coefficient C_D, A_t, mean wind speed $\bar{u}$, aerodynamic transfer function $H_a(f)$, and power spectrum of the wind $P_u(f)$. In general, the aerodynamic transfer function can be approximated as $H_a(f)^2 = 1$, as there is a minimal turbulent storage term (Amtmann, 1985; Mayer, 1987).

Stewart et al. (2012) fit equations 5.3 and 5.5 to measured spectra to determine mass, and damping. However, this involves making the assumption that system behaves like a mass-spring system. While this may be valid for a simple rod with a bucket, it is not applicable in tree canopies, which tend to exhibit a broad spectrum. In this study, therefore, equations 5.5 and 5.6 will be used to demonstrate how the frequency spectrum of the tree response depends on important tree properties, such as mass, drag coefficient, and elasticity, and to explain changes in the frequency spectra over time, through variation in tree properties.

Two characteristics of the frequency spectrum can be considered: (1) the frequency peaks, and (2) the slope of the spectrum within a certain frequency range. Peaks in the frequency spectrum indicate resonance frequencies. These might be (multiples of) the natural frequencies of the tree, or of the various subsystems (branches, leaves). To identify peaks, the local maxima in the frequency spectrum are identified. For simple systems (e.g. as in Stewart et al. (2012)), there is one governing peak in the spectrum that governs the signal. For higher-order systems like trees, which are more nonlinear, there is no single peak but a wide spectral response.

Therefore, we also look at the logarithmic slope [dB/Hz] of the frequency spectrum. The slope of the spectrum represents the damping of the driving wind force, and can be seen as a measure of momentum transfer. As the tree movement is driven by wind, a part of the wind energy is transfered to kinetic energy in the tree. The intensity of the transfer depends on the wind speed and on the tree characteristics (such as moment of inertia, mass, and the drag coefficient). Another advantage of working in term of slope, is that it is well known that for homogeneous isotropic turbulence the wind energy spectrum is expected to follow the famous Kolmogorov cascade (-5/3 slope) (Kolmogorov, 1991).

For this research we placed 19 accelerometers on 19 trees from August to December, 2015, in the Brazilian Amazon. We measured seven different canopy species, with two to four individuals per species (see Table 1). In this study, we present a phenomenological analysis of changes in peak frequency and the logarithmic slope. We interpret these with respect to with tree properties and responses, such as tree mass, canopy interception, and canopy drag.

5.2.2 SENSOR DESCRIPTION

The accelerometer used in this study is the Acceleration Logger - Model AL100 (Oregon Research Electronics, Tangent, OR, USA, http://www.orelectronics.net), which is designed to be robust and water proof. The size is 14.5x9.2x5.5 cm, and it weighs about 400 grams (Fig. 5.1a). It can measure with a frequency of up to 25 Hz, and measures the acceleration in three dimensions. A measurement frequency of 10 Hz was chosen as an optimization between accuracy and storage requirement. For further analysis, we used the acceleration component along the axis that had the largest signal, which depends on the tree species, and the orientation of the sensor, but is generally one of the horizontal axes. Depending on the sampling rate and the environment, it can log for several months on 2 C-size cell batteries. The 8 GB data card has a capacity of 320 days with 10 Hz data. Data were stored on a micro SD card, which can be easily replaced. To prevent data loss, data is written to a newly created file every day (Wagner, 2015 (Accessed April 9, 2015).

Figure 5.1: Picture of an accelerometer installed on a tree.

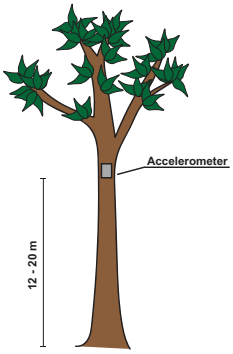

Figure 5.2: Illustration of mounting position of accelerometer in a tree.

Figure 5.3: Location of the field site in the Amazon, Brazil.

5.2.3 MEASUREMENT SETUP AND PROTOCOL

The choice of where to place the accelerometers is governed by several factors (Wagner, 2015 (Accessed August 21, 2015). The most important is finding a location on the tree with the largest displacement and thus the largest signal. However, tree geometry is complex, and placing the accelerometer in one of the branches does not yield a signal that is representative for the whole tree. As shown by Spatz and Theckes (2013), oscillations of primary and secondary branches can significantly affect the frequency spectrum. Therefore, we placed the accelerometers on the trunk, right below the crown and the point of the main branching of the tree, see Fig. 5.2. Other factors that influence the placing are accessibility (safety and convenience for attachment and data retrieval) and safety (against e.g. weather, and flora and fauna). For longer term measurements, it is advised to regularly read out the data, and to replace the batteries.

5.2.4 DATA PROCESSING

We estimate the frequency spectrum of the horizontal, single axis acceleration using a sliding window fast Fourier transform (FFT). The spectrum was estimated every 10 minutes, using a window length of 30 minutes. To improve the frequency estimation, the raw acceleration data within the 30 minute window were detrended. To prevent leakage or contamination by spectral leaking from neighboring frequencies, the data were tapered using a Hann taper on the first and last 10 % data points of the window. We present the tree acceleration frequency spectra P_y in decibels:

$$P_y = 10 \cdot log_{10}(\frac{p}{p_0}) \tag{5.7}$$

with spectrum p, and reference value p_0. For all processing we used $p_0 = 1$. For this study, the slope of the frequency spectrum between 0.2 and 1 Hz was determined every 10 minutes. As the spectra, and thus the slope, is presented on a logarithmic scale, the slope is presented as log-log slope in section 3.

5.2.5 CASE STUDY FIELD SITE AND PLANT MATERIAL

Table 5.1: Tree characteristics: Tree number, scientific name, wood density (Chave et al., 2009; Fauset et al., 2015), estimated total height and diameter at breast height (DHB).

Tree no.	Name	[10^3kg/m3]	Wood density High - Low	Height [m]	D_{BH} [cm]
1 - 3	*Goupia glabra* (brevi-deciduous)	0.7	Low	25 - 32	135.0 - 242.5
4 - 6	*Lecythis prancei* (evergreen)	0.875	Intermediate	24 - 35	108.4 - 116.5
7 - 8	*Scleronema micranthum* (evergreen)	0.6	Low	26 - 38	81.0 - 189.5
9 - 12	*Eschweilera coriacea* (evergreen)	0.8	Intermediate	18 - 27	92.4 - 268.0
13 - 14	*Dipterix odorata* (evergreen)	1.1	High	32 - 35	177.0 - 219.5
15 - 16	*Pouteria anomala* (evergreen)	0.7	Low	22 - 23	111.0 - 117.5
17 - 19	*Maquira sclerophylla* (evergreen)	0.5	Low	18 - 35	90.6 - 264.0

This study uses data from 1 August to 31 December, 2015, obtained during a field campaign at the research station in the Amazon rainforest (2.6085° S, 60.2093° W), 60 km Northwest of Manaus (see Fig. 5.3). The study area is characterized by a wet tropical climate with an average dry season from June to October. During the measurement period, sunrise and sunset occurred at around 6 A.M. and 6 P.M., respectively. Additional meteorological data (wind speed, temperature, relative humidity, wind speed, precipitation) were measured every 15 minutes at a research tower on site. A total of 19 trees were measured with accelerometers (one per tree). Seven species were measured, with 1 to 3 individuals per species. Trees were selected to cover a broad range of heights (h), widths (diameter at breast height, D_{BH}), and wood densities (ρ_w). Wood density values were taken from the Global Wood Density Database (Chave et al., 2009; Fauset et al., 2015). Total tree height was measured using measurement tape. Tree species were determined by a classified taxonomist. Diameter at breast height (DBH) was measured using measuring tape on the day of installation of the accelerometers. Based on these dimensions, we estimated the volume (V) and mass (M) of the tree trunk using:

$$V = 2\pi h(\frac{D_{BH}}{2})^2 \tag{5.8}$$

$$M = V\rho_w \tag{5.9}$$

Note that these are approximations of the volume and mass of the tree trunk only and do not include the crown. They are intended as indicative measures of volume and mass with which we can compare and explain the results from different trees.

5.3 RESULTS AND DISCUSSION

5.3.1 INTERPRETATION OF THE SPECTRUM

To illustrate how the changes in the frequency spectrum are interpreted, results are presented for two *Goupia glabra* trees. Fig. 5.4 shows the frequency spectrum of *Goupia glabra* tree 1 at three different moments (6, 8, and 10 A.M. on 13 October, 2015). For increasing wind speeds, the energy spectrum has an increasing amount of energy and several spectral peaks emerge. One of these peaks is around 0.2 Hz, which is one of the main natural frequencies of the system. The other peaks are natural frequencies of the subsystems (e.g. branches, leaves), or peaks in the forcing load. With different wind forcing, the slope of the spectrum is clearly different, which is an indicator of the degree of interaction between the wind and the tree. As the wind speed increases the slope of the spectrum between 0.2 and 1 Hz reaches a value of almost -5/3 [dB/Hz] during higher wind speeds. This indicates that the tree sway spectrum approaches the Kolmogorov (Kolmogorov, 1991) wind energy spectrum characteristic of turbulent conditions. As hypothesized by Kolmogorov, turbulent motions in the inertial subrange are statistically isotropic, and the wind energy spectrum is only a function of frequency. This implies that at high wind speeds the tree damping is minimal compared to the forcing and could potentially be used to identify drag exerted by the tree. These results suggest that accelerometers can be used to study turbulent exchange between trees and the atmosphere.

Fig. 5.5 shows the spectra of two different *Goupia glabra* trees for a five-day period, from DOY 280 to 286 (9 to 15 October, 2015). Note that the frequency is plotted on a normal scale (not in log-scale as in Fig. 5.4) At a first glance one can see that the spectra are fairly similar, however the magnitude of the acceleration spectrum (about 0.5 dB difference) and the location of the largest frequency peak are different (0.02 Hz difference). The changes in the spectrum are mainly the result of the changing wind forcing (Fig. 5.5(c)). Differences in the frequency spectra between the two trees indicate that there is variation in the amount of energy that is absorbed and damped by each tree. Given that the available wind energy is the same for both trees, the differences in acceleration spectra are due to tree specific characteristics, such as mass, catch area or drag coefficient. For the two presented *Goupia* trees, the differences between the spectra is caused by the variation in height (25m vs 32m) and diameter (135cm vs 242.5cm). A clear peak can be seen around 0.2 Hz for both trees, which is one of the main natural frequencies. This also illustrates the difficulties of analyzing the (changes in) natural frequency, as (1) the dynamic range of the natural frequency over time is very limited, and (2) the driving wind force needs to be higher than a certain threshold to activate this frequency.

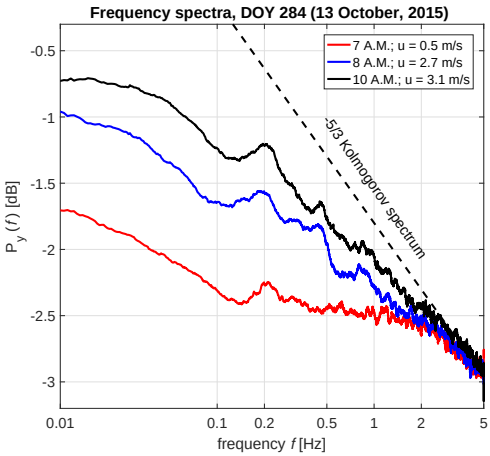

Figure 5.4: Frequency spectra of *Goupia glabra* tree no. 1 for different wind speeds on day of year (DOY) 284 (11 October, 2015), including turbulent wind spectrum (dashed black).

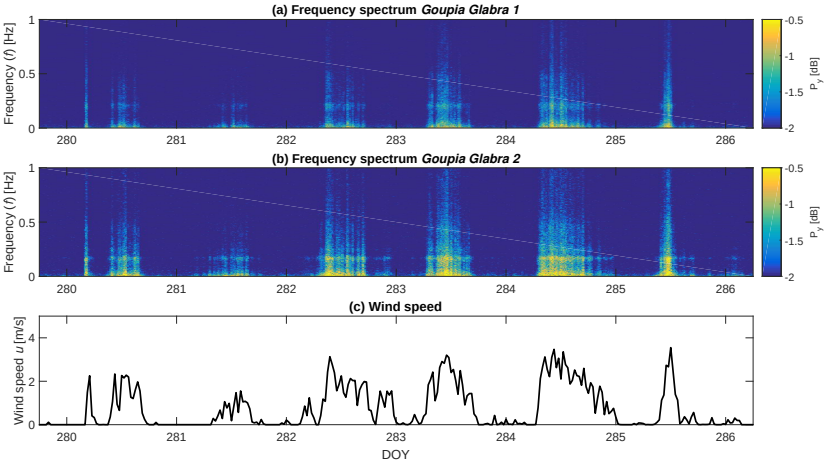

Figure 5.5: Frequency spectra of *Goupia glabra* trees no. 1 and 2 over time from DOY 280 to 286 (9 to 15 October, 2015

5.3.2 TREE MASS

The slope of the spectrum is a measure of the amount of energy transfered from the wind intro tree motion. Although taller trees catch more wind, the total energy transfer also depends on other tree properties and dimensions, such as diameter, wood density, mass, and stiffness. We also look at the sensitivity to D_{BH}/h^2, as previous work has found sensitivities of the tree sway frequency spectrum to this ratio (see e.g. Moore and Maguire (2004)). Fig. 5.6 illustrates the relationships between the mean slope of the tree response

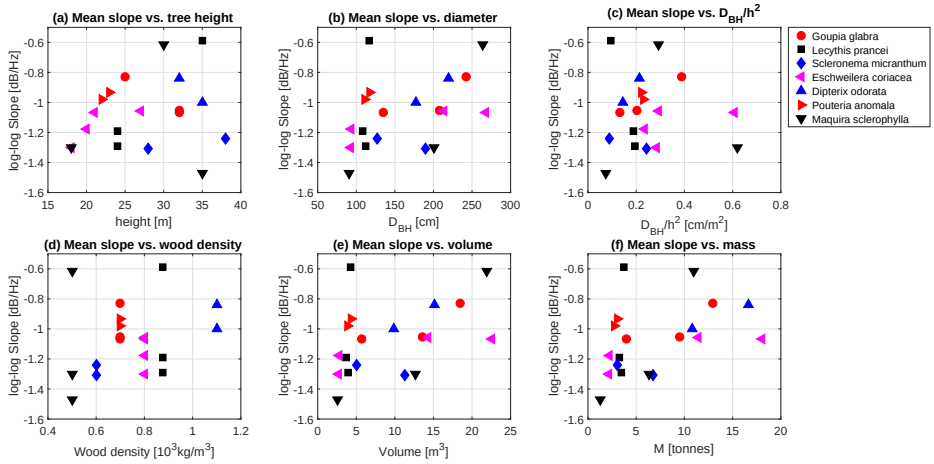

Figure 5.6: Mean slope between 0.2 and 1 Hz for each tree, plotted against (a) height, (b) diameter at breast height (D_{BH}), (c) D_{BH}/h^2, (d) wood density, (e) cylindric volume, and (f) cylindric mass.

5

frequency spectrum and tree properties. Note that we only used slopes for wind speeds higher than 2 m/s, as above this wind speed the maximum slope was reached. For the majority of the tree species, increasing height (Fig. 5.6a), D_{BH} (Fig. 5.6b), D_{BH}/h^2 (Fig. 5.6c) wood density (Fig. 5.6d) volume (Fig. 5.6e) and mass (Fig. 5.6f) corresponds with a lower slope, indicating higher damping (and hence a higher mass or stiffness). This corresponds to the idea that taller, stiffer, more robust trees, have a higher damping of the wind load. *Scleronema micranthum* trees are an exception, as both height and diameter are quite different, but the mean slope is almost equal. One of the reasons for this might be the uncertainty in the estimation of the wood density. Wood densities were estimated using the Global Wood Density Database (Chave et al., 2009; Fauset et al., 2015), as no measurements of trunk wood density were available. Another factor that influenced tree response is the crown structure and biomass. Schindler et al. (2013), for example, discussed the differences between woodland conifers and broadleaved trees. Broadleaf trees have a more complex crown structure and their sway is therefore characterized by a less dominant main axis. Additional data on the crown architecture of the trees used in this study could therefore explain the differences in measured slope of the frequency spectrum.

In all but one species we see a decreasing slope (increased damping) for increasing tree mass. This relationship between the slope of the spectra and the mass of the tree for each species, highlights the potential to measure mass in an easy and non-destructive way. Additionally, this shows that for some tree species, it might be possible to measure seasonal or even diurnal mass dynamics. By combining observations with modeling of the frequency spectrum, mass m and spring constant (tree stiffness) k can be determined separately. This allows the study of e.g. tree growth, tree responses to environmental stress, tree mortality, foliage development and loss, and tree water balance.

5.3.3 EFFECT OF PRECIPITATION

The frequency spectrum of tree acceleration is affected by precipitation events. Precipitation is associated with increased wind speed, due to cold pools generated by e.g. rain evaporation (Gentine et al., 2016), which influences the slope of the spectrum. Precipitation that is intercepted by the canopy can also lead to an increase in mass, and thus a decrease natural frequency. Fig. 5.7(a) and (b) show the changes in the spectrum and the frequency peak for increasing precipitation amounts. Note that the spectra are average spectra for the respective precipitation amounts. Fig. 5.7(b) shows the range around the frequency peak in more detail. For higher precipitation amounts, the frequency peak decreases. This is consistent with equation 5.4, as the stiffness of the system does not change. A decrease in natural frequency therefore indicates a mass increase.

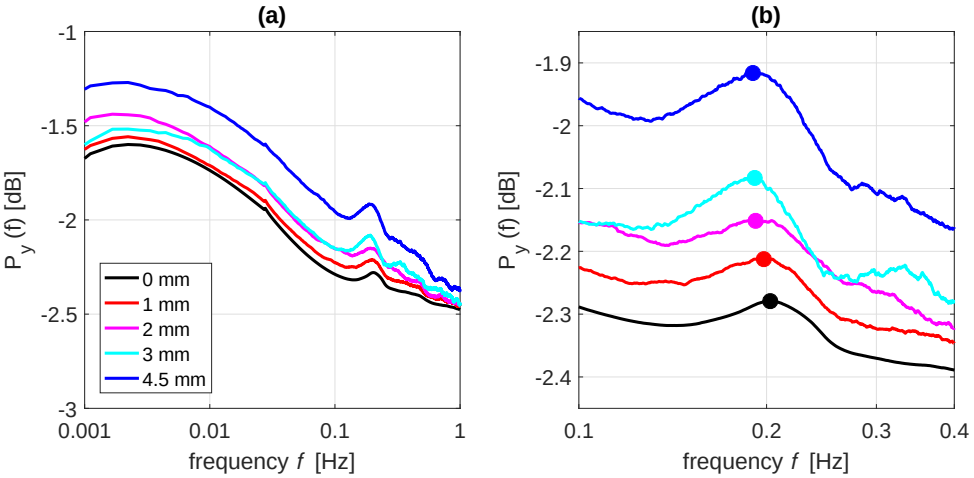

Figure 5.7: (a) Changes in the average spectra during rain events of 0, 1, 2, 3, and 4.5 mm, and (b) spectra in the natural frequency range, including frequency peaks, for *Goupia glabra* tree 1.

To further explore the sensitivity of the natural frequency f_0 to precipitation events, the difference in f_0 is plotted against the measured precipitation amount in Fig. 5.8. It can be seen that there is some variability in the degree to which this relationship can be described with a simple linear regression. For some trees (e.g. *Goupia* 2, *Scleronema* 7, *Maquira* 16), it is clear that the natural frequency decreases linearly for higher precipitation amounts. The high sensitivity of f_0 to precipitation for the *Scleronema* and *Maquira* trees might also be explained by additional mass increase through absorption of water. Both species are light wooded species, and during precipitation events these species refill internal storage (parenchyma tissue) through root water uptake. This is not the case for all trees. Some trees seem to have a change in the relationship between f_0 and precipitation amount. For example, for *Goupia* 1, *Eschweilera* 12, *Dipterix* 14, and *Pouteria* 19, f_0 seems to be linearly related to precipitation between 0 and 3-4 mm. For higher precipitation amounts the relationship becomes very uncertain.

Variations in the sensitivity of f_0 to precipitation might be explained by differences in tree height, crown architecture, or other tree properties. Fig. 5.9 therefore presents

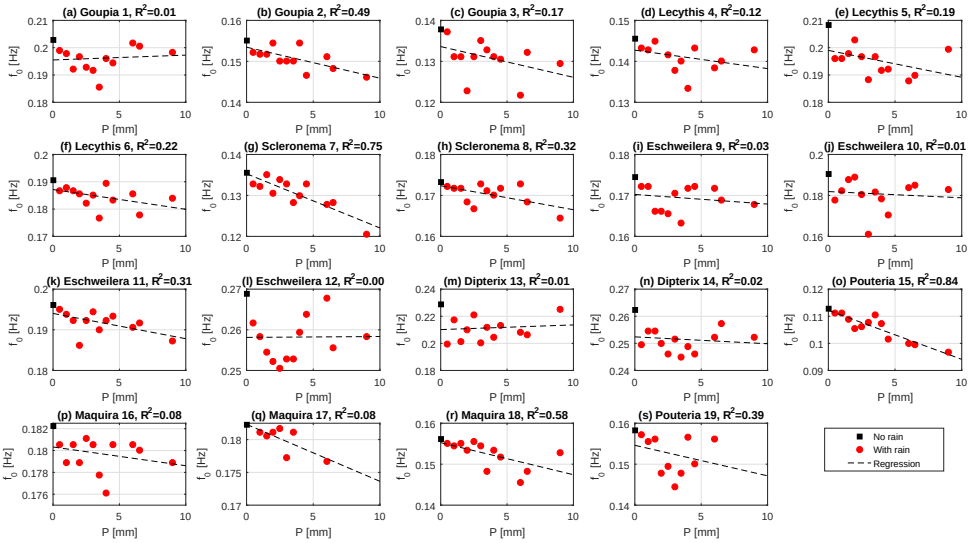

Figure 5.8: Relationship between natural frequency of the tree f_0 and the precipitation amount, for all trees. Note the first point (black square) is the natural frequency without rainfall. Also the y-axis do not all have the same scale.

the slope of the linear regressions (change in f_0 as function of precipitation, see Fig. 5.8) for each tree. To study what determines the linearity of this relationship, the slope is shown as function of height, diameter at breast height, D_{BH}/h^2, wood density, volume and mass. A steeper slope indicates a higher sensitivity to precipitation.

From Fig. 5.9 it can be seen that the sensitivity of a tree to precipitation amount is influenced by both the mechanical properties of the trees, and the location in the canopy. In Fig. 5.9(a) it can be seen that the largest trees have the highest sensitivity (-0.5 to -1.5 mHz/mm for trees higher than 30m), which can be explained by the larger amount of precipitation intercepted by the upper canopy layers. Trees with larger diameters have a lower sensitivity (Fig. 5.9(b)). This is expected, as the slope is proportional to moment of inertia, which varies with the 4^{th} power of the diameter. Trees with larger wood density, and mass (Fig. 5.9 (d), and (f)) all have a lower sensitivity to increased precipitation. Wood density is positively related to the elasticity of the tree (Evans and Ilic, 2001), and one would therefore expect a lower sensitivity to precipitation for trees with higher wood density. In addition to the elasticity, the moment of inertia considerably affects tree displacement. This is largely influenced by the tree diameter, which explains why wider trees are less sensitive to precipitation. Finally, the shorter trees intercept less precipitation than those above them.

The weaker dependence of f_0 on precipitation amount at higher precipitation values (2-4mm) could be related to precipitation intensity. Higher intensity rainfall results in splashing, causing drops to fall of the leaves. Canopy architecture also has a significant influence on the sensitivity to rainfall. Intercepted rainfall depends on the location, orientation, and size of the leaves. The sensitivity of the tree sway spectrum to intercepted rainfall is in turn influenced by leaf orientation, shape, and position with respect to the

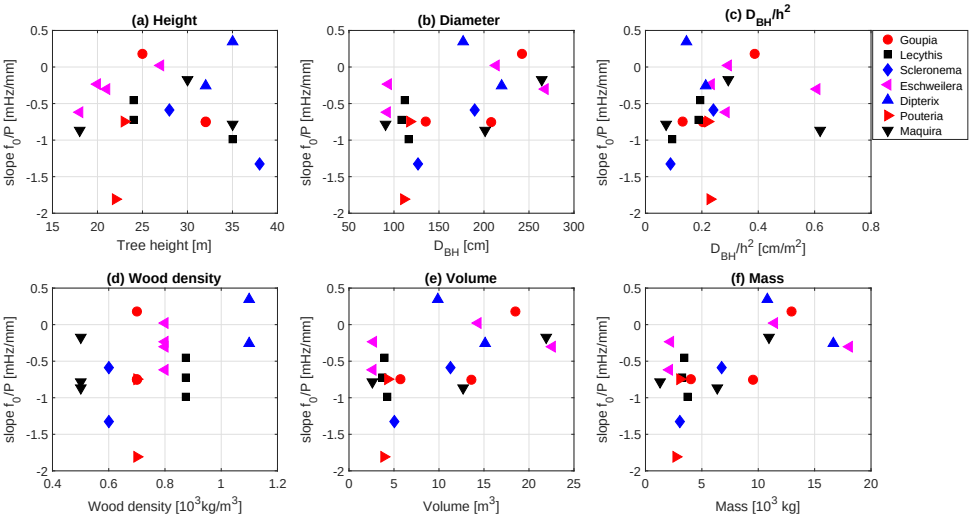

Figure 5.9: Slope of the change in natural frequency f_0 with precipitation amount [mHz/mm] against (a) tree height, (b) diameter at breast height, D_{BH}/h^2, (d) wood density, (e) volume, and (f) mass.

trunk. Additional information on canopy architecture can give insight in its influence on sensitivity of the f_0 to intercepted rainfall. This preliminary analysis suggests that it might be able to estimate canopy interception by analyzing the change in the frequency spectrum.

5.3.4 ENERGY TRANSFER FROM WIND TO TREE SWAY

Energy transfer between the atmosphere and vegetation has a significant influence on biotic and abiotic processes, such as tree mortality, and exchange of water, heat and CO_2 (Aumond et al., 2013). The amount of energy that is transfered from wind to tree motion is significantly influenced by the drag coefficient of a tree. The drag coefficient is in turn a function of tree architecture, geometry, and dimensions (Mayer, 1987; Schindler et al., 2013). As we show in Section 1, the slope of the frequency spectrum is a measure of energy transfer from the wind to the tree. As current field methods for measuring canopy drag (Koizumi et al., 2010) are difficult to apply for extended periods, especially in remote and challenging locations, we can use the slope as an approximation and analyze its variations with wind speed, dynamics in time, and differences between trees.

Fig. 5.10 presents the monthly averaged slope from August to December, 2015, for a *Goupia glabra* (a), *Lecythis prancei* (b), and *Scleronema micranthum* (c) trees. Drag coefficient is a function of wind speed (Stull, 2012), as vegetation streamlines and reconfigures as wind speed changes (Koizumi et al., 2010; Whittaker et al., 2015; Koizumi et al., 2016). Generally, higher wind speeds result in lower drag coefficients for trees. As wind speed increases from 0 to 1.5 m/s, the slope, and thus energy transfer, increases. This means that for increasing available wind energy, relatively less energy is transferred into tree motion, indicating a lower drag coefficient. The rate of energy transfer clearly varies per month as function of wind speed, and between trees. For all three trees the energy

transfer seems to increase between August and December, 2015. This is most likely a reflection of phenological changes, such as leaf flushing or drop (Lopes et al., 2016). Also the differences between trees are considerable. The inflection point for the *Scleronema micranthum* tree is less clear, indicating a higher drag coefficient than the *Goupia glabra* and *Lecythis prancei* trees. The *Lecythis prancei* shows the largest dynamic range over time, with a difference in maximum slope of 0.6 for wind speeds over 2 m/s between August and December, 2015, against an almost negligible difference for the *Goupia glabra* tree. Recall from equations 5.1-5.6 that drag coefficient, catch area and mass are important parameters that determine the energy transfer from atmosphere to tree. The large variations observed for *Lecythis* are therefore likely to be caused by changing tree properties, for example leaf drop between August and September, 2015.

We show that accelerometers might be a useful method to study the interaction of a tree with the atmosphere. In large eddy simulations and meteorological models, the drag coefficient is often assumed constant in time and space (Shaw and Schumann, 1992; Shao et al., 2013; Aumond et al., 2013). Results presented here suggest that tree drag coefficient is variable in space and time, following changes in tree leaf biomass changes. Combining our results with auxiliary data, particularly high temporal resolution wind data, may allow us to derive the absolute drag coefficient for each tree. Also, additional information on canopy architecture will give insight in the influence of canopy architecture on the relation between the slope and wind speed, and therefore on energy transfer from atmosphere to individual trees. Future work will focus on further analysis on the temporal, spatial, and between-tree variation in energy transfer between atmosphere and trees.

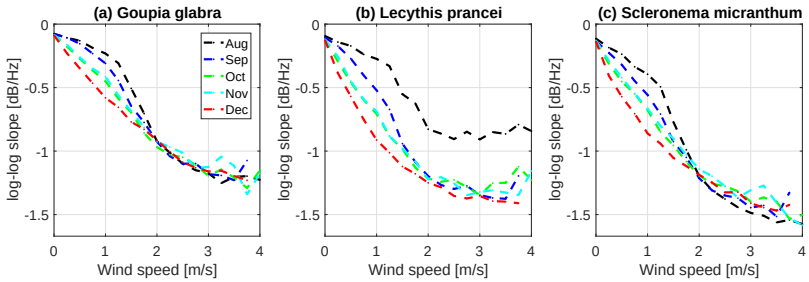

Figure 5.10: Average slope as function of wind speed from August to December, 2015, for (a) *Goupia glabra*, (b) *Lecythis prancei*, and (c) *Scleronema micranthum*.

5.3.5 SYNTHESIS AND OUTLOOK

We show several examples of information that can be extracted from analyzing frequency spectra of tree motion. We demonstrate that we can detect differences in mass, and turbulent exchange between and within species, through the relationships between the slope of frequency spectra (damping) and mass. More interestingly, this might allow analyzing seasonal or even diurnal variation in tree mass. This means that accelerometers might be used to track growth of trees, or monitor changes in diurnal mass affiliated with changing water content. Potentially, accelerometers can give more insights in the

changes in tree properties and dynamics in response to drought.

Further exploration of the possibilities of quantifying canopy interception of precipitation might contribute to a better understanding of the water cycle in forest ecosystems. Interception is one of the most important parts of the hydrological cycle. Unfortunately, it is also difficult to measure, especially on larger scales. Validation studies, including additional throughfall, stem compression measurements (Friesen, 2008), above and below canopy evaporation measurements (Schilperoort et al., 2016), or stable isotopes to separate evaporation fluxes (van Emmerik et al., 2012), will shed light on the possibilities of measuring canopy interception of individual trees using accelerometers. Note that rainfall events that occur during low wind speeds will remain difficult to detect, due to a lack of tree sway.

A novel approach is presented, using accelerometers to study the interaction between trees and the atmosphere. So far, most studies derived drag coefficients from wind speed and eddy flux measurements. Additional long time series of tree sway will increase understanding of energy and momentum transfer by individual trees. Dynamics in the energy absorption and damping might in future applications also be coupled to seasonal and diurnal mass variations due to growth, or water stress, for example to study the changes in canopy-atmosphere interaction during the dry season.

Other applications might include studying tree mortality, and wind-damage. As accelerometers are cheap and robust sensors, they might be used to study tree dynamics and properties for validation of remote sensing products in more challenging environments.

5.4 CONCLUSIONS

Accelerometers were deployed on a broad range of trees in the Amazon. They are simple, cheap and robust sensors that can last in challenging environments. We show how they can be applied in a tropical forest, and how with simple data processing algorithms valuable information on tree properties and responses can be extracted.

The slope of the frequency spectrum is related to tree mass. For all but one species, increasing tree mass clearly resulted in a lower slope. Future work will use additional data, such as throughfall, stem compression, evaporation and transpiration, to relate the frequency spectrum to mass changes due to growth on seasonal, and changing water content on a diurnal scale.

The frequency spectrum shows a clear response to precipitation events. The observed decrease in natural frequency is associated with an increased mass, due to water stored on the canopy. For several trees the relationship between natural frequency and precipitation amount is linear, which highlights the potential of using accelerometers to estimate canopy interception by individual trees.

Preliminary results demonstrated variability in canopy-atmosphere interaction, in space and time. Changes in the frequency spectrum can be associated with variation in tree drag coefficient. The results suggest that the tree drag coefficient is more variable than currently assumed.

The affordable, easy-to-apply, robust, accelerometers used in this study provide a promising complementary technique to current measurement techniques. The results presented here demonstrate that low-cost accelerometers can yield valuable insight into

tree properties and responses. Longer deployments and their combination with other instruments in experimental studies is encouraged to reveal their full potential and to identify additional applications in vegetation monitoring.

6

Water Stress Impacts Tree-Atmosphere Interaction in the Amazon

Wenn der Wind weht,
So regen sich die Bäume

Saxon proverb

Land-atmosphere interactions depend on momentum exchange from the atmosphere to the canopy, which depends on the tree drag coefficient. It is known that the drag coefficient, and thus tree-atmosphere interaction, can vary strongly within a canopy. Yet, only few measurements are available to study the variation of tree-atmosphere interaction in time and space, and in response to vegetation water stress. In Chapter 5, Accelerometers were used to derive a measure of tree-atmosphere interaction for 19 individual trees of seven different species in the Brazilian Amazon. This Chapter demonstrates that under field conditions, tree-atmosphere interaction can vary considerably in time and space. The five-month measurement period included the transition from wet to dry months. We demonstrate that increased tree water deficit is related to observed changes in tree-atmosphere interaction, which is hypothesized to be caused by drought induced changes in tree mass.

Parts of this chapter are used in (van Emmerik et al., in review).

6.1 INTRODUCTION

The atmospheric boundary layer state is directly influenced by the surface. In turn, the atmosphere influences the land surface state through land-atmosphere interactions (Gentine et al., 2011, 2012; Green et al., 2017) Land-atmosphere interactions influence meteorological and hydrological fluxes and states, and biotic and abiotic processes, such as seed and pollen distribution (Katul et al., 2005), deposition of atmospheric pollutants (Clifton et al., 2017), and exchange of water, heat and CO_2 (Aumond et al., 2013).

Land-atmosphere interactions depend on the momentum exchange from atmosphere to the canopy, which highly depends on the turbulent drag coefficient of individual trees (Poggi and Katul, 2007). Drag causes loss of momentum, and the interplay between canopy and atmosphere is heavily affected by the transport of water, heat, and carbon between vegetation and the atmosphere (Molina-Aiz et al., 2006; Cescatti and Marcolla, 2004). In meteorological models, large-eddy simulations, and land surface models, tree-atmosphere interaction plays a crucial role in describing energy and momentum transfer from the atmosphere to the canopy. Energy and momentum transfer between trees and atmosphere greatly depend on the tree drag coefficient (Gillies et al., 2002). For computational ease, the drag coefficient is often assumed constant (Cassiani et al., 2008; Dupont and Brunet, 2008; Katul et al., 2006), both in time and space. It is known, however, that the drag coefficent, and thus the degree of tree-atmosphere interaction, can vary strongly within a canopy, and as a function of environmental conditions (Belcher et al., 2012). Assuming a constant drag coefficient may therefore be unrealistic, and introduces a large source of error.

Misrepresentation of the variability in canopy drag is largely due to a lack of (field) data. Various studies have quantified canopy drag (coefficients) in laboratory and field setups (Mayhead, 1973; Koizumi et al., 2010). Widely used drag coefficients for several tree species originate from a wind tunnel experiment by Mayhead (1973). Here it was found that drag coefficient is variable between species, and strongly depends on wind speed. Most wind tunnel studies used dwarf species, juvenile crowns, or model trees or forests, which are not representative for actual-sized trees under natural conditions (Johnson et al., 1982; Rudnicki et al., 2004; Vollsinger et al., 2005; Meroney, 1968; Novak et al., 2000; Guan et al., 2003; Poggi and Katul, 2007). Recent work (Koizumi et al., 2010, 2016) presented a novel field method that can measure stem deflection, which is used to derive the tree drag coefficient. However, this method requires a considerable amount of power, making it difficult to obtain long time series. This is especially a problem under field conditions, where power supply is limited.

The measurement technique presented in Chapter 5 used low-cost accelerometers to measure tree sway. Tree sway is a result of momentum transfer from the atmosphere to the tree, and can therefore be used to study tree-atmosphere interaction. The robustness of the sensors allows deployment in harsh conditions such as tropical environments, to obtain long time series. This Chapter uses tree sway measurements obtained during a five month period to quantify and compare the tree-canopy interaction for 19 tree in the Brazilian Amazon. The measurement period includes the transition from wet to dry months. We derived a measure for canopy-atmosphere interaction, showing clear variation between between species, over time, and response to tree water deficit.

The Amazon contains half of the world's rainforests. Yet, it remains a poorly under-

stood component of the global carbon and water cycle (Saatchi et al., 2007; Binks et al., 2016; Anber et al., 2015). For example, the extensively studied 2005 drought reversed the Amazon from a long-term carbon sink into a carbon source (Phillips et al., 2009). Amazon forests appear to be sensitive to increasing moisture stress (see Chapter 7), and future droughts have the potential to considerably change the water and carbon balance (and thus climate change) (Phillips et al., 2009). Improved understanding of the variation and dynamics of the drag coefficient will therefore contribute to a better understanding of the Amazon's role in the water and carbon cycle, and its response to deforestation.

A long time series of tree acceleration data was used to investigate tree-atmosphere interaction under field conditions, and in response to increased tree water deficit. This Chapter aims to shed a new light on the spatiotemporal variation in tree-atmosphere interaction. Specifically, we demonstrate the effect of increased tree water deficit for various tree species and individuals. We hypothesize that observed variations are related to vegetation water stress induced mass changes in the trees.

6.2 METHODS

6.2.1 STUDY AREA

The field measurements of this Chapter were obtained from August, 2015 to January, 2016 at the K34 research station in the Amazon rainforest (2.6085° S°, 60.2093° W), 60 km Northwest of Manaus, Brazil. The study area is characterized by a tropical monsoon climate with an average dry season from June to October. During the measurement period there was about 12 hours of daylight, roughly between 6 A.M. and 6 P.M. local time. Meteorological data was measured at a flux tower on site. Wind speed, temperature, and precipitation were measured every 15 minutes. For this Chapter, we use data from the period August, 2015 to January, 2016.

6.2.2 PLANT MATERIAL

A total of 19 individual trees were measured during this experiment, covering seven tree species, and a broad range of average height and wood density. An overview of the sampled tree species can be found in the Supplementary materials (Table 1). Wood density values were taken from the Global Wood Density Database (Zanne et al., 2009). Total tree height was measured using measurement tape. Tree species were determined by a classified taxonomist. Diameter at breast height (DBH) was measured using measuring tape on the day of installation of the accelerometers, between 28 July and 1 August, 2015. Volume and mass were estimated from the estimated tree dimensions using:

$$V = 2\pi h \frac{D_{BH}}{2}^2 \tag{6.1}$$

$$M = V \rho_w \tag{6.2}$$

With tree height h, diameter at breast height D_{BH}, mass M, volume V, and wood density ρ_w. These are approximations of the cylindric volume and mass, and do not include the crown.

6.2.3 EXPERIMENTAL SETUP

Water proof, robust accelerometers (Acceleration Logger - Model AL100, Oregon Research Electronics, Tangent, OR, USA, http://www.orelectronics.net) were used to measure three-dimensional acceleration with a frequency of 10 Hz. The accelerometers were placed directly below the main branching of the tree, so as to measure the largest signal can be measured, and to minimize effect of oscillations from primary and secondary branches (Spatz and Theckes, 2013). Detailed information on the accelerometer and applications can be found in Chapter 5.

Dendrometers (ZN12-T-2IP, Natkon.ch, Switzerland) were installed at 1.5 meters above ground level. Bark thickness was measured every 10 minutes. Bark time series were detrended for growth in order to use it as a direct measure of water deficit in trees. For this, the growth line of the species was determined, based on the local maximum values of stem radius (Zweifel et al., 2005; Ehrenberger et al., 2012). The actual water deficit was calculated by subtracting the measured changes in stem radius from the growth line.

$$\Delta W = D_{b,pot} - D_{b,act} \tag{6.3}$$

With total water deficit ΔW, growth line $D_{b,pot}$, and change in bark thickness $D_{b,act}$.

6.2.4 RELATING WIND TO TREE MOTION

The relation between the input wind energy spectrum P_w, and the output energy spectrum of tree motion P_y, both as function of frequency f can be described as:

$$P_y(f) = |H(f)|^2 \rho_a^2 C_D^2 A^2 \bar{u}^2 H_a(f)^2 P_u(f) \tag{6.4}$$

with mechanical transfer function H, air density ρ_a, drag coefficient C_D, tree catch area A, mean wind speed $\bar{u}$, aerodynamic transfer function $H_a(f)$, and power spectrum of the wind $P_u(f)$. In general, the aerodynamic transfer function can be approximated as $H_a(f)^2 = 1$, as there is a minimal turbulent storage term (Amtmann, 1985; Mayer, 1987).

The energy conservation and dissipation of wind turbulence depends on the scale. Large scale eddies (low frequencies) are energy containing, whereas energy dissipation mainly happens at smaller molecular scales (higher frequencies). The range in between, the inertial subrange, is where energy is transferred from low to high frequencies. Kolmogorov (1941) hypothesized that at high Reynolds numbers and under homogeneous and isotopic turbulence the inertial subrange would follow a -5/3 spectrum. The energy content P_w within the inertial subrange is a universal function of the frequency, and can therefore be expressed as (Stull, 2012, p. 390 – 391):

$$P_w = C\epsilon^{\frac{2}{3}} f^{\frac{-5}{3}} = A f^{\frac{-5}{3}} \tag{6.5}$$

With constant C, dissipation rate ϵ, frequency f. Wind in forest canopies also exhibit this spectrum (Flesch and Wilson, 1999; Odijk, 2015). For turbulent conditions, the input wind spectra (see eq. 3) and its slope are known. Comparing the input Kolmogorov wind spectrum with the output tree acceleration spectrum therefore gives a measure of the momentum damping/absorption by the tree. For eqs. 4 and 5, a constant value for the wind spectrum slope (-5/3) is used in subsequent analyses.

With known acceleration and wind spectra, we can find an expression for the transfer function, which is a measure of tree-atmosphere interaction. We use the slope of the acceleration and wind spectra:

$$\frac{dP_y}{df} = H^2 \rho^2 A^2 C_d^2 u^2 \frac{dP_w}{df} \tag{6.6}$$

$$s_a = \alpha C_d^2 u^2 s_w \tag{6.7}$$

$$\alpha C_d = \sqrt{\frac{\frac{s_a}{s_w}}{u^2}} \tag{6.8}$$

with acceleration and wind spectra slopes s_a and s_w, and transfer parameter α. The combined term αC_d is used as an expression for tree-atmosphere interaction, and accounts for the combined effect of e.g., drag coefficient, mass, density, wind catch area.

Interaction between wind and a tree is a function of wind speed. As e.g. Mayhead (1973); Koizumi et al. (2010), have shown, the drag coefficient and momentum transfer decrease with increasing wind speed. This is mainly due to streamlining of the tree, which decreases the catch area of the tree. In this Chapter, we analyze the changes in the relation between the measure of tree-atmosphere interaction αC_d and wind speed. For each week, the following function is fit to the relation between wind speed u and αC_d:

$$\alpha C_d = A \cdot \exp(-\beta \cdot u) \tag{6.9}$$

with $A = 1$, and damping parameter β. β determines the shape of the relation, and describes how the tree-atmosphere interaction changes with wind speed. The value of β is therefore used to track the variation in tree-atmosphere interaction over space and time. For better comparison between individual trees, β is presented normalized by the mean value for β per individual tree.

6.2.5 DATA PROCESSING

We estimate the frequency spectrum of the horizontal, single axis acceleration using a sliding window fast Fourier transform (FFT). The spectrum was estimated every 10 minutes, using a window length of 30 minutes. The slope of the spectrum represents the damping of the driving wind force by the tree, and can be seen as a measure of energy and momentum transfer (Chapter 5). As tree movement is driven by wind, a part of the wind energy is transferred to kinetic energy in the tree. For this study, the slope of the frequency spectrum between 0.2 and 1 Hz was determined, for every 10 minutes. The slope is presented on a logarithmic scale [Hz/dB].

6.3 RESULTS

6.3.1 ACCELERATION SPECTRA SLOPE

Fig. 6.1 presents a typical acceleration energy spectrum for a *Goupia glabra* tree, for three different wind speeds. For increasing wind speeds, the slope of the spectrum approaches the Kolmogorov -5/3 spectrum. As hypothesized by Kolmogorov (1941), turbulent motions in the intertial subrange are statistically isotropic, and the wind energy spectrum is only a function of frequency.

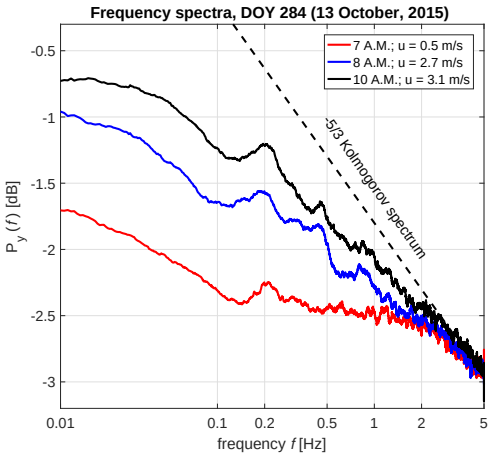

Figure 6.1: Frequency spectra of a *Goupia glabra* tree for different wind speeds on day of year (DOY) 284 (11 October, 2015), including turbulent wind spectrum (dashed black), taken from Chapter 5.

The slope varies over time, and per tree species and individual. Fig. 6.2 presents the acceleration spectra slope s_a for each tree, grouped per tree species. As expected, the slope of the acceleration spectrum increases with wind speed. The timing and magnitude does change per tree. For example, the *Scleronema* trees (Fig. 6.2C) have a consistently higher slope (1.4 Hz/dB during the day) than the *Dypterix* (Fig. 6.2E) trees (1 Hz/dB during the day). The sum of the differences between trees are captured by the paramter αC_d, which will presented later. Other clear differences can be seen between indiduals of different species. Where for the *Scleronema* (Fig. 6.2C) and *Pouteria* (Fig. 6.2F) trees the slope is similar between the individuals, for *Maquira* (Fig. 6.2G) and *Lecythis* (Fig. 6.2B) the variation between the individuals is considerably larger.

6.3.2 TREE-ATMOSPHERE INTERACTION ACROSS TIME AND SPACE

The interaction between trees and the atmosphere is expressed by the αC_d, which included effects of mass, geometry, wind catch area, and drag coefficient (see eq. 8). Streamlining of a tree for increasing wind speed affects the relation between αC_d and wind speed (Mayhead, 1973; Koizumi et al., 2010), as can be seen in Fig. 6.3. Here, the monthly averaged relation between αC_d and wind speed are presented for August to December, 2015. For wind speeds between 0 and 3-4 m/s, αC_d decreases, with the highest decrease between 0 and 1-1.5 m/s. For higher wind speeds αC_d becomes more stable. It can be seen that for αC_d varies considerably between individual trees, and that the relation between αC_d and wind speed changes over time. For example, the range of αC_d at 1 m/s changed from 0.3-0.6 to 0.4-0.8 between August and December, 2015. It is hypothesized that this is due to changes in mass, related to e.g. water content or leaf fall.

6.3.3 EFFECT OF DRY MONTHS

To further explore the changes in the relation between αC_d and wind, this relation was fit for each week of available data. The most important parameter is the damping co-

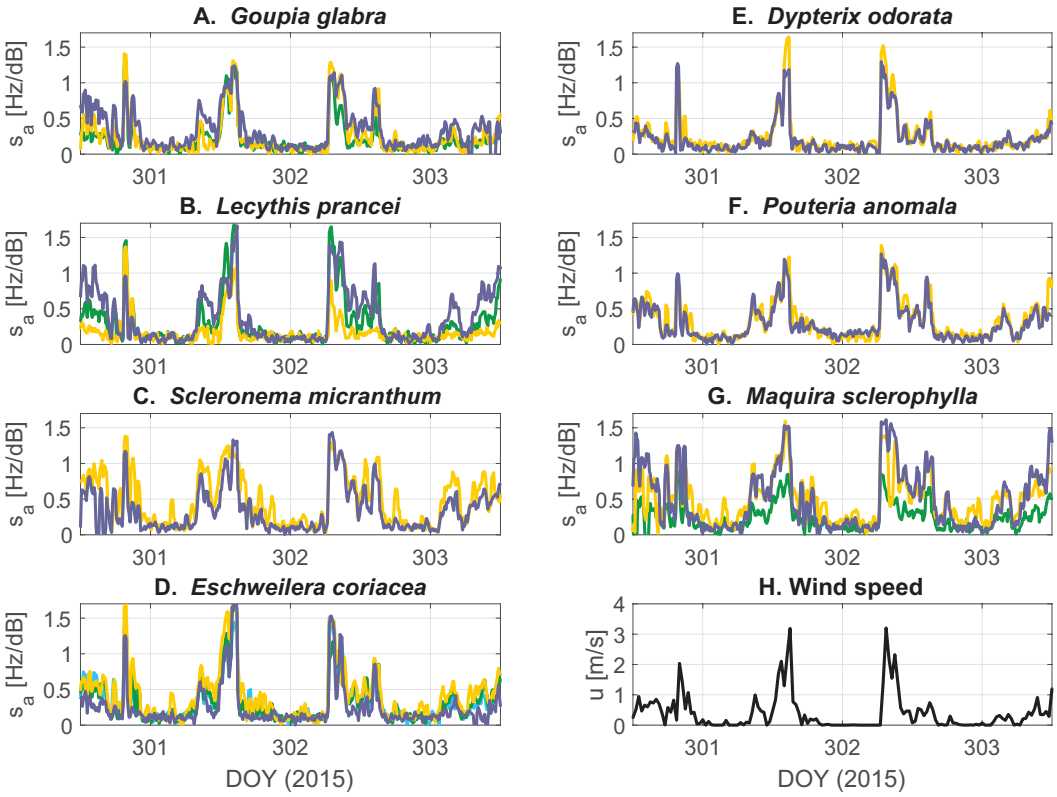

Figure 6.2: Tree acceleration spectra slope s_a [Hz/dB] over time for DOY 301 to 306 (2015), for A. *Goupia glabra*, B. *Lecythis prancei*, C. *Scleronema micranthum*, D. *Eschweilera coriacea*, E. *Dypterix odorata*, F. *Pouteria anomala*, G. *Maquira sclerophylla*, and H. wind. Each line in A-G. represents an individual tree.

efficient β (see eq. 9). Fig. 6.4 presents the weekly values for the normalized damping coefficient β between August (DOY 220) and December (365), 2015. Recall that for the normalization, time series of β are normalized by the average value of β for each individual tree. Tree water deficit measurements were also available, and are also shown in Fig. 6.4. As most trees showed similar temporal behavior, the figure presents the average water deficit based on all trees, including the minimum and maximum of the measured range.

Between DOY 230 and 280 β decreased while water deficit increased. Although water deficit decreased steeply between DOY 280 and 285, β continued decreasing until around DOY 300. Water deficit remained relatively stable between DOY 285 and 340, after which a steep increase was observed between DOY 340 and 360. β recovered between DOY 300 and 340, and decreased again between DOY 340 and 360. Changes in β are hypothesized to be caused by changes in mass related to water content, or leaf fall. The increase in water deficit supports this hypothesis, as a decreasing/increasing β

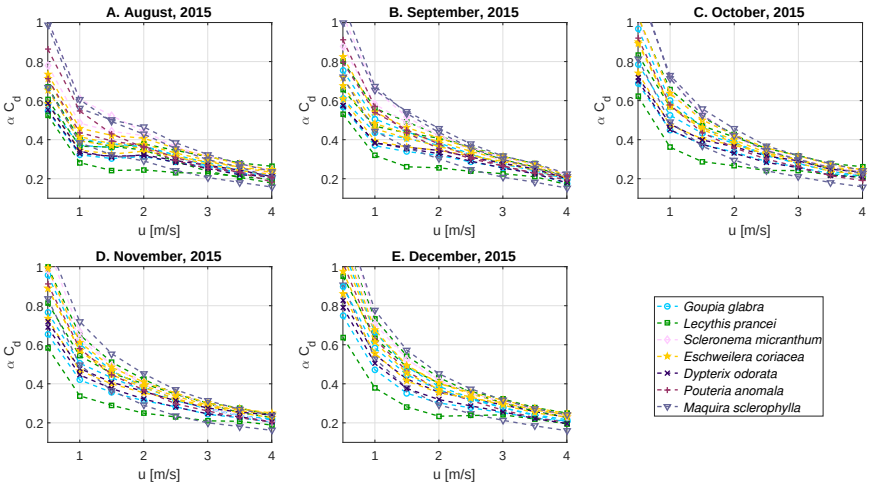

Figure 6.3: Monthly averaged tree-atmosphere interaction αC_d per individual tree as a function of wind speed u [m/s] for A. August, 2015, B. September, 2015, C. October, 2015, D. November, 2015, and E. December, 2015.

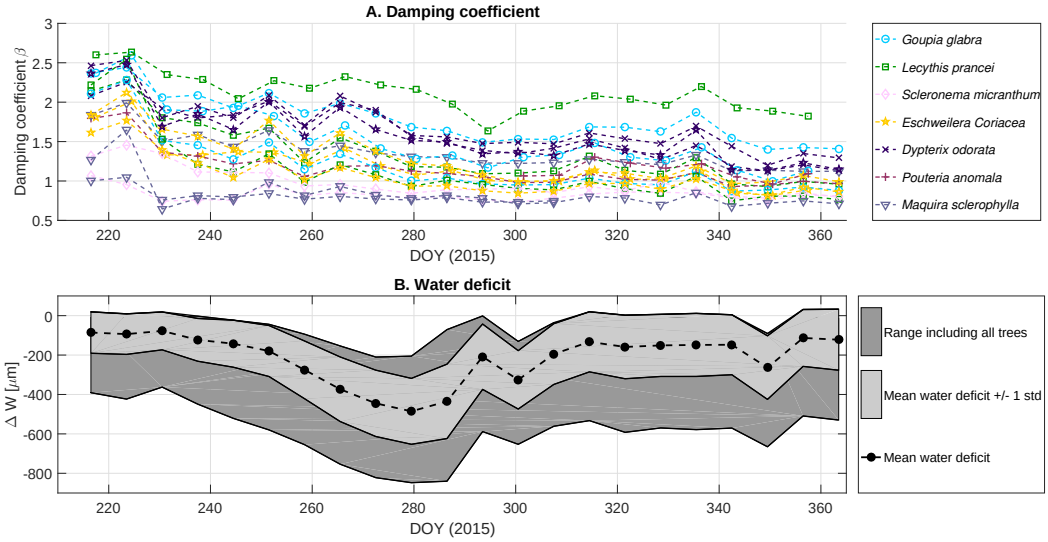

Figure 6.4: A. Normalized damping coefficient β for each individual tree, and B. mean, mean +/- 1 standard deviation, minimum and maximum water deficit ΔW, for every week from DOY 218 (August) to 365 (December), 2015.

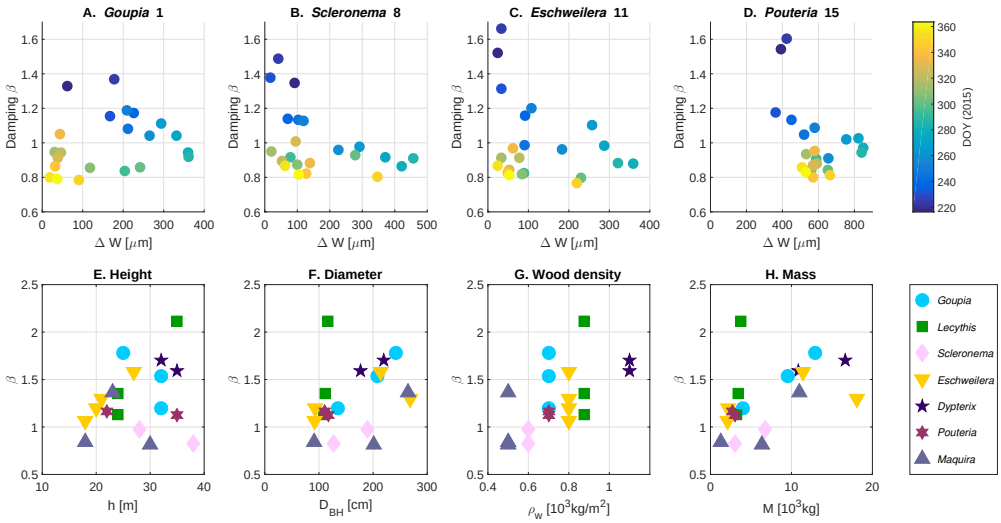

Figure 6.5: Damping coefficient β (for fitted function αC_d vs. u) for a single A. *Goupia*, B. *Scleronema*, C. *Eschweilera*, and D. *Pouteria* tree, versus water deficit ΔW, colored by day of year (DOY, 2015), and average damping coefficient β in relation to E. tree height h, F. diameter at breast height D_{BH}, G. wood density, and F. Mass, for each measured tree.

coincided with inverse changes in water deficit.

Fig. 6.5 presents the relation between β, water deficit and DOY for four trees. Here, it can be seen that there is a clear relation between increasing water deficit and decreasing β. When water deficit increases, β drops significantly (DOY 220 to 250). For higher water deficit (DOY 250 to 300), β decreases more gradually. For the recovery (DOY 300 to 340), when water deficit decreases again, the relation between β and water deficit is different. Here, β only increases gradually again for decreases water deficit. For the increase in water deficit between DOY 340 and 360, a drop in β can be seen for the *Goupia*, *Scleronema*, and *Eschweilera*.

To explore what might explain the variation in β, Fig. 6.5E-H. present the average value of β (for August to December, 2015) in relation to the estimated physical tree properties. As expected, the interaction between tree and atmosphere is the sum of various different factors. In general, it can be seen that for increased height, and diameter at breast height β is higher. It can also clearly be seen that for increased wood density the average β is higher, which can be explained by the coinciding increase in tree stiffness. We also see that there is a relation between mass and β for all trees, and for each tree species separately. Higher tree mass results in higher β. This suggests that changes in β can be explained by water variations, due to for example leaf flush or fall and water content related mass changes.

The relation between β and can explain the observations in Fig. 6.4 and 6.5A-D. During periods of increased water deficit during the dry months, β clearly decreases for

each tree. The increased water deficit suggests that this is due to water content related mass changes in the vegetation, such as decreasing tree water content and increased leaf fall during dry months. The relation between mass and β supports this hypothesis, as the observed decrease in β might be explained by decreasing tree mass during the dry months.

6.4 DISCUSSION

The results presented in this Chapter show that the degree of tree-atmosphere interaction varies considerably between species. Previous work has shown this for some species using wind tunnel experiments. This Chapter uses *in situ* measurements to demonstrate the variation in tree-atmosphere interaction in the field. Besides variation in space, significant temporal variation in tree-atmosphere interaction was found. To our knowledge, this is the first time that this has been measured under field conditions.

Changes in tree-atmosphere interaction seem to be related to vegetation water stress. For increased water deficit, measured on the tree, β decreased. There are two mechanisms that might explain the changes in β during increased water stress. First, tree mass might change through changes in water content. As insufficient water is available to refill the storage, tree water content decreases with continuing water stress. Second, increased water stress might also lead to leaf fall, which for some trees might also affect the total mass significantly (Lopes et al., 2016). Leaf fall is a direct consequence of drought-induced tree water deficit (Reich and Borchert, 1984). Peak rates of leaf fall almost always occur during the dry months in tropical forests (Wright and Cornejo, 1990). This might explain the quick response to increased tree water deficit. When tree water deficit is low again, one might expect a recovery in β as well. However, if β is mainly changed due to leaf fall, the recovery might be delayed significantly. Leaf expansion might occur only a few weeks during the early wet months (Reich and Borchert, 1984), growth of new leaves only occurs as long as soil moisture is plentiful (Bordiert, 1994). Absence of these conditions could explain the slow response in β.

The impact of water stress on tree-atmosphere is a significant finding, as this shows that tree-atmosphere interaction is also affected by the dry months, in addition to the general spatiotemporal variation. This sheds a new light on momentum transfer from the atmosphere to the tree. Previous studies on tree-atmosphere interaction used the drag coefficient C_d as a measure for tree-atmosphere interaction. It was found that this varies with wind speed, and per tree species. So far, this has not been done on trees in forests. Also, no studies have investigated the effect of drought on tree drag coefficient, or any other measure of tree-atmosphere interaction.

This Chapter demonstrates that the variation in momentum transfer can change considerably during the shift from the wet to the dry months. This has important implications for the water and carbon balance, as these depend strongly on the momentum transfer from atmosphere to the canopy.

Additional measurements of the input wind spectra, and its variation over time and space, will allow further exploration of the relation between wind, tree sway, and momentum transfer. Combining the current data with plant physiological measurements will allow further testing of the hypothesis that the temporal changes in tree-atmosphere interaction are related to drought-induced tree mass changes.

6.5 CONCLUSIONS

Tree-atmosphere interaction was measured on 19 trees during a transition from the wet to the dry months in the Brazilian Amazon. It was found that tree-atmosphere interaction varies considerably between individuals, and between species.

Tree-atmosphere interaction, and its relation with wind speed also changes over time. Especially during the transition from the wet to the dry months, a clear change in tree-atmosphere interaction was measured for all trees. The change in tree-atmosphere interaction coincided with increasing tree water deficit.

A positive relation was found between estimated tree mass, and average tree-atmosphere interaction. This suggests that the variation in accelerometer-derived measure of tree-atmosphere interaction is caused by changes in tree mass, most likely caused by water stress induced changes in water content or leaf fall.

In situ measurements of tree acceleration can be used to quantify tree-atmosphere interaction. This provides new insights in variation in tree-atmosphere interaction in time and space, and its response to increased vegetation water stress.

7

WATER STRESS DETECTION IN THE AMAZON USING RADAR

I light my torch and wave it for the
New moon on Monday
And a fire dance through the night
I stayed the cold day with a lonely satellite

Simon Le Bon, Duran Duran

The Amazon rainforest plays an important role in the global water and carbon cycle, and though it is predicted to continue drying in the future, the effect of drought remains uncertain. Developments in remote sensing missions now facilitate large-scale observations. The RapidScat scatterometer (K_u-band) mounted on the International Space Station observes the Earth in a non-sun-synchronous orbit, which allows for studying changes in the diurnal cycle of radar backscatter over the Amazon. Diurnal cycles in backscatter are significantly affected by the state of the canopy, especially during periods of increased water stress. We use RapidScat backscatter time series and water deficit measurements from dendrometers in twenty trees during a nine-month period to relate variations in backscatter to increased tree water deficit. Morning radar backscatter dropped significantly with increased tree water deficit measured with dendrometers. This chapter provides unique observational evidence that demonstrates the sensitivity of radar backscatter to vegetation water stress, highlighting the potential of drought detection and monitoring using radar.

Parts of this chapter have been published in Geophysical Research Letters (van Emmerik et al., 2017b).

7.1 INTRODUCTION

The Amazon, which contains half of the world's rainforests, plays a key role in the global water and carbon budget (Saatchi et al., 2007; Binks et al., 2016). However, the Amazon still remains a poorly understood component of the global carbon and water cycle (Samanta et al., 2010). The Amazon is predicted to continue drying in the future, which might accelerate climate change through carbon losses and change surface energy balances (Cox et al., 2008). For example, the extensively studied 2005 drought reversed the Amazon from a long-term carbon sink into a carbon source. Amazon forests appear to be vulnerable to increasing moisture stress, and future droughts have the potential to considerably change the water and carbon balance (Phillips et al., 2009). Models and observations do not all agree on the effect of drought on the Amazon. The current debate on whether or not the Amazon greens up during the dry season underscores the need for greater understanding of the effect of drought on the Amazon ((Huete et al., 2006; Saleska et al., 2007) vs. (Samanta et al., 2010; Morton et al., 2014)). Furthermore, understanding drought effects and the Amazon's resilience to drought is critical to understand their impact on the carbon and water cycles (Hilker et al., 2014).

With an increase in episodic droughts, there is a need for space borne observations, in addition to field and modeling studies (Asner and Alencar, 2010). New satellite observations provide opportunities for better detection and understanding of drought (AghaKouchak et al., 2015). Recent research suggests that radar observations might yield valuable insight into canopy water status. Several studies have identified diurnal variations in backscatter over the Amazon (Birrer et al., 1982; Satake and Hanado, 2004; Frolking et al., 2011; Jaruwatanadilok and Stiles, 2014; Paget et al., 2016) and other vegetated areas (Friesen, 2008; Friesen et al., 2012; Konings et al., 2017). Radar is sensitive to vegetation because of direct backscatter from the canopy, and attenuation of the signal as it travels through the vegetation layer (Ulaby et al., 1982a). Both are influenced by the amount of leaves in the vegetation layer, and the vegetation dielectric properties. The latter are in turn a function of vegetation water content. The number of leaves is mainly a function of tree phenology, governed by leaf flush and leaf fall. During periods of low soil moisture availability, backscatter is mainly sensitive to vegetation water content (Steele-Dunne et al., 2012). This was also demonstrated in Chapter 2 to 4. Backscatter is sensitive to vegetation, through the dielectric response of the vegetation to water stress (Chapter 2 and 3).

Diurnal differences in backscatter might be the key for water stress detection using radar. Birrer et al. (1982) found that backscatter over the Amazon rainforest at sunrise was 0.5-1 dB higher than during the rest of the day.Satake and Hanado (2004) also found diurnal variation in backscatter, and suggested that these were caused by either changes in vegetation water content or dew. Frolking et al. (2011) used QuikSCAT backscatter, in combination with a TRMM precipitation derived measure of water deficit, to hypothesize that the dry season reduction in backscatter is due to water stress induced changes in canopy water status. Strong negative anomalies in pre-dawn backscatter were found during the 2005 drought. Measured tree mortality rates during this period (Phillips et al., 2009) suggested that these anomalies were caused by changes in tree water status, rather than dew. Jaruwatanadilok and Stiles (2014) used 10 years of QuikSCAT data and found a consistent difference between ascending and descending overpasses

over tropical forests, and suggested that this is very likely due to differences in vegetation moisture content. Friesen (2008) used simple regional vegetation modeling to demonstrate that the diurnal variation in ERS C-band backscatter coincided with the onset of water stress over West Africa. The largest differences were found at the start of the dry season, ruling out interception, dew, or top soil moisture dynamics, and leaving vegetation water content as the most plausible explanation for diurnal differences. To test this hypothesis, Steele-Dunne *et al.* Steele-Dunne et al. (2012) modeled L- and C-band backscatter over a forest canopy, and demonstrated that during periods of low soil moisture availability, backscatter is mainly sensitive to changes in vegetation water content. Recent work by Paget et al. (2016) and Konings et al. (2017) used RapidScat backscatter to confirm that the theorized diurnal cycle over tropical forests definitely exists. *In situ* data in combination with backscatter is required to test the hypothesis that vegetation water content is the primary driver of water stress related diurnal variation in backscatter. This chapter presents a first study that uses field data of tree water status in combination with Ku-band radar backscatter to confirm that changes in vegetation water content associated with water stress are apparent in backscatter.

Data from the RapidScat scatterometer (Cooley, 2013) on board the International Space Station (ISS) offer a unique opportunity to investigate diurnal variations in backscatter with spaceborne radar. Due to the orbit of the ISS, the daily ascending and descending overpass times shift and eventually cover a complete diurnal cycle. These unique orbit characteristics allow us to study changes in backscatter for specific hours of the day. A diurnal cycle for backscatter can be constructed each month, allowing us to study how the diurnal cycle changes in time and to confirm the hypothesis of Friesen et al. (2012), Steele-Dunne et al. (2012), and this thesis (Chapter 1 to 4) that diurnal variations in backscatter are related to water stress. Here we compare backscatter data from RapidScat to dendrometer data from 20 trees in the Amazon rain forest from July 2015 to April 2016. Diurnal cycles of horizontally (HH) and vertically (VV) co-polarized backscatter are determined for each month. First, these are compared to the water deficit calculated from the dendrometer data to investigate how the diurnal cycle of backscatter changes in the transition from the wet to dry season. Second, the temporal variation in pre-dawn backscatter will be compared to the water status of the measured trees to confirm the hypothesis that increasing water stress leads to a decrease in pre-dawn vegetation water content and backscatter.

7.2 METHODS

7.2.1 STUDY AREA

For this study we use ground data obtained at a research station in the Amazon rainforest (2.6085° S, 299.8107° W), 60 km Northwest of Manaus, Brazil. The study area is characterized by a tropical climate with an average dry season from June to October. During the measurement period, there was about 12 hours of daylight, roughly between 6 A.M. and 6 P.M. local time. A land cover map of the study area is presented in the Supplementary materials (S1), including the location of the measurement site, and the footprint of the radar data used. The land cover classification was retrieved from the ESA Climate Change Initiative (CCI) land cover map (ESA–European Space Agency, 2016). Radar data

from July, 2015 to August, 2016 and ground measurements from August, 2015 to April, 2016 were available.

7.2.2 RADAR DATA

RapidScat, launched in September, 2014, is a rotating pencil-beam scatterometer installed on the International Space Station (ISS). Scatterometers are a type of active microwave remote sensing, which emits microwave energy towards the Earth's surface and measures the reflected energy. RapidScat measures both horizontally (HH) and vertically polarized (VV) K_u-band (13.6 GHz) backscatter. The incidence angle various between 44-54° (HH) and 51-61° (VV), and the resolution for the normalized backscatter is 26x37km. The ISS, and therefore RapidScat, has a non-sun-synchronous orbit, which allows for different local time of day observations as the orbit progresses (Paget et al., 2016). Every day the overpass time shifts to an earlier time of the diurnal cycle by around 30 minutes, meaning that a complete diurnal cycle for each overpass mode is covered after two months. Combining ascending and descending data will cover a diurnal cycle every single month. For more details on the sensor, and initial data processing see Paget et al. (2016) and Madsen and Long (2016). For this study we use HH and VV polarized backscatter from July to August, 2016, that was retrieved over the Amazon between 1.6-3.6°S and 298.8-300.8° W.

The backscatter from the 2°x2° area was resampled into 25 sub-areas of 0.4° by 0.4°, which was chosen as a compromise to maximize the number of data per sub-area, but minimizing spatial information loss. For this study we only use backscatter that has its entire footprint within 1° longitude and latitude from the measurement location. We applied a land cover based mask to filter out the observations influenced by urban areas, water bodies, and flooded forests. The applied masked was based on the ESA CCI landuse map (ESA–European Space Agency, 2016). All sub-areas that were water bodies, urban areas, flooded forests, or croplands were filtered out. Fig. 7.1. shows the map of the field site, the land classes and the footprint, the mean backscatter per sub-area, the applied mask, and the final sub-areas that were used in the analyses, including mean backscatter. Finally, the spatially filtered backscattered was averaged for each time step, arriving at the final backscatter time series for both HH and VV.

We found that depending on the hour of the day, the spatial variability in backscatter can vary over the forest canopy. Therefore, in the following analyses data retrieved at 5 and 6 A.M. and P.M. were used for morning and evening data, respectively. The spatial variation of backscatter depends on the time of day. Fig. 7.2 presents the standard deviation for spatial averaging for each hour. The time of day chosen has a considerable influence on the magnitude and the range of the data. At night, all vegetation, independent of the species, comes to an equilibrium with the atmospheric and hydrologic conditions. Before sunrise the standard deviation for both VV and HH is between 0.7 and 0.72 dB. During the day, the transpiration rates, and therefore water status, of each individual tree might vary considerably, leading to an increased spatial variability. After sunrise this increases to 1.0 - 1.1 dB (VV, HH) at 10 A.M.. In the afternoon it decreases again to 0.7-0.8 dB.

Combining ascending and descending overpass data, diurnal cycles of radar backscatter were constructed for every month. For the measurement period of July, 2015 to Au-

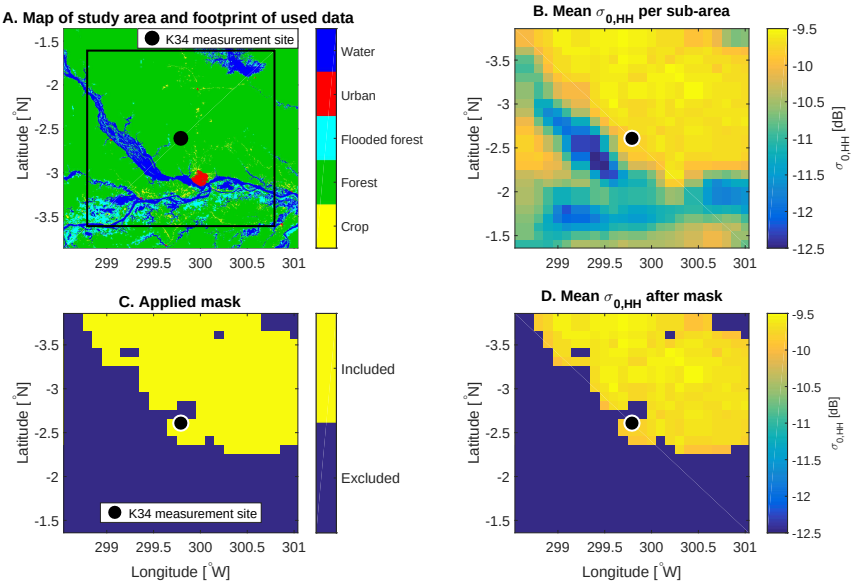

Figure 7.1: A. Mean HH backscatter per sub-area, after resampling, B. mean HH backscatter of the area, C. applied mask based on the ESA CCI landuse map, D. the mean HH backscatter on the area after applying the mask.

gust, 2016, this resulted in 14 diurnal cycles. From these diurnal cycles we also extracted backscatter for specific hours of the day. For this analysis, data at 5 and 6 A.M./P.M. were used, which yield a time series of morning and evening backscatter at these specific times. We also computed the diurnal variation $\Delta\sigma^0_t$ by subtracting the evening backscatter from the morning backscatter:

$$\Delta\sigma^0_t = \sigma^0_{t,AM} - \sigma^0_{t,PM} \tag{7.1}$$

with chosen time of day t.

7.2.3 GROUND DATA

A total of 20 individual trees were measured during this experiment, covering seven tree species, with a broad range of average height and wood density. In total 7 species were measured, with 1 to 3 individuals per species. Trees were selected to cover a broad range of heights (h), widths (diameter at breast height, D_{BH}), and wood densities (ρ_w). An overview of the measured trees is found in Table 7.1. Data from August, 2015 to April, 2016 were used.

We used the same dendrometer data as presented in Chapter 6. Dendrometers (ZN12-T-2IP, Natkon.ch, Switzerland) were installed at 1.5 meters above ground level. Two potentiometers measured the thickness of the bark and the xylem every 10 minutes. From back thickness, the water deficit was determined (see Chapter 6.2.3). To compare the dendrometer data with radar backscatter, the water deficit time series was resampled at

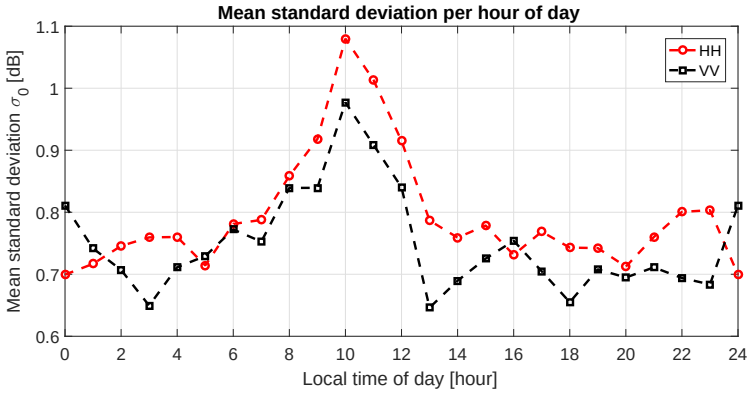

Figure 7.2: Standard deviation as function of local time of day for VV and HH backscatter.

Table 7.1: Tree characteristics: Tree number, scientific name, wood density, estimated total height and diameter at breast height (D_{BH}).

Tree no.	Name	Estimated wood density $[10^3 kg/m^3]$	Estimated height [m]	D_{BH} [cm]
1 - 3	*Goupia glabra*	0.7 (High)	25 - 32	135.0 - 242.5
4 - 6	*Lecythis prancei*	0.875 (Intermediate)	24 - 35	108.4 - 116.5
7 - 9	*Scleronema micranthum*	0.5 - 0.7 (Low)	26 - 38	81.0 - 189.5
10 - 13	*Eschweilera coriacea*	0.8 (Intermediate)	18 - 27	92.4 - 268.0
14 - 15	*Dypterix odorata*	1.1 (High)	32 - 35	177.0 - 219.5
16 - 17	*Pouteria anomala*	0.7 (Low)	22 - 23	111.0 - 117.5
18 - 20	*Maquira sclerophylla*	0.5 (Low)	18 - 35	90.6 - 264.0

the same time of day as the backscatter data used (5-6 A.M./P.M.), yielding daily morning and evening values. Subsequently, these were subtracted to calculate the daily diurnal difference. We use the Spearman rank coefficient to evaluate the significance of the relationship between water deficit and backscatter. We also looked at the changes in xylem thickness, as this is a good indicator of tree water status and water use, transpiration rate, and leaf water status (Perämäki et al., 2005; Sevanto et al., 2008). Also, this is not affected by absorption and evaporation of water from the bark tissue (Sevanto et al., 2011). Wet conditions result in an increase in the xylem diameter, and drought leads to a decrease. The exact relationship between xylem thickness and sap flow varies with species and over time.

7.3 RESULTS

7.3.1 BACKSCATTER TIME SERIES AND DIURNAL CYCLES

Fig. 7.3A presents the average backscatter over the study area from July, 2015 to April, 2016. Here it can be seen how the non-sun-synchronous orbit affects the data availability. After two months, a full diurnal cycle is covered. Three clear periods can be distinguished. From July to October, 2015, the backscatter in the morning was higher than in the evening. From October, 2015 to April, 2016 the diurnal variation decreased, and backscatter is quite stable during the day. From April onwards, the morning backscatter

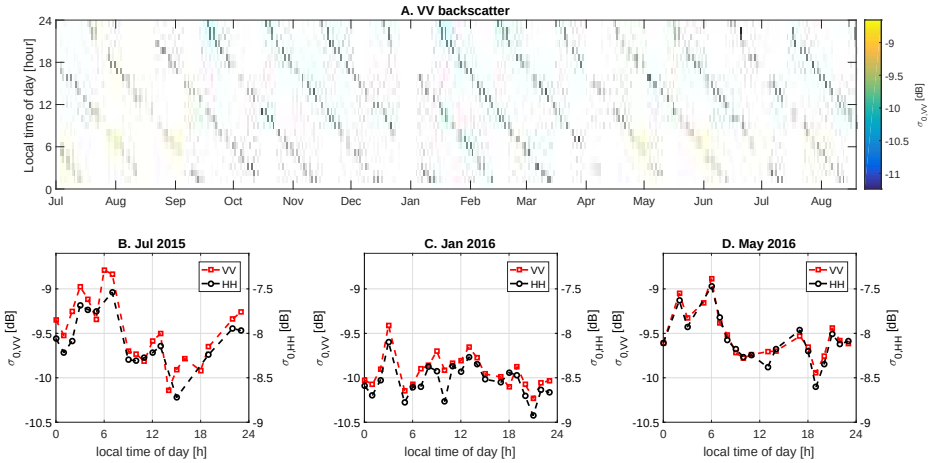

Figure 7.3: A.Backscatter per hour of the day for VV polarized backscatter from July, 2015 to August, 2016, and diurnal cycles of VV and HH backscatter in B. July, 2015 (wet period), C. January, 2016 (dry period), and D. May, 2016 (wet period).

increases again. For the periods with a considerable difference between morning and evening backscatter, the difference can reach up to 1.2 dB for both VV and HH.

Fig. 7.3B-D present diurnal cycles for these three distinct periods. In July, 2015 (Fig. 7.3B), the maximum backscatter was around 6 A.M., after which it decreased during the day. In January, 2016(Fig. 7.3C) the morning backscatter had decreased and the diurnal variation is low. In May, 2016, the diurnal variation increased again (Fig. 7.3D), with again the maximum backscatter around 6 A.M. The diurnal variation in backscatter was similar to the expected variation in vegetation water content in the canopy. Right before sunrise, when photosynthetic activity was low, the water content was at its daily maximum. With increasing net solar radiation, the vegetation loses water through transpiration, decreasing to a minimum in the evening (Fig. 7.3B, 7.3D). At night vegetation replenishes its water storage again. However, during dry periods (Fig. 7.3C) there might not be sufficient water available in the soil, leading to decreasing maximum water content. Eventually, the diurnal variation will also decrease (Slayter et al., 1967).

In addition to Fig. 7.3B-D, Fig. 7.4 shows all diurnal cycles for each orbit, for both VV and HH. The diurnal cycles of VV and HH are similar, except for the range of values. VV backscatter ranges between -8.8 and -10.5 dB, HH between -7.5 and 8.8 dB. Both exhibit a diurnal cycle, with the highest values in the morning, between 4 and 7 A.M., after which it decreases to a minimum around 2-4 P.M. In the 2nd and 3rd cycle of VV and HH a diurnal difference can also be seen. This changes over time, as especially the morning values decrease in the following cycle. In the 5th cycle the morning values are higher again. Cycles 4 to 18 show relatively low diurnal variation. From Cycle 9 to 14, the diurnal variation increases again to about 1 to 1.5 dB for both VV and HH.

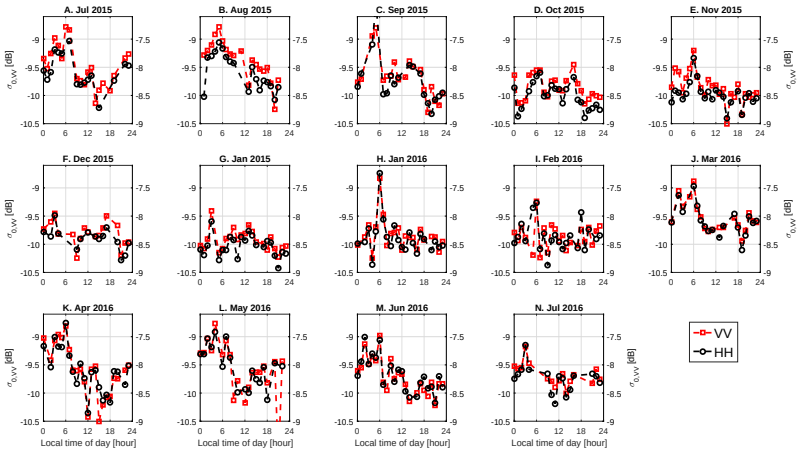

Figure 7.4: Diurnal cycles of VV and HH backscatter, constructed using each two-month orbit.

7.3.2 PRE-DAWN TIME SERIES

The plant water deficit, xylem thickness, and VV and HH backscatter are presented in Fig. 7.5A-C. For the water deficit and xylem thickness, three individual trees, and the mean values of all trees are shown. The individual trees were selected to illustrate the range of values across species. In addition to Fig. 7.5, Fig. 7.6 shows the water deficit and xylem thickness of all trees. Also, the mean value of all trees is shown. For all trees, the dry periods from October to November, 2015, December, 2016 and, January to February, 2016 can be seen. The degree of exact timing of the increased water deficit, or decreased xylem thickness depends strongly on the individual tree.

The periods from July, 2015 to April, 2016, can be separated in three phases. In the first phase, water deficit was low, the xylem thickness was stable, and backscatter was high. In September, 2015, water deficit started to increase. At the same time, the xylem thickness also decreased, indicating lower transpiration rates and lower water content in plant tissues. Backscatter for both VV and HH also dropped significantly from -9 to -9.6 dB (VV) and from -7.5 to -8.4 dB (HH). From October, 2015 to February, 2016, a second phase of increased water deficit can be distinguished. Backscatter during this period did not show much variability, even though the water deficit recovers in November and December, 2015. Xylem thickness in the *Goupia glabra* was still lower, which suggests that the leaf water content might not have recovered. The water deficit was determined using the bark thickness, which is a measure of the total water content in the tree. However, a decreasing water deficit in the trunk might not have resulted yet in recovery of leaf water content. As RapidScat measured at high frequency (13.4 GHz), backscatter was mainly sensitive to changes in leaf water content (Ulaby and Jedlicka, 1984). Therefore, the recovery might not have been as clear in the backscatter signal. The moment water deficit increased to a maximum in February, 2016, backscatter again dropped with 0.5 dB. Af-

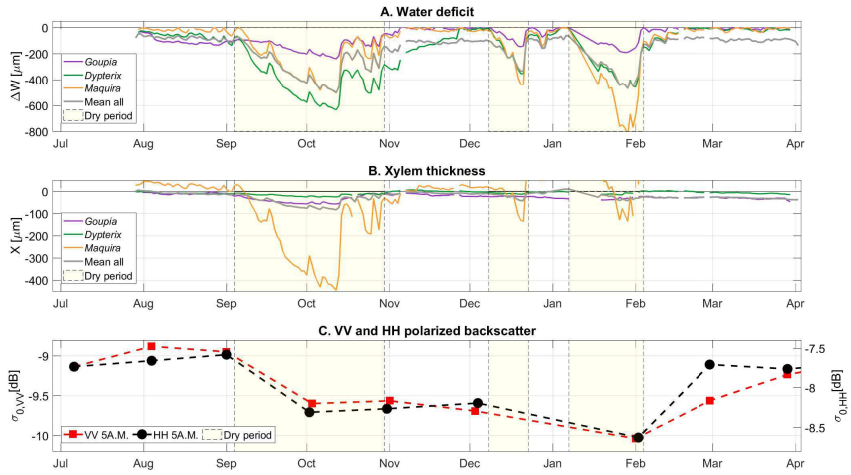

Figure 7.5: A. Water deficit and B. Xylem thickness for *Goupia glabra*, *Dypterix odorata*, *Maquira sclerophylla* trees, and mean of all trees, and C. VV and HH polarized 5 A.M. backscatter, from July, 2015 to August, 2016. The periods of increased water deficit are indicated with the yellow background.

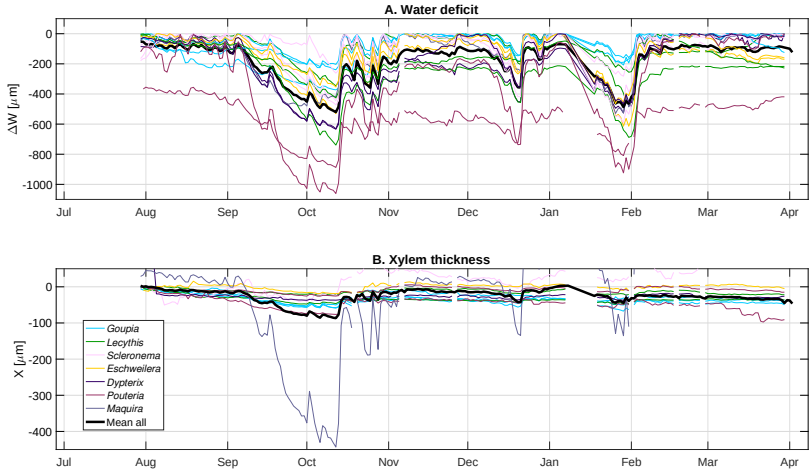

Figure 7.6: A. Water deficit and B. Xylem thickness for all measured trees, and mean of all trees, from July, 2015 to August, 2016.

ter February, 2016, water deficit went back to zero for all three trees, suggesting recovery of the vegetation. Also backscatter increased from -10 to -9.2 dB (VV) and from -8.7 to

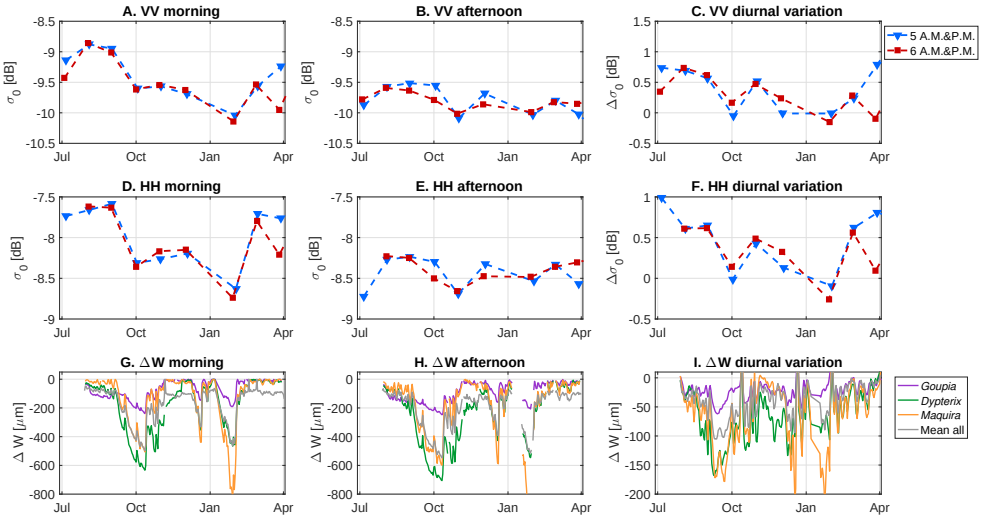

Figure 7.7: VV backscatter time series for A. 5 and 6 A.M. in the morning, B. 5 and 6 P.M. in the evening, and C. diurnal difference at 5 A.M./P.M. and 6 A.M./P.M., HH backscatter time series for D. 5 and 6 A.M. in the morning, E. 5 and 6 P.M. in the evening, and F. diurnal difference at 5 A.M./P.M. and 6 A.M./P.M., water deficit time series for G. 5 A.M., H. 5 P.M. and diurnal difference at 5 A.M./P.M.

-7.7 dB (HH) between February and April, 2016. In this phase, the plant water content recovered more than after the first dry period (September-November, 2015). Also, during this period leaf flush might have occured. Although water deficit was low, it takes some time before leaf development results in biomass increase. This would explain the delayed increase in backscatter.

During the peaks in water deficit in October, 2015 and February, 2016, both HH and VV backscatter significantly dropped by 0.5 to 0.9 dB. The effect of water stress is not only visible in the morning values. Fig. 7.7 presents morning and evening VV (Fig. 7.7A and B), HH (Fig. 7.7D and E) backscatter values, and the diurnal variation for both VV (Fig. 7.7C) and HH (Fig. 7.7F), and water deficit during morning (Fig. 7.7G), evening (Fig. 7.7H) and its diurnal variation (Fig. 7.7I). In addition to the pre-dawn measurements, the evening values clearly dropped around 0.5 dB for both VV and HH. Also the diurnal variation decreased from 1 to 0 dB during the peaks in water deficit. Ground measurements on the trees give a measure of water stress, which was largest in October, 2015 and February, 2016. In these months, morning backscatter, evening backscatter and the diurnal variation in backscatter significantly dropped.

From Fig. 7.5 and 7.7 it can be seen that the drop (and increase) in backscatter during the wet to dry (and dry to wet) period is significant (0.7-1.0 dB). These two transition phases will be discussed separately, to investigate the sensitivity of backscatter to changing water status in the canopy. Fig. 7.8 presents the relationship between measured

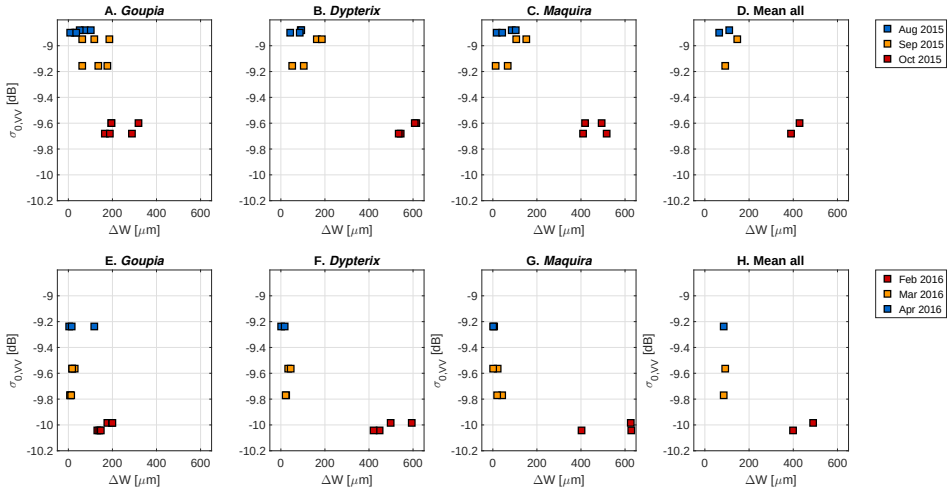

Figure 7.8: Water deficit ΔW and backscatter σ_0 for three tree species, and mean water deficit of all trees at 5 A.M. and 6 A.M.. Each marker type corresponds to an individual (circle, triangle or square), and the color refers to the time of measurement (A-D: August to October, 2015 for the top row. E-H: February to April, 2016 for the bottom row). A/E: Three *Goupia glabra* individuals. B/F: two *Dypterix odorata* individuals. C/G: two *Maquira sclerophylla* individuals. D/H: mean water deficit using all trees. Note that the y-axis values are the same across all columns.

7

water deficit of four tree species during (1) the transition from wet to dry, from August - November, 2015 (Fig. 7.8A-D), and (2) the transition from dry to wet, from February to April, 2016 (Fig. 7.8E-H). For the first transition, water deficit was strongly related to backscatter. The water deficit was different in magnitude for all tree species. Water deficit is influenced by tree size, and stress coping mechanisms. In general the different individuals react similarly, also compared to the mean water deficit using data from all trees (Fig. 7.8D/H). From Fig. 7.8A-D it is clear however, that although the variability in water deficit varies between species, the canopy as a whole significantly affects backscatter. Using the Spearman rank test, it was found that the relation between lower backscatter and increased water deficit is statistically significant. Confidence boundaries ranged from 0.9 for water deficit of individual trees, to 0.99 for mean water deficit. For the second transition, from dry to wet, again a clear correlation can be seen. However, though the dendrometer data indicates a reduction in water stress by March, the backscatter continues to increase in April. This suggests that there may be a delay between recovery in the trunk and the leaves, which could be associated with leaf development after the decrease of water deficit (leaf flushing).

7.4 DISCUSSION

The most significant sign of vegetation water stress was the change in morning backscatter. During periods with the highest water deficit across the measured trees, VV and HH

backscatter were lowest. This is in line with previous studies that associated anomalies in morning backscatter to drought effects in the canopy, such as Saatchi et al. (2013) and Frolking et al. (2011). The ground measurements provide the first observational evidence of the effect of vegetation water stress on radar backscatter.

During periods of increased water deficit, based on in situ tree measurements, the diurnal variation decreased. This was attributed to decrease in morning backscatter, which can be explained by the decrease in canopy moisture content. The inability to refill completely during the night is one of the signs of vegetation water stress (Hsiao, 1973). For the first time, changes in diurnal backscatter cycle were linked to changes in vegetation water status based on ground measurements. This allows studying sub-seasonal variations, such as the observed transitioning from wet to dry conditions. Vegetation dynamics change on a significantly shorter time scale, and the diurnal backscatter cycles obtained on a shorter timescale gave additional insight in the effect of water stress on vegetation.

A difference was observed between the transition from wet to dry, and the transition from dry to wet. Water deficit has an immediate effect on leaves (Slayter et al., 1967; Tardieu et al., 1993), and this is observed as a drop in backscatter. There is a delay between increase in xylem thickess and leaf development/recovery after the dry period (Sevanto et al., 2002). Results show that backscatter continues to increase after xylem has recovered, suggesting leaf development or recovery after the transition from dry to wet period. Leaf flushing is likely to occur when water deficit is low. After leaf flushing, new leaves need time to develop and gain biomass (Asner and Alencar, 2010; Samanta et al., 2012), which causes a delay in the backscatter response. Besides variation in canopy water content, changes in leaf area can have a considerable impact on backscatter. The drop in backscatter as observed between September and October, 2015, coincides with a steep increase in water deficit. During periods of decreased water deficit, canopy water content decreases first. Eventually, sustaining water deficit will lead to leaf fall, decreasing the leaf area. Decreased leaf area can be an explanation for the delay in recovery in November, 2015 and February, 2016. Although water deficit decreases to almost zero, the recovery is not directly observed in the backscatter. After November, 2015 no increase is observed at all, and after February, 2016 an increase in backscatter is observed after one month. When water deficit is decreased, the leaf area does not directly increase as trees need time to gain biomass and develop new leaves. In November, 2015, the recovery was not sufficient to allow for increase in leaf area. After February, 2016, biomass gain did result in increased leaf area. In-situ observations of leaf-area are not available for this study period. However, this seasonal pattern corresponds to observations from earlier years at the same measurement site (Lopes et al., 2016). For 2012 and 2013, leaf flush occurred one to two months after the transition to the wet season, with increased precipitation and low tree water deficit.

This chapter demonstrates the value of coincident backscatter and field measurements of tree water status. The trees measured during this fieldwork had a temporally similar response. In other canopies this might not be the case. Additional research is essential to understand and quantify if the backscatter time series over a less temporally similar canopy also contains a clear stress signature. For this study, only 9 months of data were available. Future work might extend the length of the data series to not only at inci-

dental dry periods, but also investigate seasonality, phenology, and monthly anomalies. This will give more insight in how to quantify the effect of vegetation water stress.

7.5 CONCLUSIONS

Simultaneous ground measurements and RapidScat K_u-band radar backscatter were used to relate variation in backscatter to increased tree water deficit. During two dry periods, increased vegetation water stress resulted in drops in radar backscatter.

Pre-dawn backscatter showed the largest sensitivity to increased vegetation water stress. Both VV and HH backscatter dropped 0.5 to 1 dB as a result of increased tree water deficit. Also evening VV and HH backscatter, and the diurnal variation in radar backscatter dropped considerably during periods of vegetation water stress. This clearly demonstrates the strong relation between water status of the canopy and radar backscatter.

Changes in the diurnal cycle of backscatter were found, associated with the change in water status of the vegetation canopy. During the wet period, morning backscatter was up to 1 dB higher than in the evening. During the dry period the diurnal variation in backscatter decreased to nearly zero.

RapidScat backscatter is mainly sensitive to changes in leaf water content. The largest variation in backscatter were observed during the transition phases from a wet period to a dry period and vice versa. At the start of the first dry period, increased water deficit in the canopy resulted in an immediate drop in backscatter. During the wetting phase, backscatter followed, although with a delay, the recovery of the vegetation. During recovery, the trunk recovers faster than the leaves.

Drought detection and monitoring in tropical forests is a major challenge. This chapter found that radar backscatter is sensitive to increased water deficit in the Amazon, which demonstrates the value of drought monitoring and detection using radar remote sensing.

8

Conclusions

Finally, from so little sleeping and so much reading,
his brain dried up and he went completely out of his mind.

Miquel de Cervantes - Don Quixote

This thesis tested the hypothesis that vegetation water stress leads to observable variations in radar backscatter. Using field measurements in corn canopies, and tropical forests, a link was made between increased vegetation water stress and changes in vegetation water content, vegetation dielectric properties, and radar backscatter. In this final chapter, the conclusions are presented on (1) the effects of water stress on plant dynamics, (2) the effects of water stress on vegetation dielectric properties, and (3) the effects of water stress on radar backscatter. Finally, a synthesis and outlook for future work is presented.

8.1 EFFECT OF WATER STRESS ON PLANT DYNAMICS

Field measurements in three different environments demonstrated the significant effect of water stress on plant dynamics. The timing and magnitude of the impact of water stress varies between species, and varies per environment. In the controlled greenhouse experiment on tomato plants (Chapter 2), the changes in leaf water content were relatively small. However, a significant downward trend of leaf water content was found for the stressed tomato plants, in contrast to the leaf water content of the unstressed plants. The slow response of leaf water content and dielectric properties to decreased soil moisture availability is explained by the low expected photosynthetic activity, as only 10 % of the summertime net radiation was available for photosynthesis, and the fruits were already fully developed.

Results from the field measurements on corn (Chapter 2 and 3) under low water availability demonstrated that plant water content clearly responds to water stress. Diurnal destructive sampling of leaf and stalk water content showed that leaf water content can vary up to 40 % diurnally. Total bulk water content changed up to 30% between 6 A.M. and 6 P.M., mainly governed by the changes in stalk water content. The field measurements also give insight in the diurnal differences on plant water content for corn. Corn is an isohydric species, meaning that its water content is stable during the day for normal conditions. In the week preceding the onset of water stress, plant water content was stable. Diurnal variation in water content increased shortly after irrigation was stopped. Persisting water stress eventually causes the diurnal variation in vegetation water content to decrease again, although overall water content remains to decrease.

The transition from wet to dry season in the Amazon rainforest was clearly observed in the changing tree-atmosphere interactions derived from tree sway, measuring using accelerometers (Chapter 5 and 6). At the onset of the dry season, a sudden drop in energy transfer from atmosphere to the trees was observed. Since a relation between tree mass and tree-atmosphere interaction was found, the drop in energy transfer from atmosphere to tree might be explained by changes in tree mass.

The trees in the Amazon demonstrated a clear change in water content in response to the start of the dry season (Chapter 7). The measured trees also showed isohydric behavior, as diurnal variation in measured water deficit increased significantly during periods of low moisture availability. A sudden drop in water content was measured in all trees, at the same time. This suggests that forests such as the Amazon rainforests can have a relatively homogeneous respond to the onset of the dry season.

By comparing different plant types we can conclude that different plant species respond differently to water stress. However, there are also similarities. For both the corn

and the Amazon trees, the onset caused a sudden change in plant water content. For corn, this resulted in a sudden increase in diurnal variation of leaf water content, while in Amazon trees water stress resulted in a rapid increase in tree water deficit, and a clear increase in diurnal variation of tree water content. This is favorable for radar remote sensing, because these sudden drops in tree water content can have an observable effect on radar backscatter.

8.2 EFFECT OF WATER STRESS ON PLANT DIELECTRIC PROPERTIES

To study the influence of vegetation water stress on leaf dielectric properties, a novel sensor was used in a controlled greenhouse experiment (Chapter 2), and under field conditions (Chapter 3). First, it was demonstrated that the dielectric response of the sensor changes with leaf water content. The relation between leaf water content and dielectric response was found to vary between different plant species. For tomatoes, the relation between leaf water content and dielectric response was found to be non-monotonic. For corn, a clear relation was found between leaf water content and dielectric response.

During the controlled experiment (Chapter 2) the leaf dielectric properties of tomato plants with and without water stress were compared. Despite the non-monotonic relation between leaf water content and dielectric response, a significant difference in temporal trends were found, showing water stress can affect plant dynamics considerably.

The used sensor allowed unique measurements under field conditions, which suggest that leaf dielectric properties are dynamic in time and space (Chapter 3). First, it was found that the variation in leaf dielectric properties respond to plant growth or water stress. The unstressed corn canopy showed only very little variation in leaf dielectric response over time. The dielectric properties of the stressed canopy on the other hand, were clearly affected.

Second, it was found that the dielectric response to plant growth and water stress depends on leaf height. The leaf at the corn cob showed an increase in diurnal variation in dielectric response, as well as a negative trend in evening values. Leaves at other heights did not show this change in diurnal variation.

The unique in vivo measurements allowed coupling of changes in plants water dynamics to leaf dielectric properties, in response to water stress. In addition to day-to-day changes in leaf dielectric properties, the diurnal variations in leaf dielectric properties can also change significantly with persisting water stress.

8.3 EFFECT OF WATER STRESS ON RADAR BACKSCATTER

For the corn canopy, increasing water stress resulted in significantly changing water content, as well as leaf dielectric properties (Chapter 3). A sensitivity study using a water-cloud model demonstrated that at high frequencies (8.6-35 GHz), backscatter was influenced by both vegetation water content and soil moisture (Chapter 4). For increasing frequency, the influence of vegetation water content increases, mainly due to increased sensitivity to leaf water content.

Modeled time series of backscatter demonstrated that during periods of low soil mois-

ture variability, as is the case during water stress, the dynamics in radar backscatter are caused by changes in vegetation water content (Chapter 4). Statistically significant diurnal differences in backscatter were found. When radar is most sensitive to changes in soil moisture, vegetation affects the attenuation, leading to diurnal differences in total backscatter. When total backscatter is mainly sensitive to vegetation, diurnal differences are caused by direct backscatter from the canopy.

Over the Amazon, field measurements of tree water deficit were linked to radar backscatter (Chapter 7). Diurnal cycles in backscatter changes seasonally. During the wet season, the diurnal variation between morning and evening can be 1.5 dB, with the maximum around 6 A.M. (just before sunrise). During the transition to the dry season the diurnal variation decreases, up to 0 dB during periods of high tree water deficit.

Pre-dawn backscatter dropped 1 dB as a result of increased tree water deficit, demonstrating the strong relation between canopy water content and radar backscatter. Backscatter at Ku-band is mainly sensitive to changes in leaf water content. During the transitions from wet to dry season and vice versa, it is also the leaf water content that has the strongest reaction. For increased water stress at the onset of the dry season leaf water content decreases, or leaves are lost. After the start of the wet season, leaf flush leads to biomass gained and increased water content, resulting in higher backscatter.

8.4 IMPACT OF THIS THESIS AND OUTLOOK TO FUTURE RESEARCH

Testing the hypothesis that vegetation water stress significantly affects radar backscatter has been found to be challenging. This thesis presents a combination of field measurements of vegetation water content, leaf dielectric properties, tree sway, and modeled and observed radar backscatter. For both corn and tropical forest canopies, increased water stress results in changes in diurnal variation in water content. For corn, it was demonstrated how this affects leaf dielectric properties, eventually leading to significant diurnal differences in radar backscatter. For tropical forests, tree acceleration was used to show the effect of tree water deficit on tree-atmosphere interaction. Furthermore, the timing of increased tree water deficit coincided with a significant drop in radar backscatter, as well as changes in the diurnal cycle of backscatter over the Amazon.

The in vivo leaf dielectric properties datasets, and their response to vegetation water stress, give new insights in the dynamics of canopy dielectric properties. Although it has been known that dielectric properties are primarily influenced by water content, the in vivo measurements of leafs have revealed a vertical profile of the canopy dielectric properties. This has shed a new light on the within canopy heterogeneity of its dielectric properties, and the different responses at different layers to vegetation water stress. A better understanding of canopy dielectric properties can in turn be used to study the interaction between the vegetation layer, and radar with different frequencies, polarizations and incidence angles. The measurement periods were relatively short, and it would be interesting to extend the measurement period in future campaigns. In addition to the sudden change in response to water stress, this might also allow studying the effect of plant growth, and recovery after water stress relieve, on leaf dielectric properties. Furthermore, current measurements were only done on tomato and corn, and measurements on different crops (e.g. anisohydric species like sorghum, sunflower) would give additional insight in dielectric response to water stress. Understanding the stress

response from different crops will also contribute in better understanding and interpretation of radar backscatter from more heterogeneous canopies.

Additional modeling of radar backscatter over stressed canopies will also give additional insight in which radar frequencies, polarizations and incidence angles are most sensitive to water stress. In this thesis, the rather simple water-cloud model was used for a limited number of frequencies, polarizations and incidence angles. This mainly demonstrated radar is sensitive to vegetation water stress. However, for the design of future measurement campaigns or remote sensing missions, more extensive modeling will give additional insight in how the signatures of water stress can be detected most accurately.

This thesis shows that observed variations in radar backscatter can be explained by increased vegetation water stress. Depending on the time scale of interest, taking into account diurnal variations in backscatter can improve current radar applications. For example, for applications such as soil moisture and fuel load estimation, diurnal and day-to-day vegetation dynamics are important. Soil moisture retrieval algorithms use an estimation of vegetation water content, which is often assumed to only change on a seasonal scale. A better understanding of the influence of vegetation dynamics on diurnal variations in backscatter will help to improve soil moisture estimation algorithms. Similarly, fuel load estimations, used to monitor fire threats in forests, will improve by better taking into account vegetation related diurnal variations in backscatter.

A significant part of this thesis is based on measurements using new techniques and approaches, which have resulted in various new insights. In addition to the revealed vertical profile in vegetation dielectric properties, the low-cost accelerometers were found to give very insightful information in tree properties and responses. At first these were deployed with the aim to monitor diurnal variations in tree acceleration, related to changing tree mass. With the current dataset, this was not achieved yet. However, the results did demonstrate the potential of accelerometers to study tree properties and responses. The acceleration was shown to be depending on tree mass. Further research will focus on not only using accelerometers to discriminate between trees, but also to monitor changing tree mass on seasonal and diurnal scales. Also, a clear relation was found between tree acceleration and intercepted rainfall. Not only does this show the sensitivity of tree sway to changes in mass (interception or water content related), but also provides a useful new technique to measure intercepted rainfall on individual trees. Finally, the accelerometers were used to derive a measure of tree-atmosphere interaction. This is very useful for land-atmosphere modeling on different scales. More importantly, it was demonstrated that tree-atmosphere interaction is impacted by vegetation water stress. Instead of using accelerometers to measure tree mass directly and estimate the impact of water stress on trees, tree-atmosphere interaction can be used to quantify and monitor water stress for individual trees.

The effect of water stress in the Amazon forest was clearly detected using Ku-band radar from RapidScat. Future research might include longer time series, and data from different missions, to better explore the possibilities for water stress detection and monitoring. In this thesis only two transitions between seasons were studied. This thesis is limited to using RapidScat backscatter, a mission that only has a two-year data record. The analysis of signatures of water stress could be extended to other missions with longer

time series, such as the QuikScat mission, or the recently launched Sentinel-1 mission. Comparing transitions during different years will give additional insight in the potential extent of drought in the Amazon, and to what degree radar backscatter is sensitive to this. This might be of particular interest when studying the effect of the El Niño Southern Oscillations on the annual dry period in the Amazon. Future research could include the studying of other crop and forest ecosystems. As demonstrated using the dendrometer data, the study site in the Amazon responded relatively homogeneously in terms of timing of the response to tree water deficit. In other ecosystems there might be a larger variation in the timing and response to water stress, and it should be explored under what conditions radar is still sensitive to water stress.

Most importantly, this thesis provides a starting point for further exploration of the potential of using radar for vegetation water stress detection and monitoring. Whether it is for tropical forests or crops, water stress has a significant, negative effect on vegetation, especially from a human perspective. At the same time, new opportunities to use radar remote sensing for water stress detection are emerging. On the one hand through major new radar missions, such as ESA's Sentinel-1 program, providing data with high spatial and temporal resolution. On the other, through a shift of the field of Earth observation from being mainly government funded to for/non-profit organizations and individuals (McCabe et al., 2017). This development is expected to result in many new data sources, and this thesis provides a foundation for using these for vegetation water stress detection.

For years, the hypothesis that radar backscatter is sensitive to vegetation water stress has been debated. Finally, this thesis provides first observational evidence of the relation between plant water content, dielectric properties, and radar backscatter in response to water stress. Vegetation water stress is observable through variations in diurnal differences in radar backscatter. There is more work to be done, but potential of vegetation water stress detection using radar has been demonstrated.

REFERENCES

Abendroth, L. J., Elmore, R., Boyer, M., and Marlay, S.: Corn Growth and Development. PMR 1009., Iowa State University Extension., 2011.

Acevedo, E., Fereres, E., Hsiao, T. C., and Henderson, D. W.: Diurnal Growth Trends, Water Potential, and Osmotic Adjustment of Maize and Sorghum Leaves in the Field, Plant Physiology, 64, 476–480, 1979.

AghaKouchak, A., Farahmand, A., Melton, F., Teixeira, J., Anderson, M., Wardlow, B., and Hain, C.: Remote sensing of drought: Progress, challenges and opportunities, Reviews of Geophysics, 53, 452–480, 2015.

Allen, R. G., Pereira, L., Raes, D., and Smith, M.: FAO Irrigation and Drainage Paper No. 56, Food and Agriculture Organization of the United Nations, pp. 26–40, 1998.

Amtmann, R.: Data acquisition system for wind induced tree vibration, in: The Forest-Atmosphere Interaction, pp. 149–159, Springer, 1985.

Anber, U., Gentine, P., Wang, S., and Sobel, A. H.: Fog and rain in the Amazon, Proceedings of the National Academy of Sciences, 112, 11 473–11 477, 2015.

Asner, G. P. and Alencar, A.: Drought impacts on the Amazon forest: the remote sensing perspective, New Phytologist, 187, 569–578, 2010.

Attema, E. and Ulaby, F. T.: Vegetation modeled as a water cloud, Radio Science, 13, 357–364, 1978.

Aumond, P., Masson, V., Lac, C., Gauvreau, B., Dupont, S., and Berengier, M.: Including the drag effects of canopies: real case large-eddy simulation studies, Boundary-Layer Meteorology, 146, 65–80, 2013.

Baldocchi, D. D. and Amthor, J. S.: Canopy photosynthesis: history, Terrestrial Global Productivity, pp. 9–31, 2001.

Baldocchi, D. D., Luxmoore, R. J., and Hatfield, J. L.: Discerning the forest from the trees: an essay on scaling canopy stomatal conductance, Agricultural and Forest Meteorology, 54, 197–226, 1991.

Belcher, S. E., Harman, I. N., and Finnigan, J. J.: The wind in the willows: flows in forest canopies in complex terrain, Annual Review of Fluid Mechanics, 44, 479–504, 2012.

Bindlish, R. and Barros, A. P.: Parameterization of vegetation backscatter in radar-based, soil moisture estimation, Remote Sensing of Environment, 76, 130–137, 2001.

Bindlish, R., Jackson, T., Sun, R., Cosh, M., Yueh, S., and Dinardo, S.: Combined passive and active microwave observations of soil moisture during CLASIC, IEEE Geoscience and Remote Sensing Letters, 6, 644–648, 2009.

Binks, O., Meir, P., Rowland, L., Costa, A. C. L., Vasconcelos, S. S., Oliveira, A. A. R., Ferreira, L., Christoffersen, B., Nardini, A., and Mencuccini, M.: Plasticity in leaf-level water relations of tropical rainforest trees in response to experimental drought, New Phytologist, 2016.

Birrer, I., Bracalente, E., Dome, G., Sweet, J., and Berthold, G.: σ signature of the Amazon rain forest obtained from the SeaSat scatterometer, IEEE Transactions on Geoscience and Remote Sensing, pp. 11–17, 1982.

Bohnert, H. J. and Jensen, R. G.: Strategies for engineering water-stress tolerance in plants, Trends in Biotechnology, 14, 89–97, 1996.

Bongiovanni, T., Liu, K., Nagarajan, D., Preston, P., Rush, P., van Emmerik, T., Terwilleger, R., Mosivais-Huertero, A., Judge, J., Steele-Dunne, S., Akbar, R., Baar, E., Wallace, K., and England, A.: Field Observations During the Eleventh Microwave Water and Energy Balance Experiment (MicroWEX-11): From April 25 Through December 9, 2012, Center for Remote Sensing, University of Florida, Available at UF/IFAS EDIS website at http://edis.ifas.ufl.edu/pdffiles/ae/ae51400.pdf, 2015.

Bordiert, R.: Water status and development of tropical trees during seasonal drought, Trees-Structure and Function, 8, 115–125, 1994.

Brakke, T. W., Kanemasu, E. T., Steiner, J. L., Ulaby, F. T., and Wilson, E.: Microwave radar response to canopy moisture, leaf-area index, and dry weight of wheat, corn, and sorghum, Remote Sensing of Environment, 11, 207–220, 1981.

Brisco, B., Brown, R., Koehler, J., Sofko, G., and Mckibben, M.: The diurnal pattern of microwave backscattering by wheat, Remote Sensing of Environment, 34, 37–47, 1990.

Brocca, L., Crow, W. T., Ciabatta, L., Massari, C., de Rosnay, P., Enenkel, M., Hahn, S., Amarnath, G., Camici, S., Tarpanelli, A., et al.: A review of the applications of ASCAT soil moisture products, IEEE Journal of Selected Topics in Applied Earth Observations and Remote Sensing, 2017.

Buckley, T. N.: The control of stomata by water balance, New Phytologist, 168, 275–292, 2005.

Burgess, S. S., Adams, M. A., Turner, N. C., Beverly, C. R., Ong, C. K., Khan, A. A., and Bleby, T. M.: An improved heat pulse method to measure low and reverse rates of sap flow in woody plants, Tree Physiology, 21, 589–598, 2001.

Burke, E. J., Harlow, R. C., and Ferré, T. P.: Measuring the dielectric permittivity of a plant canopy and its response to changes in plant water status: An application of Impulse Time Domain Transmission, Plant and Soil, 268, 123–133, 2005.

Carlson, T. N., Belles, J. E., and Gillies, R. R.: Transient water stress in a vegetation canopy: Simulations and measurements, Remote Sensing of Environment, 35, 175–186, 1991.

Cassiani, M., Katul, G., and Albertson, J.: The effects of canopy leaf area index on airflow across forest edges: large-eddy simulation and analytical results, Boundary-Layer Meteorology, 126, 433–460, 2008.

Cescatti, A. and Marcolla, B.: Drag coefficient and turbulence intensity in conifer canopies, Agricultural and Forest Meteorology, 121, 197–206, 2004.

Chambers, J. Q., Asner, G. P., Morton, D. C., Anderson, L. O., Saatchi, S. S., Espírito-Santo, F. D., Palace, M., and Souza, C.: Regional ecosystem structure and function: ecological insights from remote sensing of tropical forests, Trends in Ecology & Evolution, 22, 414–423, 2007.

Champion, I., Prevot, L., and Guyot, G.: Generalized semi-empirical modelling of wheat radar response, International Journal of Remote Sensing, 21, 1945–1951, 2000.

Chave, J., Coomes, D., Jansen, S., Lewis, S. L., Swenson, N. G., and Zanne, A. E.: Towards a worldwide wood economics spectrum, Ecology Letters, 12, 351–366, 2009.

Clifton, O. E., Fiore, A. M., Munger, J., Malyshev, S., Horowitz, L., Shevliakova, E., Paulot, F., Murray, L., and Griffin, K.: Interannual variability in ozone removal by a temperate deciduous forest, Geophysical Research Letters, 44, 542–552, 2017.

Cooley, V.: Unique offerings of the ISS as an Earth observing platform, in: Proc. 64th Int. Astron. Congr., Beijing, pp. 1–6, IAC-13-D9.2.8, 2013.

Correia, M. and Pereira, J.: The control of leaf conductance of white lupin by xylem ABA concentration decreases with the severity of water deficits, Journal of Experimental Botany, 46, 101–110, 1995.

Cox, P. M., Harris, P. P., Huntingford, C., Betts, R. A., Collins, M., Jones, C. D., Jupp, T. E., Marengo, J. A., and Nobre, C. A.: Increasing risk of Amazonian drought due to decreasing aerosol pollution, Nature, 453, 212–215, 2008.

Dabrowska-Zielinska, K., Inoue, Y., Kowalik, W., and Gruszcynska, M.: Inferring the effect of plant and soil variables on C- and L-band SAR backscatter over agricultural fields, based on model analysis, Advances in Space Research, 39, 139–148, 2007.

Davies, W. and Meinzer, F.: Stomatal Responses of Plants in Drying Soil, Biochemie und Physiologie der Pflanzen, 186, 357–366, 1990.

Davies, W. J. and Zhang, J.: Root signals and the regulation of growth and development of plants in drying soil, Annual Review of Plant Biology, 42, 55–76, 1991.

Ding, R., Kang, S., Du, T., Hao, X., and Zhang, Y.: Scaling Up Stomatal Conductance from Leaf to Canopy Using a Dual-Leaf Model for Estimating Crop Evapotranspiration, PloS One, 9, e95 584, 2014.

Dobson, M., DeLaSierra, R., and Christensen, N.: Spatial and temporal variation of the microwave dielectric properties of loblolly pine trunks, in: Geoscience and Remote Sensing Symposium, 1991. IGARSS'91. Remote Sensing: Global Monitoring for Earth Management., International, vol. 3, pp. 1107–1110, IEEE, 1991.

Dobson, M. C., Ulaby, F. T., LeToan, T., Beaudoin, A., Kasischke, E. S., and Christensen, N.: Dependence of radar backscatter on coniferous forest biomass, IEEE Transactions on Geoscience and Remote Sensing, 30, 412–415, 1992.

Drew, D. M. and Downes, G. M.: The use of precision dendrometers in research on daily stem size and wood property variation: a review, Dendrochronologia, 27, 159–172, 2009.

Dubois, P. C., van Zyl, J., and Engman, T.: Measuring Soil Moisture with Imaging Radars, IEEE Transactions on Geoscience and Remote Sensing, 33, 915–926, 1995.

Dupont, S. and Brunet, Y.: Edge flow and canopy structure: a large-eddy simulation study, Boundary-Layer Meteorology, 126, 51–71, 2008.

Dwyer, L. and Stewart, D.: Effect of leaf age and position on net photosynthetic rates in maize (*Zea mays* L.), Agricultural and Forest Meteorology, 37, 29–46, 1986.

Egea, G., Verhoef, A., and Vidale, P. L.: Towards an improved and more flexible representation of water stress in coupled photosynthesis–stomatal conductance models, Agricultural and Forest Meteorology, 151, 1370–1384, 2011.

Ehrenberger, W., Rüger, S., Fitzke, R., Vollenweider, P., Günthardt-Goerg, M., Kuster, T., Zimmermann, U., and Arend, M.: Concomitant dendrometer and leaf patch pressure probe measurements reveal the effect of microclimate and soil moisture on diurnal stem water and leaf turgor variations in young oak trees, Functional Plant Biology, 39, 297–305, 2012.

El-Rayes, M. A. and Ulaby, F. T.: Microwave dielectric spectrum of vegetation - Part I: Experimental observations, IEEE Transactions on Geoscience and Remote Sensing, pp. 541–549, 1987.

Entekhabi, D., Njoku, E. G., O'Neill, P. E., Kellogg, K. H., Crow, W. T., Edelstein, W. N., Entin, J. K., Goodman, S. D., Jackson, T. J., Johnson, J., et al.: The soil moisture active passive (SMAP) mission, Proceedings of the IEEE, 98, 704–716, 2010.

ESA–European Space Agency: CCI Land Cover Product User Guide version 2.5, ESA CCI LC project, 2016.

Evans, R. and Ilic, J.: Rapid prediction of wood stiffness from microfibril angle and density, Forest Products Journal, 51, 53, 2001.

Fauset, S., Johnson, M. O., Gloor, M., Baker, T. R., Monteagudo, A., Brienen, R. J., Feldpausch, T. R., Lopez-Gonzalez, G., Malhi, Y., Ter Steege, H., et al.: Hyperdominance in Amazonian forest carbon cycling, Nature Communications, 6, 2015.

Ferrazzoli, P., Paloscia, S., Pampaloni, P., Schiavon, G., Solimini, D., and Coppo, P.: Sensitivity to microwave measurements to vegetation biomass and soil moisture content: A case study, IEEE Transactions on Geoscience and Remote Sensing, 30, 750–756, 1992.

Ferrazzoli, P., Paloscia, S., Pampaloni, P., Schiavon, G., Sigismondi, S., and Solimini, D.: The potential of multifrequency polarimetric SAR in assessing agricultural and arboreous biomass, IEEE Transactions on Geoscience and Remote Sensing, 35, 5–17, 1997.

Flesch, T. K. and Wilson, J. D.: Wind and remnant tree sway in forest cutblocks. II. Relating measured tree sway to wind statistics, Agricultural and Forest Meteorology, 93, 243–258, 1999.

Foody, G., Curran, P., Groom, G., and Munro, D.: Multi-temporal airborne synthetic aperture radar data for crop classification, Geocarto International, 4, 19–29, 1989.

Friesen, J.: Regional vegetation water effects on satellite soil moisture estimations for West Africa, Ph.D. thesis, TU Delft, Delft University of Technology, 2008.

Friesen, J., Winsemius, H. C., Beck, R., Scipal, K., Wagner, W., and Van De Giesen, N.: Spatial and seasonal patterns of diurnal differences in ERS Scatterometer soil moisture data in the Volta Basin, West Africa, IAHS PUBLICATION, 316, 47, 2007.

Friesen, J., Steele-Dunne, S. C., and van de Giesen, N.: Diurnal differences in global ERS scatterometer backscatter observations of the land surface, IEEE Transactions on Geoscience and Remote Sensing, 50, 2595–2602, 2012.

Frolking, S., Milliman, T., McDonald, K., Kimball, J., Zhao, M., and Fahnestock, M.: Evaluation of the SeaWinds scatterometer for regional monitoring of vegetation phenology, Journal of Geophysical Research: Atmospheres, 111, 2006.

Frolking, S., Milliman, T., Palace, M., Wisser, D., Lammers, R., and Fahnestock, M.: Tropical forest backscatter anomaly evident in SeaWinds scatterometer morning overpass data during 2005 drought in Amazonia, Remote Sensing of Environment, 115, 897–907, 2011.

Gardiner, B.: The interactions of wind and tree movement in forest canopies, Wind and Trees. Cambridge University Press, Cambridge, pp. 41–59, 1995.

Gauthier, T. D.: Detecting trends using Spearman's rank correlation coefficient, Environmental Forensics, 2, 359–362, 2001.

Gentine, P., Entekhabi, D., and Polcher, J.: The diurnal behavior of evaporative fraction in the soil–vegetation–atmospheric boundary layer continuum, Journal of Hydrometeorology, 12, 1530–1546, 2011.

Gentine, P., Entekhabi, D., and Heusinkveld, B.: Systematic errors in ground heat flux estimation and their correction, Water Resources Research, 48, 2012.

Gentine, P., Garelli, A., Park, S.-B., Nie, J., Torri, G., and Kuang, Z.: Role of surface heat fluxes underneath cold pools, Geophysical Research Letters, 43, 874–883, 2016.

Gerrits, A. and Savenije, H.: Interception, in: Treatise on Water Science, edited by Wilderer, P., pp. 89 – 101, Elsevier, Oxford, doi:http://dx.doi.org/10.1016/B978-0-444-53199-5.00029-4, URL http://www.sciencedirect.com/science/article/pii/B9780444531995000294, 2011.

Gerrits, A., Savenije, H., Hoffmann, L., and Pfister, L.: New technique to measure forest floor interception: an application in a beech forest in Luxembourg, Hydrology and Earth Systems Sciences, 2007.

Gerrits, A. M. J.: The role of interception in the hydrological cycle, TU Delft, Delft University of Technology, 2010.

Gillies, J., Nickling, W., and King, J.: Drag coefficient and plant form response to wind speed in three plant species: Burning Bush (Euonymus alatus), Colorado Blue Spruce (Picea pungens glauca.), and Fountain Grass (Pennisetum setaceum), Journal of Geophysical Research: Atmospheres, 107, 2002.

Green, J. K., Konings, A. G., Alemohammad, S. H., Berry, J., Entekhabi, D., Kolassa, J., Lee, J.-E., and Gentine, P.: Regionally strong feedbacks between the atmosphere and terrestrial biosphere, Nature Geoscience, 10, 410–414, 2017.

Guan, D., Zhang, Y., and Zhu, T.: A wind-tunnel study of windbreak drag, Agricultural and Forest Meteorology, 118, 75–84, 2003.

Hassinen, A., Lemettinen, M., Peltola, H., Kellomäki, S., and Gardiner, B.: A prism-based system for monitoring the swaying of trees under wind loading, Agricultural and Forest Meteorology, 90, 187–194, 1998.

Helfter, C., Shephard, J. D., Martínez-Vilalta, J., Mencuccini, M., and Hand, D. P.: A non-invasive optical system for the measurement of xylem and phloem sap flow in woody plants of small stem size, Tree Physiology, 27, 169–179, 2007.

Hilker, T., Lyapustin, A. I., Tucker, C. J., Hall, F. G., Myneni, R. B., Wang, Y., Bi, J., de Moura, Y. M., and Sellers, P. J.: Vegetation dynamics and rainfall sensitivity of the Amazon, Proceedings of the National Academy of Sciences, 111, 16 041–16 046, 2014.

Hollinger, D., Kelliher, F., Byers, J., Hunt, J., McSeveny, T., and Weir, P.: Carbon dioxide exchange between an undisturbed old-growth temperate forest and the atmosphere, Ecology, 75, 134–150, 1994.

Hoogeboom, P.: Classification of agricultural crops in radar images, IEEE Transactions on Geoscience and Remote Sensing, pp. 329–336, 1983.

Hsiao, T. C.: Plant responses to water stress, Annual Review of Plant Physiology, 24, 519–570, 1973.

Huber, K., Vanderborght, J., Javaux, M., Schröder, N., Dodd, I. C., and Vereecken, H.: Modelling the impact of heterogeneous rootzone water distribution on the regulation of transpiration by hormone transport and/or hydraulic pressures, Plant and Soil, 384, 93–112, 2014.

Huete, A. R., Didan, K., Shimabukuro, Y. E., Ratana, P., Saleska, S. R., Hutyra, L. R., Yang, W., Nemani, R. R., and Myneni, R.: Amazon rainforests green-up with sunlight in dry season, Geophysical Research Letters, 33, 2006.

Jackson, T. and Schmugge, T.: Vegetation Effects on the Microwave Emission of Soils, Remote Sensing of Environment, 36, 203–212, 1991.

Jaruwatanadilok, S. and Stiles, B. W.: Trends and variation in Ku-band backscatter of natural targets on land observed in QuikSCAT data, IEEE Transactions on Geoscience and Remote Sensing, 52, 4383–4390, 2014.

Jarvis, P.: The interpretation of the variations in leaf water potential and stomatal conductance found in canopies in the field, Philosophical Transactions of the Royal Society of London. B, Biological Sciences, 273, 593–610, 1976.

Jasechko, S., Sharp, Z. D., Gibson, J. J., Birks, S. J., Yi, Y., and Fawcett, P. J.: Terrestrial water fluxes dominated by transpiration, Nature, 496, 347–350, 2013.

Jiang, M. and Zhang, J.: Water stress-induced abscisic acid accumulation triggers the increased generation of reactive oxygen species and up-regulates the activities of antioxidant enzymes in maize leaves, Journal of Experimental Botany, 53, 2401–2410, 2002.

Johnson, R., Ramey, G., and O'Hagan, D.: Wind induced forces on trees, Journal of Fluids Engineering, 104, 25–30, 1982.

Jones, H. and Sutherland, R.: Stomatal control of xylem embolism, Plant, Cell & Environment, 14, 607–612, 1991.

Jones, H. and Tardieu, F.: Modelling water relations of horticultural crops: A review, Scientia Horticulturae, 74, 21–46, 1998.

Joseph, A., van der Velde, R., O'neill, P., Lang, R., and Gish, T.: Effects of corn on C-and L-band radar backscatter: A correction method for soil moisture retrieval, Remote Sensing of Environment, 114, 2417–2430, 2010.

Joseph, A. T., van der Velde, R., O'Neill, P. E., Lang, R. H., and Gish, T.: Soil moisture retrieval during a corn growth cycle using L-band (1.6 GHz) radar observations, IEEE Transactions on Geoscience and Remote Sensing, 46, 2365–2374, 2008.

Katul, G., Finnigan, J., Poggi, D., Leuning, R., and Belcher, S.: The influence of hilly terrain on canopy-atmosphere carbon dioxide exchange, Boundary-Layer Meteorology, 118, 189–216, 2006.

Katul, G. G., Porporato, A., Nathan, R., Siqueira, M., Soons, M., Poggi, D., Horn, H., and Levin, S.: Mechanistic analytical models for long-distance seed dispersal by wind, The American Naturalist, 166, 368–381, 2005.

Kim, S., Kim, B., Kong, Y., and Kim, Y.-S.: Radar backscattering measurements of rice crop using X-band scatterometer, IEEE Transactions on Geoscience and Remote Sensing, 38, 1467–1471, 2000.

Kim, S., van Zyl, J., McDonald, K., and Njoku, E.: Monitoring surface soil moisture and freeze-thaw state with the high-resolution radar of the Soil Moisture Active/Passive (SMAP) mission, in: Radar Conference, 2010 IEEE, pp. 735–739, IEEE, 2010.

Kim, Y. and van Zyl, J. J.: A time-series approach to estimate soil moisture using polarimetric radar data, IEEE Transactions on Geoscience and Remote Sensing, 47, 2519–2527, 2009.

Koizumi, A., Motoyama, J.-i., Sawata, K., Sasaki, Y., and Hirai, T.: Evaluation of drag coefficients of poplar-tree crowns by a field test method, Journal of Wood Science, 56, 189–193, 2010.

Koizumi, A., Shimizu, M., Sasaki, Y., and Hirai, T.: In situ drag coefficient measurements for rooftop trees, Journal of Wood Science, pp. 1–7, 2016.

Kolmogorov, A. N.: The local structure of turbulence in incompressible viscous fluid for very large Reynolds numbers, in: Dokl. Akad. Nauk SSSR, vol. 30, pp. 299–303, 1941.

Kolmogorov, A. N.: The local structure of turbulence in incompressible viscous fluid for very large Reynolds numbers, Proceedings: Mathematical and Physical Sciences, 434, 9–13, 1991.

Konings, A. G., Yu, Y., Xu, L., Yang, Y., Schimel, D. S., and Saatchi, S. S.: Active microwave observations of diurnal and seasonal variations of canopy water content across the humid African tropical forests, Geophysical Research Letters, 2017.

Kurosu, T., Fujita, M., and Chiba, K.: Monitoring of rice crop growth from space using the ERS-1 C-band SAR, IEEE Transactions on Geoscience and Remote Sensing, 33, 1092–1096, 1995.

Larcher, W.: Physiological plant ecology, Berlin: Springer, 1995.

Lawrence, D. and Vandecar, K.: Effects of tropical deforestation on climate and agriculture, Nature Climate Change, 5, 27–36, 2015.

Le Toan, T., Beaudoin, A., Riom, J., and Guyon, D.: Relating forest biomass to SAR data, IEEE Transactions on Geoscience and Remote Sensing, 30, 403–411, 1992.

Lindner, M., Fitzgerald, J. B., Zimmermann, N. E., Reyer, C., Delzon, S., van der Maaten, E., Schelhaas, M.-J., Lasch, P., Eggers, J., van der Maaten-Theunissen, M., et al.: Climate change and European forests: What do we know, what are the uncertainties, and what are the implications for forest management?, Journal of Environmental Management, 146, 69–83, 2014.

Llamas, R., Niemeier, J., Kruger, A., Lintz, H., Kleinknecht, G., and Miller, R.: Diurnal cycles of tree mass obtained using accelerometers, in: AGU Fall Meeting Abstracts, vol. 1, p. 1575, 2013.

Lohou, F., Lopez, A., Druilhet, A., Brunet, Y., Irvine, M., and Lamaud, E.: The VENFOR Project: response of a homogeneous forest canopy to wind stress through the analysis of accelerometer measurements, Proceedings of the wind effects on trees. Germany: University of Karlsruhe, pp. 109–116, 2003.

Lopes, A. P., Nelson, B. W., Wu, J., de Alencastro Graça, P. M. L., Tavares, J. V., Prohaska, N., Martins, G. A., and Saleska, S. R.: Leaf flush drives dry season green-up of the Central Amazon, Remote Sensing of Environment, 182, 90–98, 2016.

Madsen, N. M. and Long, D. G.: Calibration and validation of the RapidScat scatterometer using tropical rainforests, IEEE Transactions on Geoscience and Remote Sensing, 54, 2846–2854, 2016.

Manzoni, S., Vico, G., Katul, G., Palmroth, S., Jackson, R. B., and Porporato, A.: Hydraulic limits on maximum plant transpiration and the emergence of the safety–efficiency trade-off, New Phytologist, 198, 169–178, 2013.

Manzoni, S., Katul, G., and Porporato, A.: A dynamical system perspective on plant hydraulic failure, Water Resources Research, 50, 5170–5183, 2014.

Martínez-Vilalta, J., Poyatos, R., Aguadé, D., Retana, J., and Mencuccini, M.: A new look at water transport regulation in plants, New Phytologist, 204, 105–115, 2014.

Mayer, H.: Wind-induced tree sways, Trees, 1, 195–206, 1987.

Mayhead, G.: Some drag coefficients for British forest trees derived from wind tunnel studies, Agricultural Meteorology, 12, 123–130, 1973.

McAdam, S. and Brodribb, T.: Separating Active and Passive Influences on Stomatal Control of Transpiration, Plant Physiol., 264, 1578–1586, 2014.

McCabe, M. F., Rodell, M., Alsdorf, D. E., Miralles, D. G., Uijlenhoet, R., Wagner, W., Lucieer, A., Houborg, R., Verhoest, N. E., Franz, T. E., et al.: The future of earth observation in hydrology, Hydrol. Earth Syst. Sci, 2017.

McDonald, K., Dobson, M., and Ulaby, F.: Using MIMICS To Model B-band Multiangle and Multitemporal Backscatter From A Walnut Orchard, IEEE Transactions on Geoscience and Remote Sensing, 28, 477–491, 1990.

McDonald, K., Zimmerman, R., and Way, J.: An Investigation Of The Relationship Between Tree Water Potential And Dielectric Constant, in: Geoscience and Remote Sensing Symposium, 1992. IGARSS'92. International, vol. 1, pp. 523–525, IEEE, 1992.

McDonald, K. C., Zimmermann, R., Way, J., and Chun, W.: Automated Instrumentation for Continuous Monitoring of the Dielectric Properties of Woody Vegetation: System Design, Implementation, and Selected *In Situ* Measurements, IEEE Transactions on Geoscience and Remote Sensing, 37, 1880–1894, 1999.

McDonald, K. C., Zimmermann, R., and Kimball, J. S.: Diurnal and spatial variation of xylem dielectric constant in Norway spruce (Picea abies [L.] Karst.) as related to microclimate, xylem sap flow, and xylem chemistry, IEEE Transactions on Geoscience and Remote Sensing, 40, 2063–2082, 2002.

McNairn, H. and Brisco, B.: The application of C-band polarimetric SAR for agriculture: a review, Canadian Journal of Remote Sensing, 30, 525–542, 2004.

McNairn, H., Shang, J., Jiao, X., and Champagne, C.: The contribution of ALOS PALSAR multipolarization and polarimetric data to crop classification, IEEE Transactions on Geoscience and Remote Sensing, 47, 3981–3992, 2009.

Meroney, R. N.: Characteristics of wind and turbulence in and above model forests, Journal of Applied Meteorology, 7, 780–788, 1968.

Molina-Aiz, F., Valera, D., Alvarez, A., and Madueno, A.: A wind tunnel study of airflow through horticultural crops: determination of the drag coefficient, Biosystems Engineering, 93, 447–457, 2006.

Moore, J. R. and Maguire, D. A.: Natural sway frequencies and damping ratios of trees: concepts, review and synthesis of previous studies, Trees, 18, 195–203, 2004.

Morison, J. I. and Gifford, R. M.: Stomatal sensitivity to carbon dioxide and humidity a comparison of two C_3 and two C_4 grass species, Plant Physiology, 71, 789–796, 1983.

Morton, D. C., Nagol, J., Carabajal, C. C., Rosette, J., Palace, M., Cook, B. D., Vermote, E. F., Harding, D. J., and North, P. R.: Amazon forests maintain consistent canopy structure and greenness during the dry season, Nature, 506, 221–224, 2014.

Naeimi, V., Bartalis, Z., and Wagner, W.: ASCAT Soil Moisture: An Assessment of the Data Quality and Consistency with the ERS Scatterometer Heritage., Journal of Hydrometeorology, 10, 2009.

Nelson, S. O.: Dielectric Properties of Agricultural Products: Measurements and Applications, IEEE Transactions on Electrical Insulation, 26, 845–869, 1991.

Novak, M. D., Warland, J. S., Orchansky, A. L., Ketler, R., and Green, S.: Wind tunnel and field measurements of turbulent flow in forests. Part I: uniformly thinned stands, Boundary-Layer Meteorology, 95, 457–495, 2000.

Odijk, T.: A tree swaying in a turbulent wind: a scaling analysis, Journal of Biological Physics, 41, 1–7, 2015.

Olioso, A., Carlson, T. N., and Brisson, N.: Simulation of diurnal transpiration and photosynthesis of a water stressed soybean crop, Agricultural and Forest Meteorology, 81, 41–59, 1996.

O'Neill, P. E., Podest, E., and Njoku, E. G.: Utilization of Ancillary Data Sets for SMAP Algorithm Development and Product Generation, in: Geoscience and Remote Sensing Symposium (IGARSS), 2011 IEEE International, pp. 2436–2439, IEEE, 2011.

Oren, R., Sperry, J., Katul, G., Pataki, D., Ewers, B., Phillips, N., and Schäfer, K.: Survey and synthesis of intra-and interspecific variation in stomatal sensitivity to vapour pressure deficit, Plant, Cell & Environment, 22, 1515–1526, 1999.

Paget, A. C., Long, D. G., and Madsen, N. M.: RapidScat diurnal cycles over land, IEEE Transactions on Geoscience and Remote Sensing, 54, 3336–3344, 2016.

Paloscia, S., Macelloni, G., Pampaloni, P., and Sigismondi, S.: The potential of C-and L-band SAR in estimating vegetation biomass: the ERS-1 and JERS-1 experiments, IEEE Transactions on Geoscience and Remote Sensing, 37, 2107–2110, 1999.

Panciera, R., Walker, J. P., Jackson, T. J., Gray, D. A., Tanase, M. A., Ryu, D., Monerris, A., Yardley, H., Rudiger, C., Wu, X., et al.: The soil moisture active passive experiments (SMAPEx): Toward soil moisture retrieval from the SMAP mission, IEEE Transactions on Geoscience and Remote Sensing, 52, 490–507, 2014.

Paris, J.: The effect of leaf size on the microwave backscattering by corn, Remote Sensing of Environment, 19, 81–95, 1986.

Patton, E. G., Sullivan, P. P., Shaw, R. H., Finnigan, J. J., and Weil, J. C.: Atmospheric Stability Influences on Coupled Boundary Layer and Canopy Turbulence, Journal of the Atmospheric Sciences, 73, 1621–1647, 2016.

Peltola, H.: Swaying of trees in response to wind and thinning in a stand of Scots pine, Boundary-Layer Meteorology, 77, 285–304, 1996.

Perämäki, M., Vesala, T., and Nikinmaa, E.: Modeling the dynamics of pressure propagation and diameter variation in tree sapwood, Tree Physiology, 25, 1091–1099, 2005.

Phillips, O. L., Aragão, L. E., Lewis, S. L., Fisher, J. B., Lloyd, J., López-González, G., Malhi, Y., Monteagudo, A., Peacock, J., Quesada, C. A., et al.: Drought sensitivity of the Amazon rainforest, Science, 323, 1344–1347, 2009.

Poggi, D. and Katul, G. G.: An experimental investigation of the mean momentum budget inside dense canopies on narrow gentle hilly terrain, Agricultural and Forest Meteorology, 144, 1–13, 2007.

Prevot, L., Dechambre, M., Taconet, O., Vidal-Madjar, D., Normand, M., and Gallej, S.: Estimating the characteristics of vegetation canopies with airborne radar measurements, International Journal of Remote Sensing, 14, 2803–2818, 1993.

Reich, P. B. and Borchert, R.: Water stress and tree phenology in a tropical dry forest in the lowlands of Costa Rica, The Journal of Ecology, pp. 61–74, 1984.

Reichstein, M., Bahn, M., Ciais, P., Frank, D., Mahecha, M. D., Seneviratne, S. I., Zscheischler, J., Beer, C., Buchmann, N., Frank, D. C., et al.: Climate extremes and the carbon cycle, Nature, 500, 287–295, 2013.

Rochette, P., Pattey, E., Desjardins, R., Dwyer, L., Stewart, D., and Dube, P.: Estimation of maize (*Zea mays* L.) canopy conductance by scaling up leaf stomatal conductance, Agricultural and Forest Meteorology, 54, 241–261, 1991.

Rudnicki, M., Mitchell, S. J., and Novak, M. D.: Wind tunnel measurements of crown streamlining and drag relationships for three conifer species, Canadian Journal of Forest Research, 34, 666–676, 2004.

Saatchi, S., Halligan, K., Despain, D. G., and Crabtree, R. L.: Estimation of forest fuel load from radar remote sensing, IEEE Transactions on Geoscience and Remote Sensing, 45, 1726–1740, 2007.

Saatchi, S., Asefi-Najafabady, S., Malhi, Y., Aragão, L. E., Anderson, L. O., Myneni, R. B., and Nemani, R.: Persistent effects of a severe drought on Amazonian forest canopy, Proceedings of the National Academy of Sciences, 110, 565–570, 2013.

Sade, N., Gebremedhin, A., and Moshelion, M.: Risk-taking plants. Anisohydric behavior as a stress-resistance trait, Plant Signaling & Behavior, 7, 767–770, 2012.

Salas, W., Ranson, K., Rock, B., and Moss, D.: Diurnal changes in the dielectric properties and water status of eastern hamlock and red spruce from Howland, ME, in: Geoscience and Remote Sensing Symposium, 1991. IGARSS'91. Remote Sensing: Global Monitoring for Earth Management., International, vol. 3, pp. 1111–1113, IEEE, 1991.

Salas, W., Ranson, J., Rock, B., and Smith, K.: Temporal and spatial variations in dielectric constant and water status of dominant forest species from New England, Remote Sensing of Environment, 47, 109–119, 1994.

Saleska, S. R., Didan, K., Huete, A. R., and Da Rocha, H. R.: Amazon forests green-up during 2005 drought, Science, 318, 612–612, 2007.

Samanta, A., Ganguly, S., Hashimoto, H., Devadiga, S., Vermote, E., Knyazikhin, Y., Nemani, R. R., and Myneni, R. B.: Amazon forests did not green-up during the 2005 drought, Geophysical Research Letters, 37, 2010.

Samanta, A., Knyazikhin, Y., Xu, L., Dickinson, R. E., Fu, R., Costa, M. H., Saatchi, S. S., Nemani, R. R., and Myneni, R. B.: Seasonal changes in leaf area of Amazon forests from leaf flushing and abscission, Journal of Geophysical Research: Biogeosciences, 117, 2012.

Satake, M. and Hanado, H.: Diurnal change of Amazon rain forest σ_0 observed by Ku-band spaceborne radar, IEEE Transactions on Geoscience and Remote Sensing, 42, 1127–1134, 2004.

Schilperoort, B., Coenders-Gerrits, M., Luxemburg, W., Cisneros Vaca, C., and Ucer, M.: Verifying the distributed temperature sensing Bowen ratio method for measuring evaporation, in: EGU General Assembly Conference Abstracts, vol. 18, p. 8486, 2016.

Schindler, D., Schönborn, J., Fugmann, H., and Mayer, H.: Responses of an individual deciduous broadleaved tree to wind excitation, Agricultural and Forest Meteorology, 177, 69–82, 2013.

Schlesinger, W. H. and Jasechko, S.: Transpiration in the global water cycle, Agricultural and Forest Meteorology, 189, 115–117, 2014.

Selker, J., Lane, J., Rupp, D., Hut, R., Abou Najm, M., Stewart, R., Van De Giesen, N., and Selker, F.: The answer is blowing in the wind: using wind induced resonance of trees to measure time varying canopy mass, including interception, in: AGU Fall Meeting Abstracts, vol. 1, p. 1155, 2011.

Sellers, P., Dickinson, R., Randall, D., Betts, A., Hall, F., Berry, J., Collatz, G., Denning, A., Mooney, H., Nobre, C., et al.: Modeling the exchanges of energy, water, and carbon between continents and the atmosphere, Science, 275, 502–509, 1997.

Sellier, D., Brunet, Y., and Fourcaud, T.: A numerical model of tree aerodynamic response to a turbulent airflow, Forestry, 81, 279–297, 2008.

Sevanto, S., Vesala, T., Perämäki, M., and Nikinmaa, E.: Time lags for xylem and stem diameter variations in a Scots pine tree, Plant, Cell & Environment, 25, 1071–1077, 2002.

Sevanto, S., Nikinmaa, E., Riikonen, A., Daley, M., Pettijohn, J. C., Mikkelsen, T. N., Phillips, N., and Holbrook, N. M.: Linking xylem diameter variations with sap flow measurements, Plant and Soil, 305, 77–90, 2008.

Sevanto, S., Hölttä, T., and Holbrook, N. M.: Effects of the hydraulic coupling between xylem and phloem on diurnal phloem diameter variation, Plant, Cell & Environment, 34, 690–703, 2011.

Shao, Y., Liu, S., Schween, J. H., and Crewell, S.: Large-Eddy atmosphere–land-surface modelling over heterogeneous surfaces: model development and comparison with measurements, Boundary-Layer Meteorology, 148, 333–356, 2013.

Shaw, R. H. and Schumann, U.: Large-eddy simulation of turbulent flow above and within a forest, Boundary-Layer Meteorology, 61, 47–64, 1992.

Shinozaki, K. and Yamaguchi-Shinozaki, K.: Gene Expression and Signal Transduction in Water-Stress Response., Plant Physiology, 115, 327, 1997.

Simunek, J. and van Genuchten, M.: Estimating unsaturated soil hydraulic properties from tension disc infiltrometer data by numerical inversion, Water Resources Research, 32, 2683–2696, 1995.

Slayter, R. et al.: Plant-water relationships., Plant-water relationships., 1967.

Soudani, K. and François, C.: Remote sensing: A green illusion, Nature, 506, 165–166, 2014.

Spatz, H.-C. and Theckes, B.: Oscillation damping in trees, Plant Science, 207, 66–71, 2013.

Steduto, P. and Hsiao, T. C.: Maize canopies under two soil water regimes.: I. Diurnal patterns of energy balance, carbon dioxide flux, and canopy conductance, Agricultural and Forest Meteorology, 89, 169–184, 1998a.

Steduto, P. and Hsiao, T. C.: Maize canopies under two soil water regimes: II. Seasonal trends of evapotranspiration, carbon dioxide assimilation and canopy conductance, and as related to leaf area index, Agricultural and Forest Meteorology, 89, 185–200, 1998b.

Steele-Dunne, S. C., Friesen, J., and van de Giesen, N.: Using diurnal variation in backscatter to detect vegetation water stress, IEEE Transactions on Geoscience and Remote Sensing, 50, 2618–2629, 2012.

Steele-Dunne, S. C., McNairn, H., Monsivais-Huertero, A., Judge, J., Liu, P. W., and Papathanassiou, K.: Radar Remote Sensing of Agricultural Canopies: A Review, IEEE Journal of Selected Topics in Applied Earth Observations and Remote Sensing, pp. 1–25, 2017.

Stephenson, N. L., Das, A., Condit, R., Russo, S., Baker, P., Beckman, N., Coomes, D., Lines, E., Morris, W., Rüger, N., et al.: Rate of tree carbon accumulation increases continuously with tree size, Nature, 507, 90–93, 2014.

Stewart, R. D., Hut, R., Rupp, D. E., Gupta, H., and Selker, J. S.: A resonating rainfall and evaporation recorder, Water Resources Research, 48, 2012.

Stull, R. B.: An introduction to boundary layer meteorology, vol. 13, Springer Science & Business Media, 2012.

Taconet, O., Benallegue, M., Vidal-Madjar, D., Prevot, L., Dechambre, M., and Normand, M.: Estimation of soil and crop parameters for wheat from airborne radar backscattering data in C and X bands, Remote Sensing of Environment, 50, 287–294, 1994.

Tardieu, F. and Simonneau, T.: Variability among species of stomatal control under fluctuating soil water status and evaporative demand: modelling isohydric and anisohydric behaviours, Journal of Experimental Botany, 49, 419–432, 1998.

Tardieu, F., Bruckler, L., and Lafolie, F.: Root clumping may affect the root water potential and the resistance to soil-root water transport, Plant and Soil, 140, 291–301, 1992a.

Tardieu, F., Zhang, J., and Davies, W.: What information is conveyed by an ABA signal from maize roots in drying field soil?, Plant, Cell & Environment, 15, 185–191, 1992b.

Tardieu, F., Zhang, J., and Gowing, D.: Stomatal control by both [ABA] in the xylem sap and leaf water status: a test of a model for draughted or ABA-fed field-grown maize, Plant, Cell & Environment, 16, 413–420, 1993.

Tardieu, F., Lafarge, T., and Simonneau, T.: Stomatal control by fed or endogenous xylem ABA in sunflower: interpretation of correlations between leaf water potential and stomatal conductance in anisohydric species, Plant, Cell & Environment, 19, 75–84, 1996.

Thuiller, W., Lavergne, S., Roquet, C., Boulangeat, I., Lafourcade, B., and Araujo, M. B.: Consequences of climate change on the tree of life in Europe, Nature, 470, 531–534, 2011.

Turner, N. C.: Stomatal Behavior and Water Status of Maize, Sorghum, and Tobacco under Field Conditions II. At Low Soil Water Potential, Plant Physiology, 53, 360–365, 1974.

Tuzet, A., Perrier, A., and Leuning, R.: A coupled model of stomatal conductance, photosynthesis and transpiration, Plant, Cell & Environment, 26, 1097–1116, 2003.

Ulaby, F.: Radar measurement of soil moisture content, IEEE Transactions on Antennas and Propagation, 22, 257–265, 1974.

Ulaby, F.: Radar response to vegetation, IEEE Transactions on Antennas and Propagation, 23, 36–45, 1975.

Ulaby, F. and Batlivala, P.: Diurnal variations of radar backscatter from a vegetation canopy, IEEE Transactions on Antennas and Propagation, 24, 11–17, 1976.

Ulaby, F., Bush, T., and Batlivala, P.: Radar response to vegetation II: 8-18 GHz band, IEEE Transactions on Antennas and Propagation, 23, 608–618, 1975.

Ulaby, F. T. and El-Rayes, M. A.: Microwave dielectric spectrum of vegetation - Part II: Dual-dispersion model, IEEE Transactions on Geoscience and Remote Sensing, pp. 550–557, 1987.

Ulaby, F. T. and Jedlicka, R.: Microwave dielectric properties of plant materials, IEEE Transactions on Geoscience and Remote Sensing, pp. 406–415, 1984.

Ulaby, F. T., Dobson, M. C., and Bradley, G. A.: Radar reflectivity of bare and vegetation-covered soil, Advances in Space Research, 1, 91–104, 1981.

Ulaby, F. T., Aslam, A., and Dobson, M. C.: Effects of vegetation cover on the radar sensitivity to soil moisture, IEEE Transactions on Geoscience and Remote Sensing, pp. 476–481, 1982a.

Ulaby, F. T., Li, R. Y., and Shanmugan, K.: Crop classification using airborne radar and Landsat data, IEEE Transactions on Geoscience and Remote Sensing, pp. 42–51, 1982b.

Ulaby, F. T., Moore, R. K., and Fung, A. K.: Microwave Remote Sensing, Active and Passive, II, Radar Remote Sensing and Surface Scattering and Emission Theory, Artech House, Norwood, Mass, 1982c.

Ulaby, F. T., Sarabandi, K., Mcdonald, K., Whitt, M., and Dobson, M. C.: Michigan microwave canopy scattering model, International Journal of Remote Sensing, 11, 1223–1253, 1990.

van Emmerik, T., Coenders-Gerrits, A., and Wenninger, J.: Partitioning of evaporation fluxes in summer and winter using stable isotope approach, in: EGU General Assembly Conference Abstracts, vol. 14, p. 3779, 2012.

van Emmerik, T., Steele-Dunne, S., Judge, J., and van de Giesen, N.: A comparison between leaf dielectric properties of stressed and unstressed tomato plants, in: Geoscience and Remote Sensing Symposium (IGARSS), 2015 IEEE International, pp. 275–278, IEEE, 2015a.

van Emmerik, T., Steele-Dunne, S. C., Judge, J., and van de Giesen, N.: Impact of diurnal variation in vegetation water content on radar backscatter from maize during water stress, IEEE Transactions on Geoscience and Remote Sensing, 53, 3855–3869, 2015b.

van Emmerik, T., Steele-Dunne, S., Hut, R., Gentine, P., Guerin, M., Oliveira, R., Wagner, J., Selker, J., and van de Giesen, N.: Measuring Tree Properties and Responses Using Low-Cost Accelerometers, Sensors, 17, 1098, 2017a.

van Emmerik, T., Steele-Dunne, S., Paget, A., Oliveira, R., Bittencourt, P., de V. Barros, F., and van de Giesen, N.: Water stress detection in the Amazon using radar, Geophysical Research Letters, 2017b.

van Emmerik, T., Steele-Dunne, S. C., Judge, J., and Van De Giesen, N.: Dielectric Response of Corn Leaves to Water Stress, IEEE Geoscience and Remote Sensing Letters, 14, 8–12, 2017c.

van Emmerik, T., Steele-Dunne, S., Gentine, P., Oliveira, R., Bittencourt, P., de V. Barros, F., and van de Giesen, N.: Water stress impacts tree-atmosphere interaction in the Amazon, in review.

van Genuchten, M. T. and Nielsen, D. R.: On describing and predicting the hydraulic properties of unsaturated soils, Annales Geophysicae, 3, 615–628, 1985.

Vollsinger, S., Mitchell, S. J., Byrne, K. E., Novak, M. D., and Rudnicki, M.: Wind tunnel measurements of crown streamlining and drag relationships for several hardwood species, Canadian Journal of Forest Research, 35, 1238–1249, 2005.

Vreugdenhil, M., Dorigo, W. A., Wagner, W., de Jeu, R. A., Hahn, S., and van Marle, M. J.: Analyzing the Vegetation Parameterization in the TU-Wien ASCAT Soil Moisture Retrieval, IEEE Transactions on Geoscience and Remote Sensing, 54, 3513–3531, 2016a.

Vreugdenhil, M., Hahn, S., Melzer, T., Bauer-Marschallinger, B., Reimer, C., Dorigo, W. A., and Wagner, W.: Assessing Vegetation Dynamics Over Mainland Australia With Metop ASCAT, IEEE Journal of Selected Topics in Applied Earth Observations and Remote Sensing, 2016b.

Wagner, J.: Beta Prototype Product Manual Acceleration Logger – Model AL100, Oregon Research Electronics, 31677 N. Lake Creek Drive, Tangent, OR 97389 USA, http://www.orelectronics.net, 2015 (Accessed April 9, 2015).

Wagner, J.: Application Note AL100: Optimizing Accelerometer Placement in Trees - Preliminary, Oregon Research Electronics, 31677 N. Lake Creek Drive, Tangent, OR 97389 USA, http://www.orelectronics.net, 2015 (Accessed August 21, 2015).

Wagner, W., Lemoine, G., and Rott, H.: A method for estimating soil moisture from ERS scatterometer and soil data, Remote Sensing of Environment, 70, 191–207, 1999.

Way, J., Paris, J., Dobson, M. C., McDonals, K., Ulaby, F. T., Weber, J., Ustin, L., Vanderbilt, V. C., and Kasischke, E. S.: Diurnal change in trees as observed by optical and microwave sensors: The EOS synergism study, IEEE Transactions on Geoscience and Remote Sensing, 29, 807–821, 1991.

Weber, J. and Ustin, S.: Diurnal water relations of walnut trees: implications for remote sensing, IEEE Transactions on Geoscience and Remote Sensing, 29, 864, 1991.

Whittaker, P., Wilson, C. A., and Aberle, J.: An improved Cauchy number approach for predicting the drag and reconfiguration of flexible vegetation, Advances in Water Resources, 83, 28–35, 2015.

Wright, S. J. and Cornejo, F. H.: Seasonal drought and leaf fall in a tropical forest, Ecology, 71, 1165–1175, 1990.

Yu, G.-R., Nakayama, K., Matsuoka, N., and Kon, H.: A combination model for estimating stomatal conductance of maize (*Zea mays* L.) leaves over a long term, Agricultural and Forest Meteorology, 92, 9–28, 1998.

Zanne, A., Lopez-Gonzalez, G., Coomes, D., Ilic, J., Jansen, S., Lewis, S., Miller, R., Swenson, N., Wiemann, M., and Chave, J.: Global wood density database. Dryad, Also available at http://hdl. handle. net/10255/dryad, 235, 2009.

Zhang, J. and Davies, W.: Does ABA in the Xylem Control the Rate of Leaf Growth in Soil-Dried Maize and Sunflower Plants?, Journal of Experimental Botany, 41, 1125–1132, 1990.

Zimmermann, R., McDonald, K., Way, J., and Oren, R.: Microclimate, water potential, transpiration, and bole dielectric constant of coniferous and deciduous tree species in the continental boreal ecotone of central Alaska, in: Geoscience and Remote Sensing Symposium, 1994. IGARSS'94. Surface and Atmospheric Remote Sensing: Technologies, Data Analysis and Interpretation., International, vol. 1, pp. 226–228, IEEE, 1994.

Zimmermann, R., McDonald, K., Oren, R., and Way, J.: Xylem dielectric constant, water status, and transpiration of young Jack Pine (Pinus banksiana Lamb.) in the southern boreal zone of Canada, in: Geoscience and Remote Sensing Symposium, 1995. IGARSS'95.'Quantitative Remote Sensing for Science and Applications', International, vol. 2, pp. 1006–1008, IEEE, 1995.

Zweifel, R., Zimmermann, L., and Newbery, D.: Modeling tree water deficit from microclimate: an approach to quantifying drought stress, Tree Physiology, 25, 147–156, 2005.

ACKNOWLEDGEMENTS

Although my thesis has one author, it is thanks to very long list of people that I was able to finish it. Scientifically, and definitely also personally. I hope that I give credit to all the people who deserve it. In case you don't find your name here, please know that you might still have a special place in my heart. But, it could also be a good reason to unfriend me.

Susan, I am indefinitely grateful for your supervision. It's been very inspiring to work with you, and I've learned a lot. Not only in the science department, but also, for example, that it's allowed to switch hotels when you find yourself in the middle of a cockroach parade. Five years is a long time, and I'm very thankful that you managed to keep your trust in me for this whole journey. Go raibh maith agat!

Nick, ik wil je bedanken voor alle fantastische mogelijkheden die je mij hebt gegeven om mijzelf te ontwikkelen als wetenschapper, als persoon, en als veldwerkfanaat. Je hebt me (letterlijk, Binaba) laten zien hoe ik mijn hoofd boven water moet houden, in goede en in slechte tijden. Je hebt altijd goed door waar ik warm (of koud) van word, en dat heeft me enorm geholpen in het vormgeven van mijn bewandelde pad.

Huub, alhoewel je weinig met mijn promotie te maken hebt gehad, ben ik ook dankbaar voor alle steun en wijze lessen die ik van jou heb gekregen. Tijdens de artikelen die we samen hebben gepubliceerd. Maar misschien nog wel belangrijker, door alle deuren die je hebt geopend voor opzetten van de Young Hydrologic Society, en alle goede dingen die daar uit voort zijn gevloeid!

Hoe onwaarschijnlijk het klinkt, ik wil Maurits ook bedanken! Je hebt mij ooit de kans geboden om mijn bacheloreindwerk zelf vorm te geven, en dit project heeft mijn eerste interesse in wetenschap aangewakkerd.

De echte vlam voor onderzoek is echter aangewakkerd tijdens de isotopenstudie die ik met Miriam Coenders-Gerrits en Jochen Wenninger mocht doen. Es ist schade, dass die grösste Entdeckung war dass unsere Methode nicht so gut funktionierte wie gehofft. Trotzdem, dieses Projekt hat mich inspiriert um das wissenschaftliche Pfad zu nehmen.

Half of my thesis uses data I obtained at a Florida cornfield, and I would like to thank Jasmeet, and all of her group at the University of Florida Center for Remote Sensing, for the opportunities to work with her during my M.Sc. thesis. Our papers weren't the easiest ones to get published, but I'm very happy we made it.

An important period for my academic development was the time I spent working with Siva at the University of Illinois at Urbana-Champaign. Thank you very much for the guidance, opportunities and academic freedom that you provided me.

The tropical part of my thesis would not have been possible without Rafael, Paulo, Fernanda, Tomas, and Laura. Muito obrigado por permitir me vir junto com você para trabalho de campo. Obrigado especialmente a Rafael. Você me ensinou muitas coisas sobre florestras e Brazil. Ademas, você fez nosses artigos muitos melhor.

From Columbia University in New York, I want to thank Pierre, Marceau, Julia and Daniel. Pierre, je suis impressionné par ton train de pensées brillant et inârretable.

C'etait trés inspirant de travailler avec toi. Marceau, Julia, and Daniel, thank you for our unforgettable time in the Brazilian Amazon! Julia, I look forward doing and sharing science on many more continents.

Alhoewel ik veel van mijn data zelf heb verzameld, was dit nooit mogelijk geweest zonder de hulp van iedereen waar ik mijn veldwerk heb gedaan. Ik wil graag de Botanische Tuin van de TU Delft, en Bob Ursem specifiek, bedanken voor alle hulp die ik heb gekregen bij het uittesten van sensoren. Ook ben ik Kees Scheffers en de Wageningen University and Research Glastuinbouw in Bleiswijk dankbaar voor de metingen die ik heb mogen doen aan tomatenplanten. De familie De Pater uit Zeewolde wil ik bedanken voor de metingen die ik heb mogen doen aan maisplanten op hun land.

Daarnaast wil ik iedereen bedanken van de TU die mij gesteund heeft en mijn thesis mede mogelijk heeft gemaakt: Lydia, Betty, Luz, Boran, Frank, Marie, Camille, Heloise, Anna, Prof. Geert Leus, Wim, Dong, Aagje, Remko.

I am also very thankful to the myriad of friends, colleagues and co-authors from all over the world, who helped me grow as a person and as a scientist: Gert Mulder, Marja Haagsma, Lieke Melsen, Yvonne Smit, Koen Hilgersom, Anna Kauffeldt, Dario Del Guidice, Josh Larsen, Saket Pande, Alon Rimmer, Scott Tyler, and John Selker.

Anna, vaše role v dokončení této práce překračuje moje schopnosti popisovat ji. Vaše přátelství, podpora a kolegiality jsou víc, než bych si přál. Během posledních čtyř let jsem s tebou strávil více času než s někým jiným a doufám, že se brzy neskončí. Jedinečná kombinace našich preferencí pro vtipné vtipy, alkoholické nápoje a šťavnaté klepy mě držely na správné cestě. Dékuji.

Emma, ik ben heel erg dankbaar voor de speciale band die wij hebben. We weten elkaar toch altijd weer goede moed, en goede tijden te bezorgen. Ik kijk er naar uit om nog veel geld te laten rollen dat we nooit zullen hebben.

Het noodzakelijke combineren met het aangename, dat is misschien nog wel de wijste les die ik van jou heb geleerd, Wouter. Ik ben jou ontzettend dankbaar voor jouw vriendschap en inspiratie, en ik ben er ontzettend trots op wat we samen hebben bereikt. Met YHS, met gezamelijke papers, en met onze kunst levensgenieten.

Laurène, kantoorgenoten, buren, vrienden, wat zijn we niet! Bedankt voor alle mooie tijden die we samen hebben beleefd, in binnen- en buitenland. De kraan zal altijd voor je open staan.

Dirk, bedankt voor het onvergetelijke avontuur in de Oost. Nog lang zullen we doorpraten over ons legendarische project in Cambodja, wat ook het begin was van een mooie vriendschap, met ontelbare uren squash, sauna, en glazen bier.

Franca, we zijn ooit door het lot bij elkaar gebracht in het 48e bestuur van het dispuut, en ik blij dat het zo gelopen is! Bedankt voor al jouw geweldige Indische maaltijden, en jouw fijne gezelschap!

Defne, ik ben jou ook ongelooflijk dankbaar. Vanaf het moment dat de eerste rook was opgetrokken op civiel wisten we elkaar te vinden, en ik ga ervan uit dat we nog vele jaren zoveel voor elkaar kunnen betekenen als dat we tot nu toe hebben gedaan.

Daarnaast wil ik ook alle vrienden bedanken die mij de afgelopen jaren vreugde hebben gebracht. Daan, voor alle goede gesprekken, autoritjes en Mark Knopfler. Pierre, obrigado voor je warmte, inspiratie en gezelligheid. Maurits, voor alle heerlijkeberenavonturen. Marieke, voor het feit dat ik nu snel kan afwassen, en de mooie jaren sinds

Londen. Sjoerd, voor onze altijd leuke uitjes. Lotte, voor de interessante nieuwe gezamelijke inzichten. Stefanie, danke dass trotz ich immer zu spät bin, du immer noch Freunden sein möchte. Andrea, vielen dank für alle schöne Unterhaltungen, und dass du dir immer die Zeit nimmst um meine Grammatik zu verbessern. Rolf, voor al je can-domentaliteit die je op mij hebt afgestraald, je al altijd oppeppende woorden en het delen van de mooiste geheime plekjes in binnen- en buitenland.

Katharina, danke für alli Gipfeli, diini Erüchtich, Magnetismus und Gsellschaft. Du bisch äs urigs Gschänkli.

Since 2012 I've spent a fair amount of time on organizing networks, events, and sessions for early career scientists. I'm very proud that the Young Hydrologic Society (YHS) is, what it currently is. However, this would not have been possible without all the fantastic dedication by current active scientists. Specifically I want to thank the people who supported YHS from the beginning, and built the foundation of the success it is now: Shaun Harrigan, Maarten Smoorenburg, Hannes Müller, Juernjakob Dugge.

A large part of YHS' success is thanks to many dedicated people from EGU and AGU. Without the organizations, and the people, the global community of young hydrologists would not have been so strong. In particular, I want to thank Eric Wood, Efi Foufoula-Georgiou, and Jeff McDonnell from the AGU Hydrology Section, Kara Smedly Rodean from AGU, Gerrit de Rooij and Elena Toth from the EGU Hydrology Division, and Sheila, Mousa, Evan, Kevin, Frank, Natasha, and Adam from the AGU Hydrology Student Subcommittee (and its unofficial predecessor).

Sommige vrienden heb je niet voor even, die heb je voor het leven. Bedankt Ronald, Thomas, Carlijn en Lotte voor de onverwoestbare band die wij hebben. In tegenstelling tot het pad der destructie dat menigmaal door de Vedettes achter wordt gelaten.

Ook ben ik al mijn lieve (oud-)huisgenootjes van de ZAB dankbaar. Tijdens mij hele Delftse leven heb ik hier gewoond en ik ben eeuwig dankbaar dat ik hier terecht ben gekomen. Het komt zeker voor een groot deel door jullie dat ik ben geworden wie ik ben. Bedankt Piers Titus, Ewout, Bart, Hannah, Maaike, Gerben, Floor, Ruben, Marte, Nicolien, Arie, Sylvia, Pelin, Keimpke, Dolores, Koen, Joshua, Louise, Bas, Frederike, Nadine, Cher, en natuurlijk Bink, Yuki, Meimei, Scarlett, Bob en Keira.

Marjolein, ik ben je ontzettend dankbaar voor de tijd die wij samen hebben gehad en de steun die ik van jou heb gekregen tijdens een groot deel van mijn promotie, en natuurlijk tijdens onze hele gezamelijke reis. Ik ben blij dat we samen groot zijn geworden.

Heel veel dank aan alle lieve (stief)familie, en vooral al mijn grootouders. Jullie hebben zo veel bijgedragen aan wie ik nu ben, waar ik van houd, hoe ik denk, en ik ben blij dat jullie mij (nog steeds) ontzettend veel inspiratie weten te geven.

Lina, du är verkligen en av dem modigaste och starkaste personer jag känner. Jag är jätte glad och tacksam för alla våra momenter ihop, och din stöd under dem sista två år. Jag vet inte vad framtiden ska ge, men jag är tacksam för du har kommit i mit liv.

Robin, bedankt dat je er altijd voor me bent, en bent geweest. Je bent een van de tofste en belangrijkste mensen in mijn leven.

Mama, papa, bedankt voor alle kansen die jullie mij hebben gegeven. Het leven is niet altijd even makkelijk, maar ik had me geen betere ouders kunnen wensen.

CURRICULUM VITÆ

Tim Hans Martin VAN EMMERIK

03-10-1989	Born in Delft, The Netherlands.

EDUCATION

2001–2007	Atheneum Ashram College, Alphen aan den Rijn
2007–2011	B.Sc. Civil Engineering Delft University of Technology *Thesis:* Agriculture in Kenya: Design of a small-scale irrigation system to stimulate agricultural activities in Kilole
2010–2013	M.Sc. Civil Engineering Delft University of Technology *Thesis:* Diurnal differences in vegetation dielectric constant as a measure of water stress
2013–2017	Ph.D. Civil Engineering Delft University of Technology *Thesis:* Water stress detection using radar

AWARDS

2016	Winner Youth Contest for Sustainable Deltas, Delta Coalition, The Netherlands
2016	Outstanding presentation, 17th WaterNet Symposium, Botswana
2010	Winner Wetskills Student Competition, Shanghai, China

APPOINTMENTS AND ACTIVITIES

2010–2011	**Council Member**, Student Council, Faculty of Civil Engineering & Geosciences, Delft University of Technology
2011	**President**, Dispuut Watermanagement
2012–2016	**Founder and co-chair**, Young Hydrologic Society
2014–2016	**Student Representative**, AGU Hydrology Section Executive Committee
2015–2016	**Chair**, AGU Hydrology Section Student Subcommittee
2015–2017	**Member**, AGU Meetings Committee
2013–present	**Reviewer**, e.g. IEEE Journal of Selected Topics in Applied Earth Observations and Remote Sensing, Frontiers in Earth Science, Hydrology and Earth System Sciences, Water Resources Research, International Journal of Remote Sensing, Journal of Geophysical Research: Biogeosciences
2017–present	**Student Member**, AGU Council

List of Publications

Peer-Reviewd Journals

15. **van Emmerik, T.**, S. Steele-Dunne, P. Gentine, R.S. Oliveira, P. Bittencourt, F. Barros, and N. van de Giesen, *Water impacts tree-atmosphere interaction in the Amazon*, in review.

14. **van Emmerik, T.**, A. Popp, A. Solcerova, H. Müller, H. Beria, and R. Hut, *Reporting on negative results to revive experimental hydrology*, in review.

13. Roobavannan, M., **T. van Emmerik**, Y. Elshafei, J. Kandasamy, M. Sanderson, S. Vigneswaran, S. Pande, and M. Sivapalan, *Norms and values in socio-hydrological models*, Hydrol. Earth Syst. Sci. Discuss., in review (2017).

12. **van Emmerik, T.**, S. Steele-Dunne, A. Paget, R.S. Oliveira, P.R.L. Bittencourt, F. de V. Barros, and N. van de Giesen, *Water stress detection in the Amazon using RapidScat*, Geophysical Research Letters, (2017).

11. Berghuijs, W., J. Larsen, **T. van Emmerik**, and R. Woods, *A Global Assessment of Runoff Sensitivity to Changes in Precipitation, Potential Evaporation, and Other Factors*, Water Resources Research, (2017).

10. Yoshihide Wada, Marc F. P. Bierkens, Ad de Roo, Paul A. Dirmeyer, James S. Famiglietti, Naota Hanasaki, Megan Konar, Junguo Liu, Hannes Müller Schmied, Taikan Oki, Yadu Pokhrel, Murugesu Sivapalan, Tara J. Troy, Albert I. J. M. van Dijk, **T. van Emmerik**, Marjolein H.J. Van Huijgevoort, Henny A. J. Van Lanen, Charles J. Vörösmarty, Niko Wanders, and Howard Wheater, *Human-water interface in hydrological modeling: Current status and future directions*, Hydrol. Earth Syst. Sci. (2017).

9. Peters-Lidard, C. D., Clark, M., Samaniego, L., Verhoest, N. E. C., **van Emmerik, T.**, Uijlenhoet, R., Achieng, K., Franz, T. E., and Woods, R., *Scaling, Similarity, and the Fourth Paradigm for Hydrology*, Hydrol. Earth Syst. Sci., (2017).

8. **van Emmerik, T.**, S. Steele-Dunne, R. Hut, P. Gentine, M. Guerin, R.S. Oliveira, J. Wagner, J. Selker, and N. van de Giesen, *Measuring Tree Properties and Responses Using Low-Cost Accelerometers*, Sensors **17:5**, 1098, (2017).

7. **van Emmerik, T.**, S. Steele-Dunne, J. Judge and N. van de Giesen, *Dielectric Response of Corn Leaves to Water Stress*, IEEE Geosciences and Remote Sensing Letters **14:1**, 79–90 (2017).

6. Hut, R., S. Tyler and **T. van Emmerik**, *Proof of concept: Temperature sensing waders for environmental sciences*, Geosci. Instrum. Method. Data Syst. **5**, 45–51 (2016).

5. Hilgersom, H., **T. van Emmerik**, A. Solcerova, W. Berghuijs, J. Selker and N. van de Giesen, *Practical Considerations for enhanced-resolution coil-wrapped Distributed Temperature Sensing setups*, Geosci. Instrum. Method. Data Syst. **5**, 151–162 (2016).

4. **van Emmerik, T.**, G. Mulder, D. Eilander, M. Piet and H. Savenije, *Predicting the ungauged basin: Model validation and realism assessment*, Front. Earth Sci. **3**, 62 (2015).

3. **van Emmerik, T.**, S. Steele-Dunne, J. Judge and N. van de Giesen, *Impact of Diurnal Variation in Vegetation Water Content on Radar Backscatter of Maize During Water Stress*, Geosciences and Remote Sensing, IEEE Transactions on **52**, 7 (2015).

2. **van Emmerik, T.H.M.**, Z. Li, M. Sivapalan, S. Pande, J. Kandasamy, H.H.G. Savenije, A. Chanan and S. Vigneswaran, *Socio-hydrologic Modeling to Understand and Mediate the Competition for Water between Agriculture Development and Environmental Health: Murrumbidgee River Basin, Australia*, Hydr. Earth Syst. Sci. **18**, 4239–4259 (2014).

1. **van Emmerik, T.H.M.**, A. Rimmer, Y. Lechinsky, K.J.R. Wenker, S. Nussboim, N.C. van de Giesen, *Measuring heat balance residual at lake surface using Distributed Temperature Sensing*, Limnology and Oceanography: Methods **11**, 79–90 (2013).

CONFERENCE PROCEEDINGS

1. **van Emmerik, T.**, S. Steele-Dunne, J. Judge and N. van de Giesen, *A Comparison of Leaf Dielectric Properties of Stressed and Unstressed Tomato Plants*, IGARSS 2015, Milan (2015).

OTHER

5. **van Emmerik, T.**, *Four Reasons Why All Geoscientists Should Do Fieldwork*, Streams of Thought (Young Hydrologic Society) (2015).

4. Berghuijs, W., S. Harrigan, E. Kipnis, N. Dogulu, M. Floriancic, H. Müller, I. Pohle, F. Sedlar, S. Saia, M. Smoorenburg, C. Teutschbein and **T. van Emmerik**, *Creating Community for Early-Career Geoscientists*, Eos, **96** (2015).

3. **van Emmerik, T.**, *Fall Meeting's First Student and Early Career Conference*, Eos, **96** (2015).

2. T. Bongiovanni, K. Liu, D. Nagarajan, P. Preston, P. Rush, **T. van Emmerik**, R. Terwilleger, A. Mosivais-Huertero, J. Judge, S. Steele-Dunne, R. Akbar, E. Baar, K. Wallace, and A. England, *Field Observations During the Eleventh Microwave Water and Energy Balance Experiment (MicroWEX-11): From April 25 Through December 9, 2012*, Center for Remote Sensing, University of Florida, Available at UF/IFAS EDIS website at http://edis.ifas.ufl.edu/AE514 (2015).

1. **van Emmerik, T.**, W. Berghuijs, R. Hut, *A brainstorming session about the future of scientific meetings: what will EGU 2024 look like?*, GeoQ **10** (2014).

Balnea vina venus corrumpunt corpora nostra, sed vitam faciunt balnea vina venus

Tiberius Claudius Secundus

In voorbijgevlogen jaren
Heb ik mijn onderzoek verricht
Inzichtelijk uiteengezet
In dit boek dat voor je ligt

TIM VAN
EMMERIK